The Localized-to-Delocalized Transition in Mixed-Valence Chemistry

Konstantinos D. Demadis,† Chris M. Hartshorn,‡ and Thomas J. Meyer*,§

Department of Chemistry, Venable and Kenan Laboratories, University of North Carolina at Chapel Hill, Chapel Hill, North Carolina 27599-3290, and Los Alamos National Laboratory, P.O. Box 1663, MS A127, Los Alamos, New Mexico 87545

Received May 25, 2000

Contents

I. Introduction

Mixed-valence compounds contain an element which, at least in a formal sense, exists in more than one oxidation state.[1,2] This is a common phenomenon. Prussian blue, which has a cyanide-bridged Fe(II)−Fe(III) structure, was one of the first chemical materials to be described.[3] The mixed-valence character of some minerals provides the basis for their color. Multiple-site metalloenzymes, which undergo multiple electron transfer, have mixed-valence forms.

In the 1970s the first designed mixed-valence complexes were prepared, the μ-pyrazine-bridged dimer $[(NH_3)_5Ru(pz)Ru(NH_3)_5]^{5+}$ (**1**, pz is pyrazine) by Creutz and Taube[4,5] and the cyclopentadienyl-linked biferrocenium cation $[(C_5H_5)Fe(C_5H_4-C_5H_4)Fe(C_5H_5)]^+$ by Cowan and co-workers.[6,7] They were also the first to discuss an odd-electron organic compound, the tetrathiafulvalene radical cation, as a mixed-valence molecule.[6] Mixed-valence materials had been reviewed and classified earlier by Robin and Day[8] and reviewed by Allen and Hush.[9]

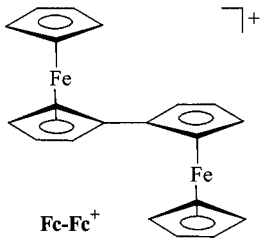

Fc-Fc$^+$

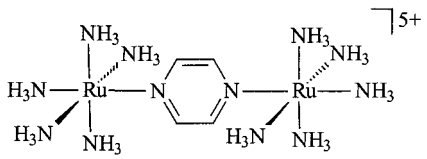

Creutz-Taube Ion
(1)

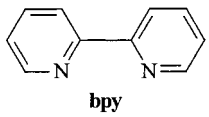

bpy

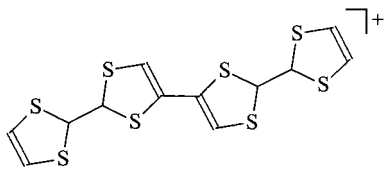

TTF-TTF$^+$

One of the reasons for interest in mixed-valence molecules was the possibility that they could be used to measure rate constants and activation barriers for intramolecular electron transfer,[4,5] e.g., eq 1 (bpy is 2,2′-bipyridine).[10,11]

$$cis,cis\text{-}[(bpy)_2(Cl)Ru^{III}(pz)Ru^{II}(Cl)(bpy)_2]^{3+} \rightleftharpoons cis,cis\text{-}[(bpy)_2(Cl)Ru^{II}(pz)Ru^{III}(Cl)(bpy)_2]^{3+} \quad (1)$$

These reactions have proven difficult to study by direct measurement, although there are notable exceptions in the work of Nelsen and co-workers on

* To whom correspondence should be addressed. E-mail: tjmeyer@lanl.gov.
† Present address: 47 Dodecanisou Street, Vrilissia 15235, Athens, Greece.
‡ Present address: Geo-Centers, Inc., c/o Naval Research Laboratory, P.O. Box 441340, Fort Washington, MD 20749-1340. E-mail: hartshorn@cbmse.nrl.navy.mil.
§ Los Alamos National Laboratory.

10.1021/cr990413m CCC: $36.00
Published on Web 09/12/2001

Konstantinos (Kostas) Demadis was born in 1967 in Komotini of Thrace, Greece. He received his B.S. degree from the National University of Athens, Greece, in 1990. He then moved to Ann Arbor, MI, where he began his graduate studies in chemistry at the University of Michigan at Ann Arbor. He earned his Ph.D. degree in 1995, after working in the Laboratories of Professor Dimitri Coucouvanis. His thesis research covered the area of structural and functional modeling of the active site of the nitrogenase enzyme. After completion of his Ph.D. degree, he joined Professor Tom Meyer's research group at the University of North Carolina at Chapel Hill. The focus of his postdoctoral research was in the fields of electron transfer, redox chemistry, and small molecule activation, with particular emphasis on the interconversion of the oxidation states of nitrogen in osmium complexes and mixed-valence chemistry. In September 1998 he moved to the Chicago area and joined the Research & Development Division of Nalco Chemical Company as a Senior Chemist. His current research interests extend over a range of scientific areas and include crystal growth and inhibition, bioinspired materials science, materials science, materials corrosion control, and technology of polymers and colloids. Kostas is a member of the American Chemical Society, the National Association of Corrosion Engineers, and the Association of Greek Chemists.

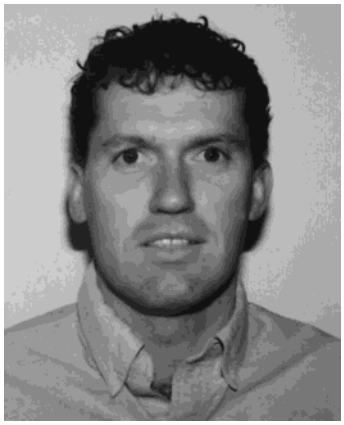

Chris M. Hartshorn was born in Christchurch, New Zealand, in 1972. He graduated with first class honors in chemistry from the University of Canterbury. He remained at the University of Canterbury for his Ph.D. degree with Associate Professor Peter J. Steel on the synthesis and coordination chemistry of new nitrogen-containing ligands. Upon completion of his Ph.D. degree in 1997, he joined the group of Professor Thomas J. Meyer at the University of North Carolina at Chapel Hill as a postdoctoral research associate. In 1999 he moved to Washington, D.C., where he was contracted to the Center of Bio/Molecular Science and Engineering at the Naval Research Laboratory. His research during this time investigated polymer-bound transition-metal complexes as catalysts for the hydrolysis of toxic materials. He has since taken a position in the Color Technology Division of GE Plastics in Selkrik, NY.

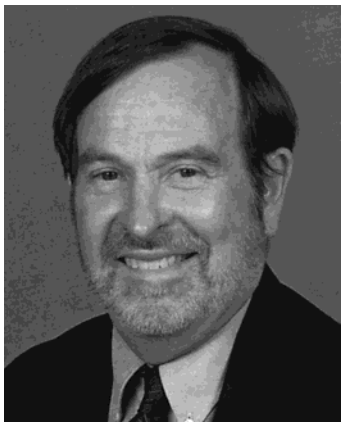

Thomas J. Meyer joined the staff of the Los Alamos National Laboratory as Associate Laboratory Director for Strategic and Supporting Research on January 3, 2000, after a long career as a faculty member and administrator at the University of North Carolina at Chapel Hill. He joined the Faculty at UNC in 1968 after a year as a NATO postdoctoral fellow at University College, London. He was promoted to Associate Professor in 1972 and Full Professor in 1975 and was named Smith Professor of Chemistry in 1982 and Kenan Professor in 1987. He served as the Head of Chemistry from 1994 to 1997 and Vice Chancellor and Vice Provost for Graduate Studies and Research from 1994 to 1999. He served on the NC Board of Science and Technology, the Executive Committees of the NC Biotechnology Center, the Research Triangle Institute, and the Triangle University Center for Advanced Study Ind., and on the Board of Associated Universities Inc. Dr. Meyer is a member of the National Academy of Sciences and the American Academy of Arts and Sciences. He has won many awards for his research in chemistry and was awarded the Order of the Long Leaf Pine of the State of North Carolina. He has published nearly 500 papers and 3 patents and is one of the most highly cited chemists in the world.

chemically linked, bis-hydrazine monocations[12−17] and by Elliott and co-workers on chemically linked, polypyridyl Fe(II)−Fe(III) assemblies.[18]

The analogous, light-driven process, eq 2, can often be observed as a broad, solvent-dependent absorption band. For symmetrical mixed-valence complexes, these bands typically appear in low-energy visible or near-infrared spectra, for example, at 7700 cm^{-1} with $\Delta\bar{\nu}_{1/2} = 4900\ cm^{-1}$ in CH_3CN for eq 2. They are called intervalence transfer (IT), metal−metal charge transfer (MMCT), or intervalence charge transfer (IVCT) bands.[19−25]

$$cis,cis\text{-}[(bpy)_2(Cl)Ru^{II}(pz)Ru^{III}(Cl)(bpy)_2]^{3+} \xrightarrow{h\nu} cis,cis\text{-}[(bpy)_2(Cl)Ru^{III}(pz)Ru^{II}(Cl)(bpy)_2]^{3+} \quad (2)$$

Hush provided an analysis of IT band shapes based on parameters that also define the electron-transfer barrier.[19,20] The barrier arises from nuclear motions whose equilibrium displacements are affected by the difference in electron content between oxidation states. This includes both intramolecular structural changes and the solvent where there are changes in the orientations of local solvent dipoles.[26−29]

The electrostatic perturbation between the electron donor and acceptor causes their electronic wave functions to mix and opens a channel for electron tunneling. For complex **1**, the geometrical distance between the metal centers (6.9 Å) is sufficiently large that direct overlap of the electronic wave functions is negligible. Electronic coupling occurs indirectly by mixing of metal-based donor and acceptor orbitals with orbitals of appropriate symmetry in the bridge. The electronic coupling matrix element arising from donor−acceptor coupling is called H_{if}, T_{if}, H_{DA}, V, or H_{ab}, all of which are used interchangeably but which

differ somewhat depending on their theoretical formulation.[19,20,30,31]

One of the continuing themes in mixed-valence chemistry is the effect of electronic delocalization on mixed-valence properties. In metal complexes, delocalization can be varied by making changes in the metal, the bridging ligand, the ancillary ligands, or the solvent. In organic molecules, variations can be made in the solvent, the redox sites, or in the chemical link that joins them.

Electronic delocalization is promoted by mixing the electronic donor and acceptor wave functions. As mixing increases, the discrete oxidation-state character of the local sites decreases and with it structural differences and dipole orientational changes in the solvent. It also mixes the donor and acceptor orbitals along the ligand bridge or organic spacer, which has the effect of decreasing the electron-transfer distance.[32−34]

If electronic coupling is sufficient, there is a complete blending of oxidation states and the odd electron is delocalized over both sites. In this limit there is no longer a structural difference between sites and local solvent dipole orientations are averaged. The odd electron occupies a delocalized molecular orbital, and the oxidation state description for a molecule such as **1** becomes Ru(II.5)−Ru(II.5) rather than Ru(III)−Ru(II).

The goal of this review is to analyze and categorize the transition between localization and delocalization in ligand-bridged, mixed-valence molecules. Although a useful theoretical framework is available for understanding this transition, recent experimental findings suggest that it is far more complex than previously thought. The focus here will be on transition-metal complexes with important and illustrative organic examples also included. These molecules reveal the extraordinarily subtle nuances that can be displayed by real mixed-valence molecules in the localized-to-delocalized transition. They also reveal a new class of mixed-valence molecules, Class II−III, whose members have properties normally associated with both localization and delocalization and, in that sense, are literally both localized and delocalized.

II. Background Theory

The localized-to-delocalized transition has been treated theoretically by many authors including an informative semiclassical treatment by Sutin[30,35] and Hush.[19,36] Application of the variational method to a linear combination of the initial, zero-order, diabatic (noninteracting) wave functions for the electron-transfer reactants (Ψ_a for Ru(III)−Ru(II)) and products (Ψ_b for Ru(II)−Ru(III)), including the interaction between them, gives rise to two new adiabatic states of energies E_1 and E_2, eq 3. The associated wave functions, Ψ_1 and Ψ_2, are linear combinations of Ψ_a and Ψ_b.[37]

In these equations $H_{aa} = \langle\Psi_a|\hat{H}|\Psi_a\rangle$ and $H_{bb} = \langle\Psi_b|\hat{H}|\Psi_b\rangle$ are the energies of the unperturbed initial and final diabatic states. $\hat{H}$ is the effective two-state Hamiltonian operator describing the system excluding the nuclear kinetic energy operator. $H_{ab} = \langle\Psi_a|\hat{H}|\Psi_b\rangle$ is the electronic or electron-transfer coupling matrix element that arises from the mixing between states.

$$E_1 = (H_{aa} + H_{bb})/2 - \{[(H_{aa} - H_{bb})^2 + 4H_{ab}{}^2]^{1/2}\}/2 \quad (3a)$$

$$E_2 = (H_{aa} + H_{bb})/2 + \{[(H_{aa} - H_{bb})^2 + 4H_{ab}{}^2]^{1/2}\}/2 \quad (3b)$$

When a coupled nuclear motion is included as an harmonic oscillator, H_{aa} and H_{bb} vary with the coordinate for this motion as shown in eq 4. These expressions assume a symmetrical mixed-valence molecule with $\Delta G° = 0$ ($H°_{aa} = H°_{bb}$) for electron transfer as in eq 1. The coordinate is x, the displacement from the energy minimum at $x = 0$. The displacement difference between the minima before and after electron transfer is a. The corresponding energies at the minima are $H°_{aa}$ and $H°_{bb}$. Equal force constants (f) are assumed for the electron-transfer reactants and products. In general, there are many coupled vibrational and solvent modes and associated coordinates, and eqs 4a and 4b describe an average of the coupled motions assumed to be harmonic.

$$H_{aa} = H°_{aa} + fx^2/2 \quad (4a)$$

$$H_{bb} = H°_{bb} + f(x - a)^2/2 \quad (4b)$$

With the dependence of H_{aa} and H_{bb} on x included, application of the variational treatment results in the energy-coordinate curves E_1 and E_2 in eq 5. They describe how the energies of the lower (E_1) and upper (E_2) states vary with the reduced nuclear coordinate X ($= x/a$) with the zero of energy taken to be $H°_{aa} = H°_{bb}$. E_1 and E_2 are parametrized in X, H_{ab} and λ with $\lambda = fa^2/2$.

$$E_1 = [\lambda(2X^2 - 2X + 1)]/2 - \{[\lambda(2X - 1)]^2 + 4H_{ab}{}^2\}^{1/2}/2 \quad (5a)$$

$$E_2 = [\lambda(2X^2 - 2X + 1)]/2 + \{[\lambda(2X - 1)]^2 + 4H_{ab}{}^2]^{1/2}\}/2 \quad (5b)$$

There are two minima in the energy-coordinate curve described by eq 5a. They occur at $X_{min} = 0$ and $X_{min} = 1$ if $H_{ab} = 0$. Including electronic coupling, the minima in the energy curves occur at $E = -H_{ab}{}^2/\lambda$ where $X_{min} = \{1 \pm (1 - (4H_{ab}{}^2/\lambda^2))^{1/2}\}/2$ rather than at $X = 0$. The vertical difference between energy curves is $E_2 - E_1 = \{[\lambda(2X - 1)]^2 + 4H_{ab}{}^{1/2}\}^{1/2}$. The intervalence transfer maximum occurs at the minima in X with $E_{IT} = \lambda$ if $H_{ab} = 0$..

Energy-coordinate curves for three different cases are illustrated in Figure 1. If there is a barrier to electron transfer, as in 1A and 1B, X varies from the minimum at $X = \{1 - (1 - 4H_{ab}{}^2/\lambda^2))^{1/2}\}/2$ to the minimum at $X = \{1 + (1 - (4H_{ab}{}^2/\lambda^2))^{1/2}\}/2$ as the barrier is traversed.

Intervalence transfer corresponds to the vertical transition at X_{min} in Figure 1A. In the classical limit with $H_{ab} \ll \lambda$, there is a Gaussian distribution of

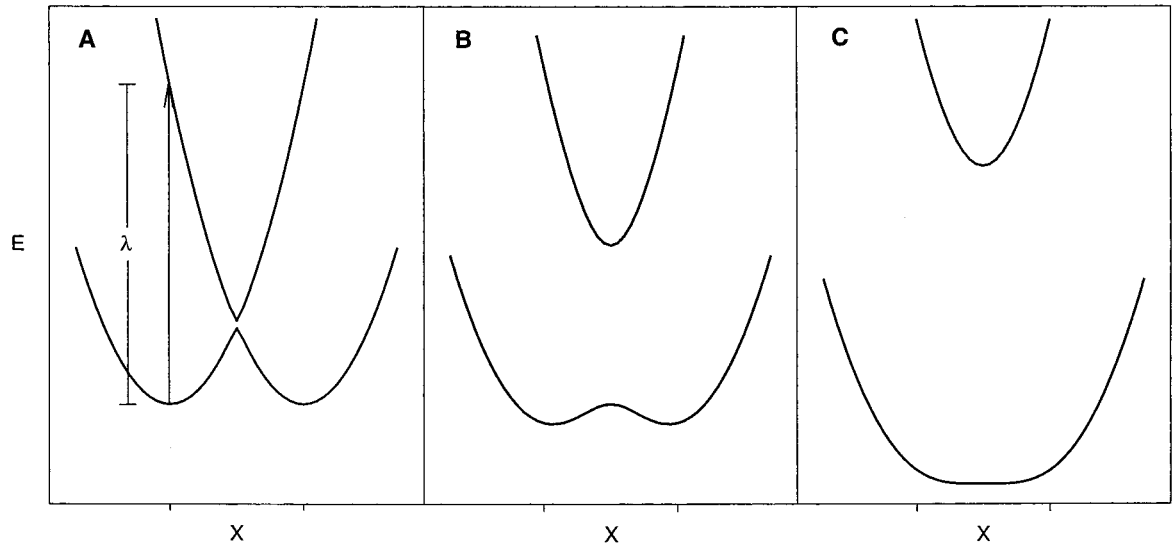

Figure 1. Energy-coordinate diagrams for E_1 and E_2 calculated by using eq 5 with $\lambda = 8000\ cm^{-1}$ and (A) $H_{ab} = 100\ cm^{-1}$, (B) $H_{ab} = 2000\ cm^{-1}$, and (C) $H_{ab} = 4000\ cm^{-1}$. The coordinate axis is the reduced coordinate X (= x/a), see text.

energies in the ground-state centered at $X = 0$, which varies with x as exp $-$ ($fx^2/2k_BT$). This results in a nearly Gaussian-shaped absorption band with a maximum at $X = 0$ and $E_{IT} = \lambda = fa^2/2$. Expressions for the band maximum, E_{IT}, and width, $\Delta\bar{\nu}_{1/2}$, in this limit are given in eqs 6 and 7, k_B is the Boltzmann constant.[19,20,38]

$$E_{IT} = \lambda \tag{6}$$

$$(\Delta\bar{\nu}_{1/2})^2 = 16k_BT\lambda \ln 2 \tag{7}$$

At the top of the barrier ($x = a/2$, $X = {}^1/_2$), $E_1 = \lambda/4 - |H_{ab}|$. The difference in energy between this point and the energy at the minimum, $E = -(H_{ab}{}^2/\lambda)$, is the classical energy of activation. It is given approximately by eq 8. The energy difference between the upper and lower energy curves at $X = {}^1/_2$ is $2H_{ab}$.[30]

$$E_a = (\lambda/4) - |H_{ab}| + (H_{ab}{}^2/\lambda) \tag{8}$$

For a Gaussian-shaped IT absorption band, H_{ab} can be calculated from characteristic band shape parameters by using eq 9 with E_{IT} and λ in cm^{-1}. In this equation ϵ is the molar extinction coefficient in M^{-1} cm^{-1} at E_{IT} and d is the electron-transfer distance in Å. More generally, H_{ab} is related to the transition moment and through it the integrated absorption band regardless of band shape, as shown in eq 10.[19,20,35,40,41]

$$H_{ab}(cm^{-1}) = [(4.2 \times 10^{-4})\epsilon\Delta\bar{\nu}_{1/2}E_{IT}]^{1/2}/d \tag{9}$$

$$H_{ab}{}^2 = [(4.2 \times 10^{-4})E_{IT}\int\epsilon(\bar{\nu})\,d\bar{\nu}]/d^2 \tag{10}$$

The electron-transfer distance d in eqs 9 or 10 can be considerably different from the center-to-center distance if there is significant electronic mixing with bridge-based orbitals and/or between redox sites across the bridge.[32,35,42,43] This distance decreases toward zero as mixing increases.[44,233] Electroabsorption (Stark effect) measurements on the IT bands of mixed-valence complexes point to charge-transfer distances that can be significantly less than center-to-center distances.[45] Results obtained by electroabsorption spectroscopy have been reviewed by Bublitz and Boxer.[46]

Because of electronic delocalization, the use of geometrical distances in eq 9 or 10 gives a *lower* limit for H_{ab}. There is an additional complication for transition-metal complexes where there is more than one IT band, section III.B. Information about delocalization in the ground state is available by analysis of the lowest energy of three IT bands, IT(1). These bands are usually overlapping, section IV and for most first- and second-row transition-metal complexes, are unresolved. The H_{ab} value obtained by the Hush analysis by assuming a single band in these cases provides an *upper* limit to ground-state electronic coupling which can differ considerably from $H_{ab}(1)$ for IT(1).

For the case in Figure 1B, H_{ab} is a sizable fraction of λ and E_a is appreciably decreased in magnitude relative to $\lambda/4$. As pointed out by Nelsen[47] and by Lambert and Nöll,[48] as E_a approaches k_BT, the population of molecules at or near the top of the electron-transfer barrier becomes significant. With $E_a = 500\ cm^{-1}$, the fraction of molecules at the top of the barrier at 298 K is ~10%.

Further motion over the barrier past $x = a/2$ results in electron transfer. From eq 5, the vertical energy difference between the upper and lower energy curves at this point ($X = {}^1/_2$) is $2H_{ab}$. This analysis predicts that the intensity of an IT band should fall to zero past this point, leading to a cutoff in the absorption band intensity on the low-energy side.

According to this analysis, the IT band shape should be Gaussian on the high-energy side, skewed on the low-energy side, and display a sharp cut off at energies past $E_2 - E_1 = 2H_{ab}$. A quantum mechanical treatment (see below) including more than one coupled vibration and solvent broadening of the individual vibronic components would "round off" the predicted abrupt decrease in band intensity at $2H_{ab}$.

An important feature that emerges from this analysis is that spectral measurements on the low-

energy tails of IT bands afford the opportunity to obtain direct spectroscopic insight into the top of the electron-transfer barrier. There is experimental evidence for skewed, asymmetrical IT bands in molecules where H_{ab} is appreciable,[4,21,23,47,48] but other origins are possible for these asymmetries, section IV.

The examples shown in Figure 1A and 1B are in Class II in the Robin and Day classification scheme.[8] In Class II there are localized valences (oxidation states) and measurable electronic coupling ($H_{ab} \neq 0$). Class I is the limiting case with $H_{ab} = 0$.

The intervalence transfer transition illustrated in Figure 1A results in intramolecular electron transfer, e.g., $Ru_a(II)-Ru_b(III) \rightarrow \{Ru_a(III)-Ru_b(II)\}$, with the electron-transfer product, $\{Ru_a(III)-Ru_b(II)\}$, formed in excited levels of the solvent and vibrational modes coupled to the transition. Subsequent relaxation occurs to the intersection region at $X = {}^1/_2$, where further relaxation or intramolecular electron transfer give a distribution of $Ru_a(II)-Ru_b(III)$ and $Ru_a(III)-Ru_b(II)$.

Class III is illustrated in Figure 1C. It occurs when $2H_{ab}/\lambda \geq 1$. In Class III there is no longer a barrier to electron transfer. The odd electron is delocalized, and the electronic wave functions are no longer time dependent.

In Class III the interpretation of the spectroscopic parameters changes. The absorption band arises from a transition between delocalized electronic levels and not from intramolecular charge transfer.[23,35,50,51] The electronic wave functions for the delocalized levels are constructed from symmetric ($\Psi_a + \Psi_b$) and antisymmetric ($\Psi_a - \Psi_b$) combinations of the initial unperturbed electronic wave functions. The modes that dominate vibrational coupling to the electronic transition between states are largely symmetrical vibrations coupled to both sites.[51,52] Solvent coupling (and λ_o) is far less than for intervalence transfer since there is no net charge transfer in the transition.

In $d\pi^5-d\pi^6$ transition-metal complexes, the initial and final wave functions are largely $d\pi$ in character but these wave functions are mixed with bridge-based π and π^* orbitals, which promote electronic coupling. In Class III, the low-energy bands that appear in the near-IR originate from $\pi(d\pi) \rightarrow \pi^*(d\pi)$ transitions that are localized on the metal−ligand−metal core and not from intervalence transfer. These mixed-valence transitions are analogous to organic $\pi \rightarrow \pi^*$ transitions with solvent effects dominated by electronic dispersion interactions with the solvent.[33,53,54,55]

The localized-to-delocalized transition has also been treated quantum mechanically by Piepho, Krausz, and Schatz (PKS).[50,52,56,57,58] With significant electronic coupling, the usual Born−Oppenheimer separation of the electronic and nuclear motions is no longer valid. PKS define electronic wave functions that are independent of the nuclear coordinates and solve the Schrödinger equation with the nuclear kinetic energy operator included. This gives vibronic energy levels and wave functions that depend on both nuclear and electronic coordinates. The wave functions are expanded in the complete orthonormal set of harmonic oscillator wave functions to give a general solution for the final mixed-coordinate wave functions.

Many of the key features of the PKS model had antecedents in the work of Fulton and Gouterman[59] and of Rice and co-workers, who applied linear response theory to electron−phonon coupling in solids.[60,61,62] The initial PKS theory included a single coupled vibrational mode, an antisymmetric combination of local modes at the donor and acceptor.[63] It was subsequently extended to include symmetric modes and more than one coupled vibration.[52,64−71]

The results of these analyses have been summarized by Reimers and Hush.[51] They note that equivalent results are obtained by starting with either localized or delocalized basis sets, if infinite basis sets are used. The localized approach is easier to implement for weak electronic coupling and the delocalized approach for strong electronic coupling, as expected. In the localized limit, both symmetric and antisymmetric modes can contribute to the energy levels and electron-transfer barrier with the latter dominating. In the delocalized limit, symmetric modes dominate.

The quantum mechanical approach provides a systematic basis for describing the localized to delocalized transition. Although somewhat complex mathematically and difficult to implement for multiple coupled vibrations, the resulting energy levels and wave functions provide a complete description of electron−vibrational coupling in mixed-valence molecules from the localized to delocalized limits.

These theories capture the essence of the localized-to-delocalized transition and describe in quantitative detail the coupling between electronic and nuclear motions that is required to traverse the electron-transfer barrier. However, recent experimental findings with transition-metal complexes reveal that the approximations often made in these theories are too limiting. They are complex molecules with multiorbital through-bridge interactions. In general, there can be many vibrations coupled to electron transfer as well as the solvent and they have different time scales. Even within the set of coupled vibrations, there are differences in how the individual modes couple to electron transfer and electronic delocalization.

III. Defining Class II–III

A. The Creutz–Taube Ion

The first designed mixed-valence complex has proven to be the most difficult to understand. A low-energy absorption band for **1** appears in the near-IR at 1560 nm (6410 cm^{-1}) in D_2O. It is narrow ($\Delta\bar{\nu}_{1/2} =$ 1480 cm^{-1}), solvent independent, and skewed with a half-bandwidth on the low-energy side narrower than on the high-enegy side.[4,5,72] Electroabsorption (Stark effect) measurements in 1:1 glycerol−water at 77 K reveal that the change in permanent electric dipole moment between the initial and final states for this transition is only 0.7 ± 0.1 D.[73] For unit electron transfer across the 6.9 Å pyrazine bridge, the calculated value is 32.7 D. On the basis of EPR data, the odd electron in **1** occupies an orbital that lies along

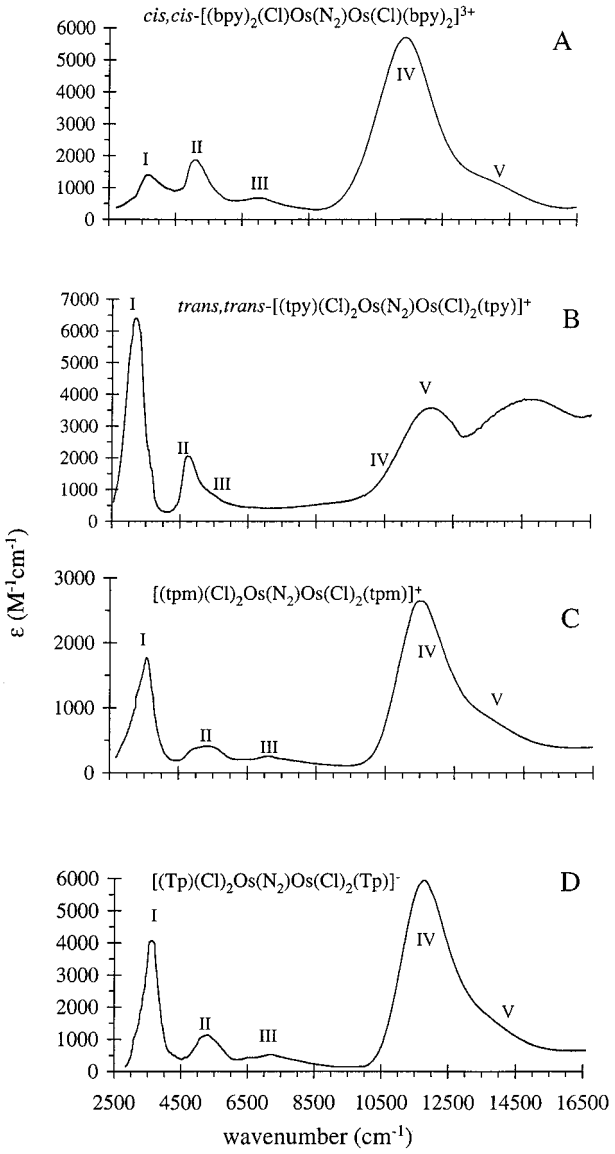

Figure 2. IR−near-IR spectra in CD_3CN. Band assignments are discussed in the text.

the Ru−pz−Ru axis.[74,75] Vibrations at 1451 cm^{-1} (ν_{19a}(pz)), 1319 cm^{-1} (δ_{HNH}), 800 cm^{-1} (ρ_{NH3}), and 449 cm^{-1} (ν_{Ru-NH_3}) are averaged compared to bands in the Ru(II)−Ru(II) and Ru(III)−Ru(III) forms.[75,76] The electronic structure of **1** has been the subject of a number of theoretical analyses which begin by assuming that the odd electron is delocalized,[66−70,77−82] including the results of a recent density functional theory (DFT) calculation.[83]

A consensus appears to have been reached that **1** is delocalized, but there is evidence for localization. In the X-ray crystal structure of the tosylate salt at 100 K, the two Ru sites have slightly different coordination geometries.[84] Three symmetrical pyrazine ring stretching vibrations appear in both the IR and Raman spectra,[85,86] which is inconsistent with a center of symmetry on the time scale of infrared absorption, section III.C.[87] Resonance Raman excitation on the high-energy side of the near-IR band in CD_3NO_2 results in resonance enhancement of the symmetric pyrazine modes, but asymmetric pyrazine modes at 1078, 1316, and 1412 cm^{-1} are enhanced to a comparable degree.[86] The most strongly coupled vibrations are Ru−N stretches at 324 and 262 cm^{-1}.

Two sets of Ru 3p ionization energies are observed in X-ray photoelectron spectra (XPS) of salts of **1**. This was initially taken as evidence for localization,[88] but as Hush pointed out, the same result could occur if **1** were delocalized.[89] Under the influence of the core hole produced by the ionization process, a delocalized orbital would relax strongly resulting in localization.[89,90] There are related delocalized examples in which only a single set of XPS binding energies are observed.[91−93] Energy minimization calculations based on INDO/1, including all of the bonding and antibonding pyrazine orbitals, predict an unsymmetrical structure. The Ru sites were predicted to differ by 0.2 of a unit Mulliken charge.[78]

The Creutz−Taube ion is commonly assumed to be "delocalized" but appears to have properties of both Class II and Class III. As discussed in section IV.A, its spectroscopic properties can be interpreted by assuming some residual localization. In fact, it may be the founding member of a new class of mixed-valence molecules, Class II−III.

B. Ligand-Bridged Os Complexes

The insight leading to the conclusion that a new class of mixed-valence molecules, Class II−III, must exist comes from experimental measurements on mixed-valence Os complexes. The X-ray structure of the BF_4^- salt of *trans,trans*-$[(tpy)(Cl)_2Os(N_2)Os(Cl)_2(tpy)]^+$ reveals that the μ-N_2-bridged Os sites are structurally inequivalent and that the BF_4^- counterion is located unsymmetrically in the lattice. It is one of a series of related μ-N_2 complexes. Other members are $[(tpm)(Cl)_2Os(N_2)Os(Cl)_2(tpm)]^+$ (**2**, tpm = tris(1-pyrazolyl)methane), $[(Tp)(Cl)_2Os(N_2)Os(Cl)_2(Tp)]^-$ (Tp = hydridotris(1-pyrazolyl)borate), and *cis,cis*-$[(bpy)_2(Cl)Os(N_2)Os(Cl)(bpy)_2]^{3+}$.[94,95] The IR−near-IR spectra of these complexes are shown in Figure 2.

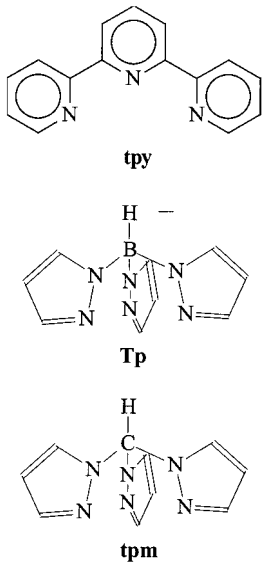

Intense $\nu(N_2)$ stretches appear for these complexes, at 2007 cm^{-1} in KBr for the tpy complex and at 2029 cm^{-1} for **2**. The molar extinction coefficients for these bands in CD_3CN are 1220 and 320 M^{-1} cm^{-1}. The

appearance of $\nu(N_2)$ is consistent with an electronic asymmetry on the time scale for IR absorption. In the IR spectra of $[(NH_3)_5Os(N_2)Os(NH_3)_5]^{5+}$ [96] and $[(CH_3CN)(NH_3)_4Os(N_2)Os(NH_3)_4(CH_3CN)]^{5+}$,[97,98] which are delocalized, $\nu(N_2)$ does not appear or is weak.[99]

These observations provide direct evidence for localization, but as shown by the appearance of the five-band pattern in the IR−near-IR spectrum in Figure 2B, **2** is an electronically complex molecule. Bands I and II in Figure 2B provide an oxidation-state marker for Os(III). Because of the effects of low symmetry, extensive metal−ligand overlap, and spin−orbit coupling (the spin−orbit coupling constant for Os(III) is $\xi \sim 3000$ cm^{-1}),[100] the dπ^5 Os(III) core is split into three Kramer's doublets (E_1', E_2', E_3') separated by thousands of cm^{-1}.[101−106] The orbital configurations of the doublet states, in order of increasing energy, are $d\pi_1^2 d\pi_2^2 d\pi_3^1 < d\pi_1^2 d\pi_2^1 d\pi_3^2 < d\pi_1^1 d\pi_2^2 d\pi_3^2$.

Bands I and II can be assigned to transitions between the Kramer's doublets. They are called d$\pi \rightarrow$ dπ or interconfigurational (IC) transitions. They are nominally parity or LaPorte forbidden but gain intensity through spin−orbit coupling and metal−ligand mixing. They also appear in related, nonbridged Os(III) polypyridyl complexes in the near-IR (at ~4000 and 6000 cm^{-1}) as narrow ($\Delta\bar{\nu}_{1/2} < 1000$ cm^{-1}), relatively weak bands ($\epsilon \leq 300$ M^{-1} cm^{-1}).[94,99,104]

The IC bands in the μ-N_2 complexes are red-shifted and of enhanced intensity compared to related nonbridged complexes. For **2** in DMSO, they appear at 3460 cm^{-1} ($\epsilon = 1500$ M^{-1} cm^{-1}, $\Delta\bar{\nu}_{1/2} = 770$ cm^{-1}) and 5200 cm^{-1} ($\epsilon = 230$ M^{-1} cm^{-1}, $\Delta\bar{\nu}_{1/2} = 1100$ cm^{-1}). The enhanced intensity comes from electronic delocalization across the bridge which has the effect of mixing Os(II) character into Os(III). This decreases the energy splittings between the Kramer's doublets and enhances the oscillator strength by mixing charge-transfer character into these nominally d$\pi \rightarrow$ dπ transitions.[107]

The remaining three bands in Figure 2B, III, IV, and V, can be assigned to IT transitions. As illustrated in the energy-level diagram in Scheme 1

Scheme 1

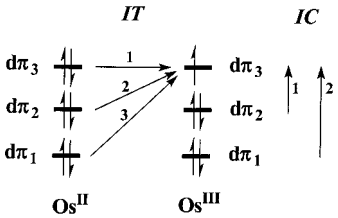

with the horizontal axis the $Os^{II}\cdots Os^{III}$ separation distance, they arise from separate electronic excitations across the bridge from the three dπ orbitals at Os(II) to the hole at Os(III). These bands are also narrow but slightly broader than the IC bands, which helps to distinguish them in making band assignments. For **2** in DMSO, they appear at 7000 cm^{-1} ($\epsilon = 100$ M^{-1} cm^{-1}, $\Delta\bar{\nu}_{1/2} = 1200$ cm^{-1}), 11 400 cm^{-1} ($\epsilon = 2100$ M^{-1} cm^{-1}, $\Delta\bar{\nu}_{1/2} = 1300$ cm^{-1}), and 12 800 cm^{-1} ($\epsilon = 750$ M^{-1} cm^{-1}, $\Delta\bar{\nu}_{1/2} = 2200$ cm^{-1}).[94]

Given these observations, any bonding scheme must include the fact that all three donor orbitals at Os(II) are mixed with the hole at Os(III). This requires low symmetry and spin−orbit coupling at Os(III) to mix the Cartesian character of the d_{xy}, d_{xz}, d_{yz} orbitals. It also requires the use of multiple π and π^* orbitals on the ligand bridge.[78] Any bonding model that assumes a single set of interactions is bound to fail. There are three orbital interactions, and all play a role in defining mixed-valence properties.

This is true for all transition-metal complexes where there are multiple orbital interactions across the bridge. Distinguishable IC bands are usually not observed for complexes in the first or second transition series unless there is a large electronic asymmetry in the ligand field. Spin−orbit coupling is lower for Ru(III) ($\xi \sim 1000$ cm^{-1}) and Fe(III) ($\xi \sim 400-500$ cm^{-1}), which has the effect of shifting the IC bands into the IR and greatly decreasing their absorptivity.[108,109] It also decreases the energy differences between the separate IT bands, which leads to broad overlapping spectra in the near-IR.

There are three IT transitions for **2**, the one at lowest energy being IT(1). In the two transitions at higher energy, IT(2) and IT(3), intramolecular electron transfer is accompanied by formation of IC excited states at Os(III), the upper two Kramer's doublets, having the electronic configurations $d\pi_1^2 d\pi_2^1 d\pi_3^2$ and $d\pi_1^1 d\pi_2^2 d\pi_3^2$.

Comparison of relative band intensities reveals that the extent of electronic coupling between Os(II) and Os(III) is different for the three IC states with $H_{ab}(1) \geq 118$ cm^{-1} for dπ_3(Os^{II}) coupling with dπ_3(Os^{III}), $H_{ab}(2) \geq 723$ cm^{-1} for dπ_2(Os^{II}) coupling, and $H_{ab}(3) \geq 595$ cm^{-1} for dπ_1(Os^{II}) coupling all in DMSO. The H_{ab} values are only lower limits since they were calculated by using eq 9 and the geometrical distance of 5.0 Å, section II.

In general, vibronic coupling and λ_i are also different for the three transitions because of symmetry differences between the dπ(Os(III)) orbitals. Assuming the classical limit and a constant λ, the energies of the IC and IT bands are related as shown in eqs 11 and 12.[104,110]

$$E_{IT}(1) = \lambda \tag{11}$$

$$E_{IT}(2) = \Delta G_1^\circ + \lambda \approx E_{IC}(1) + \lambda \tag{12a}$$

$$E_{IT}(3) = \Delta G_2^\circ + \lambda \approx E_{IC}(2) + \lambda \tag{12b}$$

For IT(2), $\Delta G^\circ(1) \sim E_{IC}(1) = 3460$ cm^{-1} and $\lambda = 7960$ cm^{-1}. For $E_{IT}(3)$, $\Delta G^\circ(2) \sim E_{IC}(3) = 5200$ cm^{-1} and $\lambda = 7600$ cm^{-1}.[110] The results of this analysis suggest that λ is reasonably constant for the three transitions since $E_{IT}(1) = \lambda = 7000$ cm^{-1}.

The two IC and three IT transitions for **2** are further illustrated in the energy-coordinate diagram in Figure 3. It was constructed by using eq 5, $\lambda = 7000$ cm^{-1}, and the H_{ab} values cited above. The energy-coordinate curves for the IC excited states, IC(1) and IC(2), were constructed by using eq 5 and offsetting the curves by $E_{IC}(1) = 3460$ cm^{-1} and $E_{IC}(2) = 5200$ cm^{-1}. This diagram shows that the higher energy transitions IT(2) and IT(3) correlate with

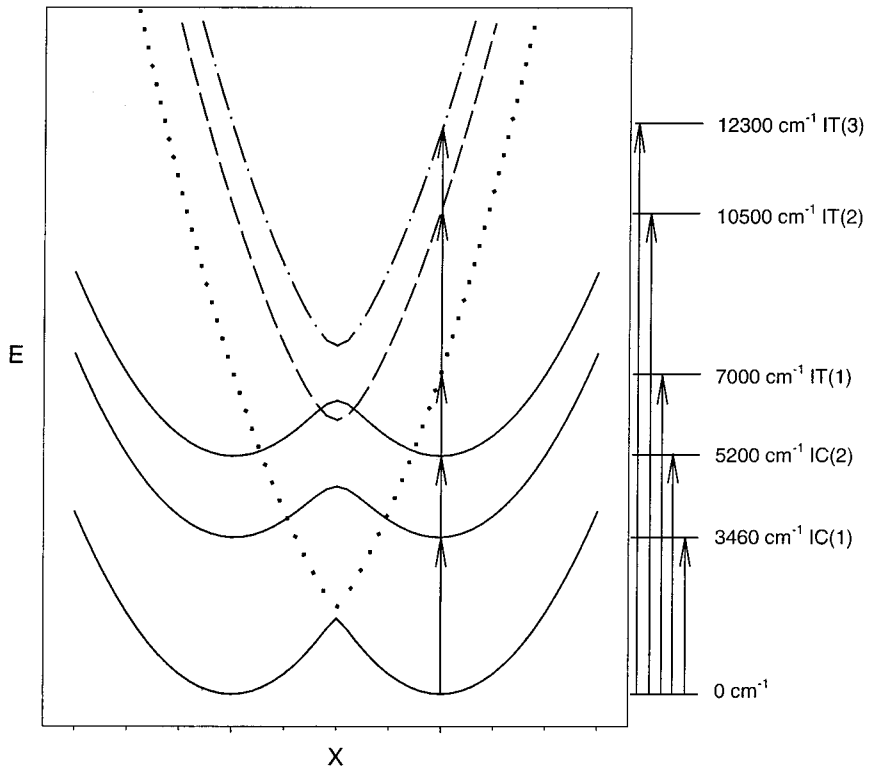

Figure 3. Schematic energy-coordinate diagram illustrating the three IT and two IC transitions for $[(tpm)(Cl)_2Os(N_2)Os(Cl)_2(tpm)]^+$. Calculated by using eq 5 with $\lambda = 7000$ cm^{-1} and $H_{ab}(1) = 118$ cm^{-1}. The upper two sets of curves were calculated similarly by using eq 5 and offsetting by $E_{IC}(1) = 3460$ cm^{-1} and $E_{IC}(2) = 5200$ cm^{-1} with $H_{ab}(2) = 723$ cm^{-1} and $H_{ab}(3) = 595$ cm^{-1}.

mixed-valence forms in which Os(III) is in the upper two Kramer's doublets, the IC excited states.

Localization vs delocalization is determined by the relative magnitudes of $H_{ab}(1)$ and $\lambda(1)$, section II, *which are characteristics of the mixed-valence ground state*. The extent to which λ is decreased relative to λ for a hypothetical analogue in which there is no electronic coupling depends on total orbital overlap and the extent of electronic coupling across the bridge. The magnitude of $H_{ab}(1)$ depends only on the extent of $d\pi_3-d\pi_3$ coupling between Os(II) and Os(III).

For mixed-valence dimer **2**, $\lambda(1) = 7000$ cm^{-1}, $2H_{ab}(1)/\lambda(1) \geq 0.033$, and this molecule is localized in the ground state. There is greater Os(II) electronic coupling with Os(III) in the mixed-valence IC excited states with $2H_{ab}(2)/\lambda(2) \geq 0.18$ and $2H_{ab}(3)/\lambda(3) \geq 0.16$, but they are also localized.

Thermal electron transfer is dominated by the $d\pi_3$(Os(II)) → $d\pi_3$(Os(III)) orbital pathway. Electron transfer from either $d\pi_2$(Os(II)) or $d\pi_1$(Os(II)) to $d\pi_3$(Os(III)) results in the formation of IC excited states at Os(III) in the electron-transfer product. $\Delta G°$ is uphill for these pathways by ~3460 and ~5200 cm^{-1} but is 0 for $d\pi_3$ → $d\pi_3$ electron transfer.

The evidence for localization in **2** is clear, but the IT bands are unusually narrow. The bandwidth calculated for IT(I) by using eq 7 is 4000 cm^{-1} compared to the experimental value of 1120 cm^{-1}. The IT bands are also nearly solvent independent.[94]

There is an explanation for this phenomenon based on relative time scales. Solvent coupling to electron transfer is dominated by reorientation of the local solvent dipoles. If electron transfer is rapid on the 0.2−10 ps time scale for these motions in typical polar organic solvents, section III.D, they can no longer contribute to the electron-transfer barrier. They would be too slow to keep up with the motion of the transferring electron. Dipole orientations in the surrounding solvent molecules would be found in averaged orientations as if the charge distribution were Os(II.5)−Os(II.5). A barrier to electron transfer would still exist arising from intramolecular structural changes at the Os(II) and Os(III) sites. In transition-metal complexes, the structural changes occur largely in low-frequency metal−ligand stetching vibrations and the transferring electron is localized on the time scale for these motions ($10^{-13}-10^{-14}$ s), section III.C.

Solvent averaging would explain narrow IT bandwidths, the absence of a significant solvent dependence for E_{IT}, and the appearance of IT bands at low energies since the solvent is no longer strongly coupled to electron transfer. In the absence of any solvent barrier, $\lambda_o \sim 0$ and $E_{IT}(1) = \lambda_i$. The solvent dependence that remains would be slight compared to solvent-coupled intervalence transfer and arises from electronic dispersion interactions as in mixed-valence transitions in delocalized mixed-valence complexes or typical $\pi - \pi^*$ transitions in organic molecules.

With solvent averaging, complex **2** is *both localized in oxidation states and averaged in solvent*. These are the characteristic features that define Class II−III: electronic localization, solvent averaging, and a residual barrier to electron-transfer arising from intramolecular structural changes.

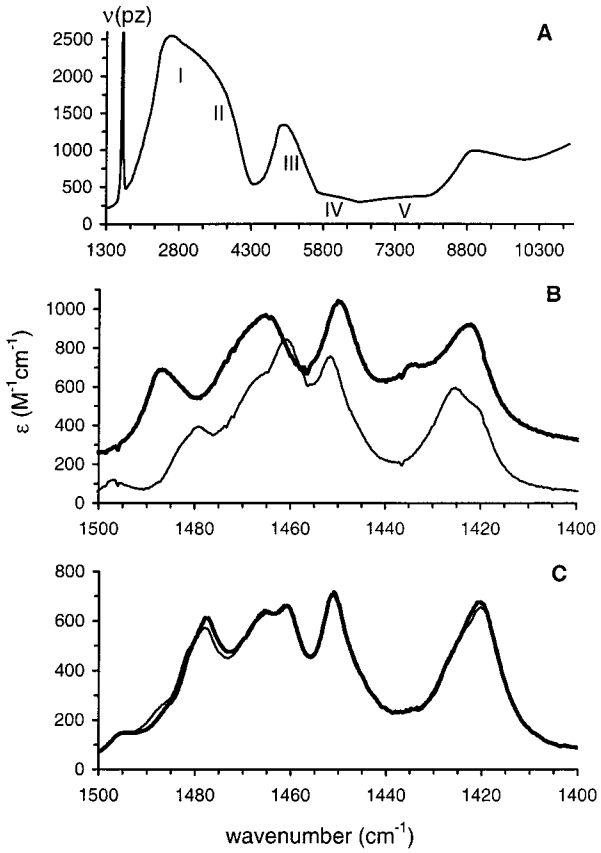

Figure 4. Near-IR−IR spectrum of *cis,cis*-$[(bpy)_2(Cl)Os(pz)Os(Cl)(bpy)_2]^{3+}$ including ν_{8a}(pz) (A) and IR spectra in the ν(bpy) region in CD_3CN of (B) *cis,cis*-$[(bpy)_2(Cl)Os-(pz)Os(Cl)(bpy)_2]^{3+}$ (thick line, −**)** and, for comparison, the average of the Os(II)−Os(II) and Os(III)−Os(III) spectra (thin line, —), and (C) the same but for *cis,cis*-$[(bpy)_2(Cl)-Os(4,4'\text{-bpy})Os(Cl)(bpy)_2]^{3+}$.

The IR−near-IR spectrum of *cis,cis*-$[(bpy)_2(Cl)Os-(pz)Os(Cl)(bpy)_2]^{3+}$ (**3**) is shown in Figure 4A.[111,112] The characteristic five-band pattern appears along with ν_{8a}(pz) at 1599 cm^{-1}. The absorption bands are also narrow and nearly solvent independent, but there is a significant difference in the pattern of band intensities compared to **2** pointing to a different electronic orbital coupling scheme.

The IC bands at 3590 and 4960 cm^{-1} provide oxidation markers for Os(III). The lowest energy band in this case, at 2620 cm^{-1} (ϵ = 2300 M^{-1} cm^{-1}), is IT(1). It is narrow ($\Delta\bar{\nu}_{1/2}$ = 1150 cm^{-1}) and solvent independent. IT(2) and IT(3) appear at 6000 and 7500 cm^{-1}. H_{ab} values for the three orbital interactions are comparable with $H_{ab}(1) \geq 247$ cm^{-1}, $H_{ab}(2) \geq 163$ cm^{-1}, and $H_{ab}(3) \geq 203$ cm^{-1}. On the basis of these values, $2H_{ab}(1)/\lambda \geq 0.19$. Mixed-valence dimer **3** is closer than **2** to being delocalized in the ground state.

The intensity of ν(pz) is unusually high for an infrared band with ϵ = 2600 M^{-1} cm^{-1} (CD_3CN) compared to 800 M^{-1} cm^{-1} for *cis*-$[Os^{II}(bpy)_2(pz)Cl]^+$. It has been suggested that this may be indicative of enhanced electronic coupling in the $v = 1$ excited vibrational level, which imparts charge-transfer character to this nominally symmetric ring-stretching mode.[111,112]

Complex **3** is also a member of Class II−III. There is evidence for electronic localization in the appearance of ν(pz) and the IC oxidation state marker bands for Os(III). There is also evidence for solvent averaging in the narrow bandwidths and the solvent independence of the IT bands.

There is additional information about Class II−III from the mid-IR spectrum of **3** in Figure 4B.[111,112] The bands in this region arise from ν(bpy) ring-stretching vibrations which undergo slight shifts (5−7 cm^{-1}) between Os(II) and Os(III). The spectrum of *cis,cis*-$[(bpy)_2(Cl)Os(4,4'\text{-bpy})Os(Cl)(bpy)_2]^{3+}$ (4,4′-bpy is 4,4′-bipyridine) is shown in Figure 4C. Electronic coupling across the longer 4,4′-bipyridine bridge is relatively weak, and the spectrum is the sum of the spectra for Os(II) ($^1/_2$Os(II)−Os(II)) and Os(III) ($^1/_2$Os(III)−Os(III)). This is not the case for **3** (Figure 4B). Bands appear in this spectrum at 1316, 1423, 1450 1465, and 1487 cm^{-1} which are the averages of bands in the Os(II)−Os(II) and Os(III)−Os(III) spectra.

Both IR band averaging and the appearance or absence of symmetrical bridging-ligand vibrations have commonly been used as markers for electronic delocalization, section IV.B.2.[21,23] However, from the spectra of **1** and **3** it is clear that different vibrations can give different answers. The most important marker band for **3** is the pyrazine stretch, ν_{8a} at 1599 cm^{-1}.[113] This band is weak or not observed in the spectrum of $[(NH_3)_5Os(pz)Os(NH_3)_5]^{5+}$, which is electronically delocalized.[114]

The absorption of IR radiation occurs roughly on the time scale of a vibrational period (= $1/\nu$), which, for ν_{8a}(pz) at 1599 cm^{-1}, is ~20 fs (2×10^{-14} s). In order for a symmetric mode such as ν_{8a}(pz) to be IR active requires that there be a local electronic asymmetry on this time scale. With the appearance of ν_{8a}(pz) in the spectrum, the vibrational period sets an approximate upper limit on the rate constant for electron transfer in **1** or **3** of $k_{ET} \leq 5 \times 10^{13}$ s^{-1}. Its absence sets a lower limit for the Os analogue of **1** of $k_{ET} \geq 5 \times 10^{13}$ s^{-1}.

IR line broadening and coalescence occur if there is chemical site exchange during the lifetime of the vibrational excited state. In mixed-valence complexes, site exchange occurs by electron transfer. The onset of coalescence depends on the electron-transfer rate constant, the IR band shape, and the difference in band energies at the exchanging sites.[115] The time scale for coalescence of the bpy vibrations is probably ~0.1 ps (10^{-11} s), see below. This allows k_{ET} to be bracketed in the range 1×10^{11} $s^{-1} < k_{ET} < 5 \times 10^{13}$ s^{-1} for **3** in CD_3CN at room temperature.

The ν(pz) and ν(bpy) modes act as "spectator" vibrations for electron transfer. The differences in equilibrium displacement for these modes between oxidation states is small. They are only weakly coupled to electron transfer and make an insignificant contribution to the electron-transfer barrier, but they provide useful oxidation-state and electron-transfer markers.

A quantitative measure of the extent that a vibration is coupled to electron transfer is given by the electron−vibrational coupling constant, S. For a coupled mode j, S_j is related to the reduced mass, M_j, the quantum spacing ($\hbar\omega_j = h\nu_j$), the change in equilibrium displacement, $\Delta Q_{e,j}$, and its contribution

to the intramolecular reorganizational barrier λ_i, as shown in eq 13. This definition neglects changes in frequency between oxidation states, but they are usually small enough to be ignored.

$$S_j = \frac{1}{2}(M_j\omega_j/\hbar)(\Delta Q_{e,j})^2 = \lambda_i/\hbar\omega_j \qquad (13)$$

There are no direct experimental measurements of S_j for the ν(bpy) or ν(pz) spectator vibrations in **3**. For the ν_{8a}(pz) mode in **1**, $S = 0.005$ as derived from an analysis of excitation-dependent resonance Raman band intensities.[86] This is too small to contribute significantly to the electron-transfer barrier. For electron transfer from initial vibrational level $v = 0$ to final level $v' = 0$, the contribution to the barrier is $\exp - S = 0.99$, section VI.A.

Infrared line broadening and coalescence arising from dynamic coupling to electron transfer have been observed experimentally. The first report was by Cannon and co-workers for Fe(III)Fe(III)Fe(II) → Fe(III)Fe(II)Fe(III) intracluster electron transfer in the triangular, μ-oxo cluster $\{[Fe(III)_2Fe(II)(\mu_3\text{-}O)(\mu\text{-}OOCCMe_3)_6(C_6D_5N)_3\}$ in the solid state.[116] A broadening of the two components of the $\nu_{as}(Fe_3O)$, in-plane vibration of the central oxygen atom was observed as the temperature was raised from 80 to 410 K. The data were treated by assuming the slow exchange limit by using eq 14. In eq 14, τ is the electron-transfer lifetime ($= 1/k_{ET}$), $\nu_{1/2}$ is the experimental half-width at half-maximum, and $\nu_{o,1/2}$ is the width in the absence of exchange. Analysis of the solid-state data gave $k_{ET} \sim 5 \times 10^{11}$ s^{-1} at 300 K.

$$\tau^{-1} = 2\pi(\nu_{1/2} - \nu_{o,1/2}) \qquad (14)$$

Itoh, Kubiak, and co-workers observed ν(CO) broadening and coalescence in the structurally related, pyrazine-bridged, mixed-valence Ru clusters $\{[Ru_3(\mu_3\text{-}O)(\mu\text{-}O_2CCH_3)_6(CO)(L)]_2(\mu\text{-pz})\}^-$ (L = 4-dimethylpyridine, pyridine, 4-cyanopyridine) in CH_2Cl_2 at room temperature.[117,118]

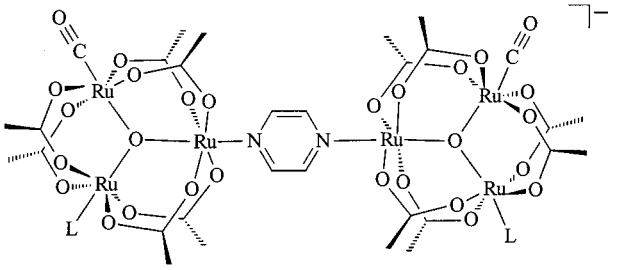

There is a difference of nearly 50 cm^{-1} in ν(CO) between the neutral and dianionic bridged clusters. Broadening and coalescence were observed, and the extent to which they occurred was found to depend on L and the extent of electronic coupling across the bridge. An analysis of the ν(CO) band shapes based on a line shape analysis by Grevels et al.[115] gave $k_{ET} = 9 \times 10^{11}$ s^{-1} (L = 4-(dimethylamino)pyridine), $k_{ET} = 5 \times 10^{11}$ s^{-1} (L = pyridine), and $k_{ET} = 1 \times 10^{11}$ s^{-1} (L = 4-cyanopyridine) in CH_2Cl_2 at room temperature.

H_{ab} values, calculated by integrating IT bands in the near-infrared at 12 100, 11 800, and 10 800 cm^{-1} were 2180, 2060, and 1310 cm^{-1}. The IT bands are broad, showing that the solvent is still coupled to electron transfer but $\Delta\bar{\nu}_{1/2}$ decreases from 5220 cm^{-1} for L = 4-cyanopyridine to 3920 cm^{-1} for L = pyridine to 3760 cm^{-1} for L = 4-(dimethylamino)pyridine. This suggests that the solvent may be partly averaged for the latter two, section V.A.

There is a time scale difference for broadening and coalescence of ν(CO) in the ligand-bridged clusters and for the ν(bpy) modes in **3**. The shifts in the ν(bpy) bands between oxidation states are only 5−7 cm^{-1} compared to 50 cm^{-1} for ν(CO), and coalescence must occur on a correspondingly slower time scale, ~10^{10}−10^{11} s^{-1}.

Other mixed-valence molecules fall in Class II but lie close to the transition to Class II−III, section V.A. The bridging ligand in $\{[(bpy)ClRu]_2(\mu_3\text{-tppz})\}^{3+}$ (tppz is tetra-2-pyridylpyrazine) is an analogue of pyrazine but occupies three coplanar coordination sites at each metal. An intense, narrow, asymmetric band appears at 6070 cm^{-1} in CD_3CN analogous to the near-IR band for **1**.[119] In the mid-IR, bands arising from ν(bpy) ring-stretching modes appear at 1428, 1459, and 1469 cm^{-1} compared to bands at 1423, 1454, and 1465 cm^{-1} for the Ru(II)−Ru(II) form. The appearance of three bands rather than six, expected for vibrational localization, is consistent with vibrational averaging, and yet a symmetric ring-stretching mode appears at 1598 cm^{-1} consistent with electronic localization.

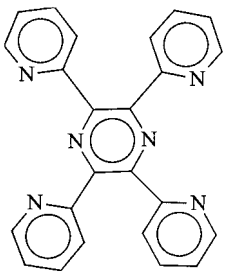

tppz

Also pointing to localization is the appearance of a band for IT(1) in the IR at 3500 cm^{-1} in CD_3CN which is broad ($\Delta\bar{\nu}_{1/2} = 1500$ cm^{-1}) and solvent dependent. From the properties of this band, $2H_{ab}(1)/\lambda \geq 0.05$, which is consistent with localization in the mixed-valence ground state.

These results show that vibrational averaging can occur even for Class II molecules for which the solvent is localized. A second example is the singly reduced form of the fulvalene-bridged carborane, $\{[(fulvalenediyl)Co]_2(Et_2C_2B_4H_4)_2\}^-$, which is a Co(III)−Co(II), d^6−d^7 (spin-paired), mixed-valence case.[120] In its IR spectrum in CH_3CN, an averaged ν(B−H) band appears for the anion at 2515 cm^{-1}. However, an IT band appears at 6300 cm^{-1} ($\epsilon = 2000$−3000 M^{-1} cm^{-1}) which is broad ($\Delta\bar{\nu}_{1/2} = 3600$ cm^{-1}) and solvent dependent.

The bandwidth points to electronic localization even though electronic coupling is significant with $H_{ab} \geq 1200$ cm^{-1} and $2H_{ab}/\lambda \geq 0.38$. The effects of

electronic coupling may also appear in the band shape, which is skewed with a narrow half bandwidth on the low-energy side, however, note section IV.

A related observation has been made by Lambert and Nöll in a study of the monocations of a series of chemically linked triarylamines.[48] For the ring−ring linked structures illustrated below, intense IT bands appear at 6360 cm^{-1} (ϵ = 28 040 M^{-1} cm^{-1}, $\Delta\bar{\nu}_{1/2}$ = 3170 cm^{-1}) for the cation of **I** and at 9530 cm^{-1} (ϵ = 22 680 M^{-1} cm^{-1}, $\Delta\bar{\nu}_{1/2}$ = 3640 cm^{-1}) for the cation of **II** in CH_2Cl_2. The IT bands are broad, solvent dependent, and skewed to low energy with the ratio of bandwidths on the high-energy side to the low-energy side of 1.45 for **I** and 1.76 for **II**. Even though there is very strong electronic coupling, the barrier to electron transfer is large and the bandwidths point to localization.

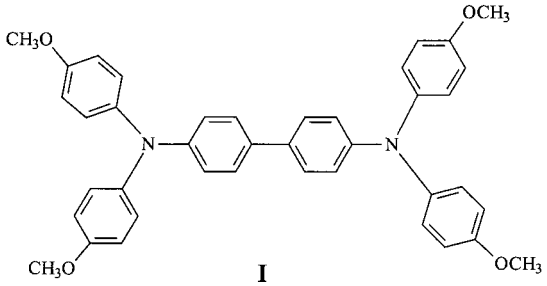

I

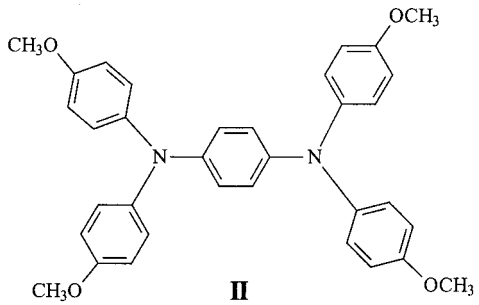

II

C. Time Scales

The features that define Class II−III and distinguish it from Classes II and III lie in the dynamical characteristics of the molecules and not the experimental time scale of the probe used to measure them. Typical time scales are $1-10^{-5}$ s for ^{1}H NMR, $10^{-5}-10^{-9}$ s for EPR, and $<10^{-11}$ s for IR. If intramolecular electron transfer is sufficiently rapid on these time scales, only averaged signals will be observed in any case.

None of these time scales, including the appearance of infrared line broadening and coalescence, is sufficient to rule out electronic localization. As described above, there are experimental examples of infrared averaging for Class II and Class II−III molecules.

The most reliable marker in the IR is the appearance or absence of symmetrical bridging-ligand stretches such as $\nu(N_2)$ or ν(pz), although even this marker must be used with care.[99] If these bands appear and are of reasonable intensity, it can be inferred that electron transfer is slow on the time scale of a vibrational period, 15−20 fs for $\nu(N_2)$ and ν(pz). In the solid state, the 10^{-17} s time scale of X-ray photoelectron spectroscopy (XPS) provides a means for distinguishing between Classes III and II or II−III, although, as noted above, there can be complications in interpreting the data.[89,90]

The appearance of IT bands provides the most systematic marker for localization and Class II (broad, solvent-dependent IT band or bands) or Class II−III (narrow, solvent-independent band or bands) behavior. The time scale for these transitions is 3×10^{-14} s or less. However, care must be taken in assigning low-energy absorption bands to IT transitions. They can also arise from mixed-valence $\pi(d\pi) \rightarrow \pi^*(d\pi)$ transitions in delocalized molecules or from local transitions such as $d\pi \rightarrow d\pi$ transitions at Os(III).

In describing mixed-valence molecules, it is important to define localization, averaging, and delocalization with care. There are three kinds of motions to consider: solvent, vibrational, and electronic. In Class II, the solvent and exchanging electron are localized. In Class II−III, the solvent is averaged and the exchanging electron is localized. In Class III, the solvent and vibrations are averaged and the exchanging electron is delocalized. Vibrational averaging can also occur in Classes II and II−III depending on the band shapes of the spectator vibrations and the time scale for electron transfer.

D. Solvent Relaxation

The solvent and its time scale for responding to changes in the local electric field caused by electron transfer are the key to the transition between Classes II and II−III. The solvent responds by changing the orientations of the local solvent dipoles. There are two components. One involves the collective reorientational motions of many solvent molecules (frictional or diffusive motions). The other occurs on a shorter time scale and involves single molecule rotations (inertial motions).[27,29]

Solvent relaxation times have been measured by ultrafast laser flash photolysis with absorption or emission monitoring. In these experiments rapid excitation with laser pulses of short duration results in the formation of excited states which are initially in the solvent orientations of the ground state (Franck−Condon Principle). Subsequent relaxation of the solvent occurs to orientations appropriate to the electronic configuration of the excited state. This causes time-dependent shifts in the absorption or emission spectra. When time resolved, they give the solvent relaxation time, τ_s.[27,29,121−130]

This technique has been applied to a series of polar organic solvents by using the excited states of organic dyes as probes. The first systematic studies were carried out by Barbara and co-workers.[28,122] The application of ultrafast pulses of durations as short as 10−20 fs has revealed an array of even shorter time scale relaxation phenomena.[27,29] An extensive study was conducted by Maroncelli and co-workers on Coumarin 153 in 24 common solvents.[27] They found clear evidence for a bimodal distribution in relaxation times in small, polar aprotic solvents with an ultrafast component appearing in the range 100−300 fs and a slower component at $\tau > 1$ ps. The contribution of the ultrafast component to spectral

shifts varied from 40% to 70% of the total spectral amplitude change. The shortest relaxation times approach the periods of molecular vibrations, and there is evidence in the early time data for contributions from vibrational relaxation in individual solvent molecules.

Even more complex behavior is observed in alcohols. For ethanol there is evidence for relaxation processes that occur on the 60 fs, 3 ps, and 27 ps time scales.[131] Average relaxation times for some common solvents are CH_3CN (0.26 ps), DMSO (2.0 ps), DMF (2.0 ps), nitromethane (0.41 ps), acetone (0.58 ps), and methanol (5.0 ps).

As noted above, the short time component of the bimodal distributions in these solvents has been attributed to inertial motions arising from single molecule rotations[27,132,133] and the longer component to collective frictional motions. The exact relationship between these relaxation times and solvent averaging by electron transfer is not clear. To a degree, solvent relaxation may be molecule specific. Strong, specific interactions exist between the solvent and certain classes of ligands. In metal complexes this includes H-bonding interactions with individual solvent molecules for NH_3 ligands and electron pair, donor−acceptor interactions for CN^- ligands.[26,134,135] These interactions have been successfully treated theoretically by using pseudo-bonding models for solvent−ligand interactions in the first solvation sphere.[136−138]

Solvent dipole reorientation times for these strongly interacting solvent molecules may be considerably slower than relaxation times in the bulk solvent or around the dye molecules used to measure solvent relaxation times. Specific solvent interactions also influence internal electronic structure.[107,134,135] Changes in these interactions, which accompany solvent reorganization, could also influence short time dynamics.

With the caveat about specific interactions noted, the results of the solvent relaxation studies provide a time scale marker for intramolecular electron transfer. If the solvent is averaged, electron transfer is more rapid than even the ultrafast solvent component. Since this component accounts for about one-half of the time-dependent solvent shift in many solvents, a considerable fraction of the solvent polarization is capable of coupling to electron transfer on the subpicosecond time scale. This is the case for acetonitrile and nitromethane for example.

The narrow bandwidth for pyrazine-bridged, mixed-valence complex **3** points to the averaging of both the fast and ultrafast solvent components in CD_3CN. This sets a lower limit on τ_{ET} of ~100 fs (10^{-13} s) since $\langle\tau_s\rangle = 260$ fs in this solvent. Also, from the appearance of ν(pz) at 1599 cm^{-1}, $\tau_{ET} \geq 20$ fs. This further brackets k_{ET} for **3** to the range $10^{13} < k_{ET} < 5 \times 10^{13}$. Electron transfer in **3** appears to occur on a time scale approaching the periods of the coupled vibrations, which raises some interesting questions about how to define the preexponential factor and barrier to electron transfer, section VI.B.

The bimodal distribution in relaxation times suggests the possibility of observing only partial solvent relaxation if the time scale for electron transfer falls between the time scales for fast and ultrafast relaxation. This would lead to a partial narrowing of the bandwidth. A second mechanism for bandwidth narrowing exists if the time scales for electron transfer and solvent relaxation are comparable since this would cause dynamical coupling. Experimental examples of partial bandwidth narrowing are discussed in section V.A.

In the absence of specific solvent effects, the inertial and collective solvent motions are incorporated in the classical barrier to electron transfer by using dielectric continuum theory. Dielectric continuum theory treats the solvent as a structureless continuum characterized by the macroscopic dielectric constants D_s, the static dielectric constant, and D_{op}, the optical dielectric constant. It has been successfully applied to optical electron transfer in mixed-valence complexes and used to account for the solvent dependences of absorption band energies and widths.[21,23,26] In other cases, it has been found to work less well or not at all.[12−17]

Application of the theory to λ_o depends on the geometrical model used to describe the molecule. For electron transfer between two noninterpenetrating spheres with a center-to-center separation distance of d, λ_o is given by eq 15. In this equation e is the unit electron charge, a_1 and a_2 are the molecular radii of spheres enclosing the redox sites, and d is the internuclear distance. If there is extensive orbital mixing with the ligand bridge, d is less than the geometrical distance, section II. In this case, eq 15 gives a lower limit for λ_o. Ellipsoidal cavity models have also been used which provide a more realistic approximation to the structures of many complexes.[139] Matyushov introduced a molecular theory which separates λ_o into a component arising from the orientational motions of the solvent dipoles and a component from density fluctuations.[140,141] It successfully predicts the sign of the temperature dependence of λ_o.

$$\lambda_o = e^2\left(\frac{1}{2a_1} + \frac{1}{2a_2} - \frac{1}{d}\right)\left(\frac{1}{D_{op}} - \frac{1}{D_s}\right) \qquad (15)$$

IV. Molecules in Class II–III

A. The Creutz–Taube Ion?

A useful way to illuminate the subtleties of Class II−III is by considering the Creutz−Taube ion in further detail. As noted in section III.A, its properties have been modeled by assuming electronic delocalization. A localized model, but with some special features, can also account for its spectroscopic properties.

Mixed-valence Os complex **2** provides a useful reference point for the localized analysis. It is electronically localized based on the appearance of $\nu(N_2)$ and the IC bands at Os(III). Electronic coupling is promoted by dπ mixing with the π, π^* orbitals of the μ-N_2 bridge. The Os−Os distance is 4.97 Å compared to 6.9 Å for pyrazine, and direct through-space overlap may play a role as well.

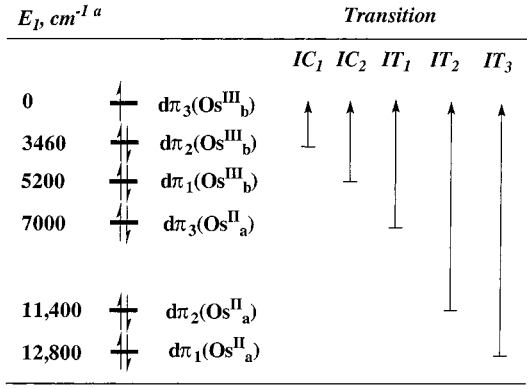

[a] Energies in d_6-DMSO for the spectroscopic (vertical) transitions

Figure 5. Energy-level diagram and band assignments for $[(tpm)(Cl)_2Os^{II}_a(N_2)Os^{III}_b(Cl)_2(tpm)]^+$ (**2**) with energy values in d_6-DMSO for the spectroscopic (vertical) transitions.

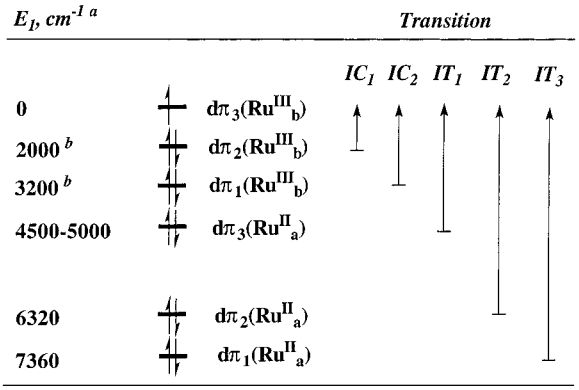

[a] Energies in H_2O for the vertical spectroscopic energies
[b] In Nafion films at low temperature (ref. 144)

Figure 6. Proposed energy-level diagram and band assignments for $[(NH_3)_5Ru(pz)Ru(NH_3)_5]^{5+}$ (**1**).

An energy-level diagram illustrating the IT and IC transitions for **2** is shown in Figure 5. It assumes localization and dπ orbitals that are premixed with π, $\pi^*(N_2)$. The energies are vertical, spectroscopic energies and include λ_i and λ_o.

On the basis of H_{ab} values for the three orbital interactions, the order of increasing mixing of dπ(Os(II)) with dπ_3(Os(III)) is dπ_2 > dπ_1 > dπ_3. The first two orbitals are stabilized relative to dπ_3(Os(II)) by a back-bonding interaction with the $\pi^*(N_2)$ orbitals. They have considerable *z* character (defining *z* to be the Os−N_2−Os axis) and are mixed with dπ_3(Os(III)) by a combination of through-space and π, $\pi^*(N_2)$ mixing. Both the ground and mixed-valence IC excited states are localized with a higher degree of delocalization in the excited states.

There is also evidence for localization in **1** based on the crystal structure[84] and the appearance of symmetrical ν(pz) modes in the IR.[76,85] Its spectroscopic properties can be explained by assuming localization in the mixed-valence ground state and delocalization or near delocalization in the IC(1) and IC(2) excited states.

The mixed-valence band at 6320 cm^{-1} in D_2O[76] is narrow with $\Delta\bar{\nu}_{1/2}$ = 1480 cm^{-1}. It is skewed with a decrease in half-bandwidth on the low-energy side. Polarized crystal spectra of the $Cl_5{\cdot}5H_2O$ and $(tosylate)_5{\cdot}4H_2O$ salts provide clear evidence for more than one electronic component in this "band". For the tosylate salt both a *Y*-polarized band at ∼8000 cm^{-1} and a *Z*-polarized band at ∼7000 cm^{-1} are observed and are of comparable intensity.[85] Pressure-dependent studies on the $Cl_5{\cdot}5H_2O$ salt reveal a general shift to higher energy with increasing pressure consistent with increased electronic coupling and a shoulder whose energy and width are medium dependent.[142] For the pyridine-substituted derivative, *trans,trans*-$[(py)(NH_3)_4Ru(pz)Ru(NH_3)_4(py)]^{5+}$ in CH_3CN, separately discernible bands appear at ∼6000 and ∼7300 cm^{-1}.[143]

Additional low-energy bands are observed for **1** at ∼2000 and ∼3200 cm^{-1} in thin polymeric films of Nafion.[144] The band at 2000 cm^{-1} also appears in the IR spectrum in H_2O/D_2O with $\Delta\bar{\nu}_{1/2}$ = 1400 cm^{-1} and ϵ = 300 M^{-1} cm^{-1}. An additional band appears at 4500−5000 cm^{-1}, which is of comparable width and molar absorptivity.[76]

On the basis of an analysis of the single-crystal EPR spectrum of the $Cl_5{\cdot}5H_2O$ salt at 3 K, the unpaired electron in **1** is predominantly in the *xz* orbital.[74,75] It lies parallel to the π^* orbitals of the pyrazine bridge. There is considerable spin density in the ligand consistent with extensive metal−ligand mixing. Low-symmetry ligand field parameters were obtained from the analysis based on an estimated value of 1000 cm^{-1} for the spin−orbit coupling constant for Ru(III). These parameters were used to calculate the energies of the two higher energy Kramer's doublets originating from the dπ^5 Ru(III) core. The calculated energy spacings between the lowest state and the two higher energy states were 2170 and 3210 cm^{-1}.[74]

To interpret the anisotropy of the EPR *g* values and MCD spectra for **1** and its Os analogue, Ferguson, et al. developed an effective pair model which assumed delocalization. It provided a satisfactory description of the spectral features of the Os analogue but not the spectral features of **1**. It was concluded that there is substantial vibronic activity in the spectrum of **1**.[145]

The same low-energy, five absorption band pattern that appears for Os complexes **2** and **3** also appears for **1**. The bands can be assigned by adopting a related energy ordering scheme. The result is shown in Figure 6.

In Figure 6, the two lowest energy bands are assigned to IC(1) and IC(2). Their energies are predicted by the parameters derived from the EPR analysis. They appear at lower energies than IC bands in Os mixed-valence complexes because of a decrease in covalency and ligand field strength and the lower spin−orbit coupling constant for Ru(III) (∼1000 cm^{-1}) compared to Os(III) (∼3000 cm^{-1}). The intensities of IC bands vary roughly as the square of the spin−orbit coupling constant. For Ru(III) they are typically of low intensity and difficult to observe experimentally.[108,109] In **1** these bands may gain intensity by mixing with the IT transitions, see below.

In the localized scheme IT(1) appears at ca. 4700 cm^{-1}. It is comparable in width (∼1400 cm^{-1}) and

absorptivity ($\epsilon \sim 300$ M^{-1} cm^{-1}) to the IC bands.[76] There is little information about this band, which is unfortunate. In this model IT(1) arises from the $d\pi_3-d\pi_3$ orbital interaction which dominates electron transfer and is the electronic interaction that determines whether the molecule is localized or delocalized in the ground state. On the basis of the estimated band shape parameters and eq 9, $H_{ab}(1) \geq 138$ cm^{-1} for IT(1). If this assignment is correct, **1** is in Class II−III. This conclusion follows from the narrow bandwidth and, with $\lambda = 4700$ cm^{-1}, $2H_{ab}(1)/\lambda \geq 0.06$.

Given the magnitude of $H_{ab}(1)$, $d\pi_3-d\pi_3$ electronic coupling is relatively weak. By inference, $d\pi_3$ lies in the $x-y$ plane orthogonal to the hole in d_{xz} at Ru(III). Depending on the relative orientation of the pyrazine plane, the orbital character of $d\pi_3(Ru^{II})$ is largely d_{xy}, $d_{x^2-y^2}$, or a linear combination of the two.[77]

On the basis of eq 12 which assumes localization, IT(2) and IT(3) should appear at ~6700 and 7900 cm^{-1}. The remaining two bands in the low-energy spectrum actually appear at ~6320 and ~7300 cm^{-1}. They are overlapped, and the overlap contributes to the band asymmetry.

The relative intensities of these bands are medium dependent. IT(2) is dominant in water, and they have comparable intensities in the solid state. They are better resolved in the related complexes $[(bpy)(Cl)Os^{III}(pz)Ru^{II}(NH_3)_5]^{4+}$ [107] and *trans,trans*-$[(py)(NH_3)_4Ru(pz)Ru(NH_3)_4(py)]^{5+}$ under certain conditions.[143] For the latter in CH_3CN, small amounts of added DMSO, which hydrogen bonds strongly to $-Ru(NH_3)_5^{3+}$, cause a dramatic enhancement in the intensity of IT(3) relative to IT(2). The change in $d\pi(Ru(II))-d\pi(Ru(III))$ coupling implied by this result is induced by selective solvation at the NH_3 groups of Ru(III) by hydrogen bonding.[26] The original band shape is restored upon addition of further DMSO, which causes both sides of the molecule to be solvated by DMSO. Selective solvation introduces a redox asymmetry by stabilizing Ru(III), and it must modify the orbital coupling scheme as well. Specific solvent effects are known to affect the internal electronic structures of related complexes.[107,134,136−138,146]

The combined high absorptivities of IT(2) and IT(3) show that there is extensive $d\pi_1,d\pi_2(Ru(II))-d\pi_3(Ru(III))$ coupling. This suggests that $d\pi_1,d\pi_2(Ru(II))$ must have considerable *xz,yz* character. The medium dependence of the IT(2)/IT(3) intensity ratio may arise from medium-induced changes in the relative orientations of the $d\pi_1$, $d\pi_2(Ru(II))$, and $d\pi_3(Ru(III))$ orbitals relative to the pyrazine plane since this would change the orbital coupling scheme.[77,107]

There is extensive mixing between $d\pi_1$, $d\pi_2(Ru(II))$, and $\pi^*(pz)$ which stabilizes these orbitals relative to $d\pi_3$. As an "electronic substituent" the remote Ru(III) lowers the pyrazine π^* levels in a way similar to methylation in $[Ru(NH_3)_5(4\text{-Mepz})]^{3+}$ (4-$Mepz^+$ is 4-methylpyrazinium cation).[72,101,147,148]

Electronic coupling with Ru(II) is sufficient that the IC excited states are electronically delocalized or nearly so. There is direct evidence for this conclusion from the electroabsorption spectrum in glycerol−water (1:1 v:v at 77 K), which demonstrates little if any charge-transfer character in the transition(s).[73,149]

There is also evidence for residual localization in the resonance Raman results of Hupp and co-workers.[86] Asymmetric $\nu(pz)$ stretches at 1412, 1316, and 1078 cm^{-1} are resonantly enhanced to the same degree as symmetric stretches at 1596, 1232, and 697 cm^{-1}. The pyrazine-based vibrations are only weakly coupled to the electronic transition with individual S values varying from 0.005 to 0.031. The largest displacements and the major contributors to the intramolecular structural change accompanying the transition(s) between states are the Ru−N(pz) mode at 324 cm^{-1} ($S = 0.79$) and the $Ru-NH_3$(axial) mode at 262 cm^{-1} ($S = 0.83$).[86,150]

Energy-coordinate curves illustrating the IT and IC transitions assuming residual localization are shown in Figure 7. The coordinate in this case can be taken to be an average of the normal coordinates for the Ru−N modes that are resonantly enhanced in the resonance Raman spectrum.[151−154]

The localized analysis provides explanations for other properties of **1**. (1) The relatively high absorptivities and bandwidths of IC(1) and IC(2) are a consequence of enhanced electronic delocalization in the $d\pi_2-d\pi_3$ and $d\pi_1-d\pi_3$ mixed-valence IC excited states. This mixes intervalence transfer character into these transitions, and they are no longer localized IC transitions. The IC bands are broader and more intense than they would be in electronically isolated Os(III) molecules. To the extent that this mixing is significant, the assumptions underlying the energy relationships among the IT and IC bands in eq 12 are no longer valid.

(2) The origin of the skewed band shape for **1** must arise from the overlap between IT(2) and IT(3) in the spectrum. An explanation based on a cutoff on the low-energy side of the band due to the population of molecules at or near the top of the electron-transfer barrier, section II,[47,48] can be ruled out in this case. Experiments at low temperature show the expected narrowing of the IT "band", but the basic band shape is retained.[73,85] If the cutoff explanation were correct, the band should become more symmetrical as the temperature is decreased.

(3) From the excitation-dependent resonance Raman analysis of **1** by Hupp et al., the extent of vibrational coupling to IT(2), IT(3) is small with $\lambda_i = 680$ cm^{-1} (480 cm^{-1} from the Ru−N modes).[86] On the basis of the energy of $E_{IT}(1)$, $\lambda \sim E_{IT}(1) = 4700$ cm^{-1}. The greatly decreased magnitude of λ for IT(2), IT(3) compared to IT(1) implied by this analysis may be a consequence of the extensive electronic delocalization in the mixed-valence excited state(s). The time-dependent analysis of Raman excitation profiles used by Hupp et al. was derived by Heller by assuming the validity of the Born−Oppenheimer approximation. The vibrational wave functions for both states are assumed to be functions of only the nuclear coordinates.[152−155] With extensive electronic delocalization, the excited-state wave functions for **1** are, in fact, strongly dependent on both electronic and nuclear coordinates, section II.

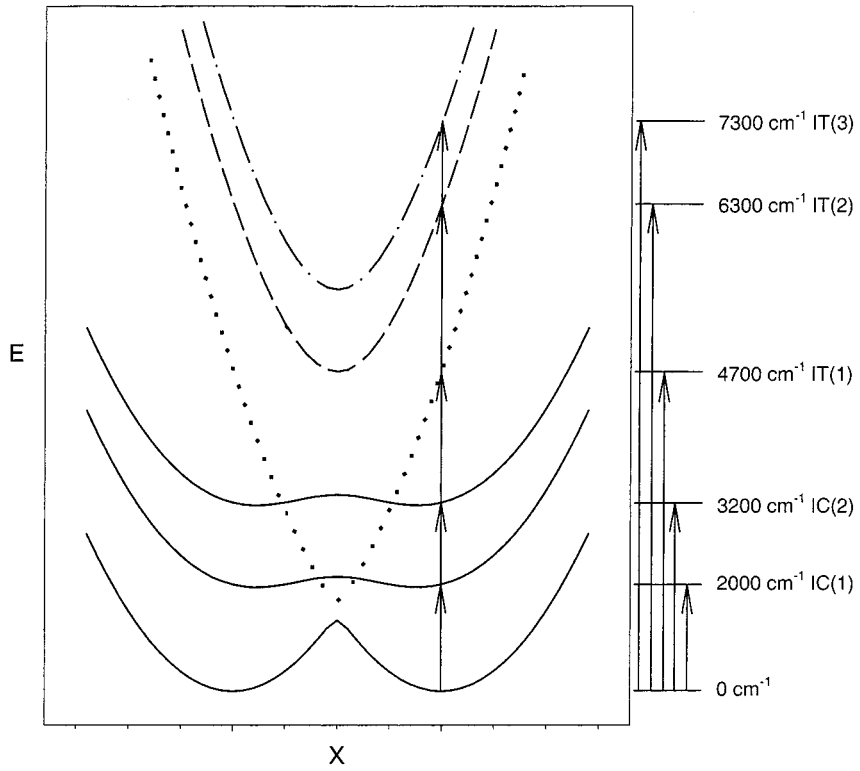

Figure 7. Schematic energy-coordinate diagram as in Figure 3 but for $[(NH_3)_5Ru(pz)Ru(NH_3)_5]^{5+}$ assuming residual localization in the mixed-valence IC excited states. Calculated from eq 5 for the separate curves illustrating IT(1), IT(2), and IT(3) by using $\lambda = 4700$ cm^{-1} and $H_{ab}(1) = 138$ cm^{-1} for IT(1) and $H_{ab}(2) = H_{ab}(3) = 1000$ cm^{-1} and $\lambda = 4700$ cm^{-1} for IT(2) and IT(3). For the latter two calculations, the curves were displaced vertically by 2000 and 3200 cm^{-1}, respectively.

(4) The electronic wave functions in the mixed-valence IC excited states are largely $d\pi-d\pi$ in character with some mixing with π, π^*(pz). This conclusion follows from the results of the resonance Raman analysis on IT(2), IT(3), which show that S values for the pyrazine modes are much smaller than for the Ru−N modes.

There is also the possibility that the mixed-valence excited states are electronically delocalized and the ground state is localized. In this case, the near-IR−IR spectra would be assigned differently. Symmetric ($d\pi + d\pi$) and antisymmetric ($d\pi - d\pi$) combinations of $d\pi_2$(Ru(II)) and $d\pi_1$(Ru(II)) with $d\pi_3$(Ru(III)) would lead to bonding, $\Psi(d\pi_2)$, $\Psi(d\pi_1)$, and antibonding, $\Psi^*(d\pi_2)$, $\Psi^*(d\pi_1)$, molecular wave functions. There would be no minima in the energy curves illustrating the mixed-valence IC excited states in Figure 7 and $2H_{ab}(2)/\lambda$, and $2H_{ab}(3)/\lambda > 1$. In this case, the assignment of the low-energy bands would change to the following. (1) Band I at 2000 cm^{-1} would become a transition from $d\pi_2$(Ru(III)) to $\Psi(d\pi_2)$ rather than IC(1). In this case, transfer of the hole from $d\pi_3$ to $d\pi_2$ increases electronic coupling sufficiently to induce delocalization in the mixed-valence excited state. (2) Band II at 3200 cm^{-1} is the analogous transition from $d\pi_1$(Ru(III)) to $\Psi(d\pi_1)$ rather than IC(2). (3) Band III at ~4700 cm^{-1} is IT(1). (4) Band IV at 6320 cm^{-1} is a transition from $d\pi_2$(Ru(II)) to $\Psi^*(d\pi_2)$ rather than IT(2). In this transition, excitation of an electron from $d\pi_2$(Ru(II)) to create the hole in $d\pi_3$(Ru(III)) enhances electronic coupling to a sufficient degree to induce delocalization. (5) Band V at 7360 cm^{-1} is the analogous transition from $d\pi_1$(Ru(II)) to $\Psi^*(d\pi_1)$ rather than IT(3).

If this interpretation is correct and both mixed-valence IC excited states are delocalized, $H_{ab}(2) \sim {}^1/_2$(Band IV − Band I) = 2160 cm^{-1} and $H_{ab}(3) \sim {}^1/_2$(Band V −Band II) = 2050 cm^{-1}.

Piepho discussed the spectroscopic properties of **1** by assuming delocalization and a single $d\pi(Ru^{II})-d\pi(Ru^{III})$ interaction.[77] The symmetry of the complex was taken to be D_{2h} with the local Ru site symmetry C_{2v}. In C_{2v} symmetry the $d\pi$ orbitals transform as a_1, b_2, and b_3. Linear combinations of the b_2 orbitals with the $b_{3u}(\pi^*)$ and $b_{2g}(\pi)$ pyrazine orbitals leads to a bonding−antibonding pair and the prediction of a single mixed-valence absorption arising from the $d\pi \rightarrow \pi^*(d\pi)$ transition, $b_{3u}(d\pi,\pi^*) \rightarrow b_{2g}^*(d\pi,\pi)$. In this model, the bands in the infrared arise from parity (LaPorte) forbidden, nonbonding to $b_{2g}^*(d\pi,\pi)$ transitions which gain intensity by spin−orbit coupling. This assignment is essentially the same as the assignments for Bands I and II above.

The available IR and resonance Raman data provide a useful map of vibronic coupling in **1**. In summary, (1) the spectator vibrations δ(HNH) at 1319 cm^{-1}, ν_{19a}(pz) at 1451 cm^{-1}, ν_{19b}(pz) at 1437 (sh) cm^{-1}, $\rho(NH_3)$ at 800 cm^{-1}, and a metal−NH_3 mode at 449 cm^{-1} are all averaged;[75,76] (2) the symmetrical pyrazine stretches at 1594, 1232, and 699 cm^{-1} provide markers for localization;[76,85,86] (3) the Ru−NH_3 and Ru−N(pz) metal−ligand stretches at 262 and 324 cm^{-1} and ν_{6a}(pz) at 697 cm^{-1} are the primary origin of the electron-transfer barrier.[86]

The analysis presented here for mixed-valence complexes **1**−**3** provides a road map for defining some of the microscopic features that lead to Class II−III behavior. They include the following: multiple d−d

interactions promoted by mixing with ligand orbitals, multiple IT transitions and mixed-valence IC excited states which can differ significantly from the ground state in the extent of electronic coupling, solvent averaging due to rapid intramolecular electron transfer, vibrations that are weakly coupled to electron transfer but which act as time scale markers, and others that are more strongly coupled and the origin of the electron-transfer barrier.

B. Class II–III. Categorization

1. Experimental Criteria

The observations made on molecules **1**−**3** also define a set of experimental criteria for deciding which molecules are in Class II−III. They include the following: (1) the appearance of narrow, solvent-independent bands at low energy which can reasonably be assigned to an IT transition or transitions; (2) direct experimental evidence for localization from a crystal structure or the appearance of an oxidation state marker such as an IC band or bands; (3) the appearance of nonaveraged spectator vibrations or of a symmetrical bridging-ligand vibration such as ν_{8a}(pz) or $\nu(N_2)$.

Criterion 1 must be applied to the appropriate absorption band or bands. For example, for {[(bpy)-ClRu]$_2$(μ_3-tptz)}$^{3+}$ (section II.B), IT(2) and IT(3) appear as an overlapped, intense, narrow solvent-independent absorption band but the key IT marker is IT(1) which appears at lower energy. It is broad and solvent dependent, consistent with solvent localization in the mixed-valence ground state and Class II behavior.[119]

IC bands and resolved IT bands appear in mixed-valence Os complexes because of the strong metal−ligand interactions and high spin−orbit coupling in the third transition series. This increases the energies and intensities of the nominally forbidden IC transitions. It also increases the energy spacings between the IT transitions, and separate IT bands are observed.

For the first- and second-row transition metals, spin−orbit coupling is lower and metal−ligand interactions are weaker. IT bands are overlapped. IC bands are shifted to lower energy and greatly decreased in intensity, which makes them difficult to observe experimentally.

Narrow, solvent-independent bands at low energy are also observed for Class III molecules. In transition-metal complexes, they arise from $\pi(d\pi) \rightarrow \pi^*(d\pi)$ or related transitions between delocalized levels. The intensities of these bands sometimes bear no relationship with other evidence for strong electronic coupling[156] or the pattern of bands is inconsistent with localization,[145] which can help in distinguishing between Class III and Class II−III.

Electrochemical measurements have been used to infer the extent of delocalization.[21,23,25] The relevant redox couples for **1** are illustrated in eq 16 for which $\Delta E_{1/2} = E_{1/2}(2) - E_{1/2}(1) = 0.39$ V in H_2O, $\mu = 0.1$.[5] The associated free energy change, ΔG°_{com}, and equilibrium constant, K_c, for the comproportionation reaction in eq 17 can be calculated from eq 18. For **1**, $K_c = 3.9 \times 10^6$ and $\Delta G^\circ_{com} = -0.39$ eV.

$$[(NH_3)_5Ru(pz)Ru(NH_3)_5]^{5+} + e^- \rightarrow [(NH_3)_5Ru(pz)Ru(NH_3)_5]^{4+} \quad (16a)$$

$$[(NH_3)_5Ru(pz)Ru(NH_3)_5]^{6+} + e^- \rightarrow [(NH_3)_5Ru(pz)Ru(NH_3)_5]^{5+} \quad (16b)$$

$$[(NH_3)_5Ru(pz)Ru(NH_3)_5]^{6+} + [(NH_3)_5Ru(pz)Ru(NH_3)_5]^{4+} \rightarrow 2[(NH_3)_5Ru(pz)Ru(NH_3)_5]^{5+} \quad (17)$$

$$\Delta G^\circ_{com}(\text{eV}) = -\Delta E_{1/2} \quad (18a)$$

$$K_c = 10^{-16.9\Delta E_{1/2}} \quad (18b)$$

A number of factors influence the magnitudes of K_c and $\Delta E_{1/2}$. They include statistical, electrostatic, and inductive effects as well as electronic delocalization and the magnitude of H_{ab} in the mixed-valence ground state.[25,43,157] To put this into perspective, for μ-N_2 complex **2**, $H_{ab}(1) \geq 118$ cm^{-1} (0.015 eV) which is only 2% of the 0.61 V difference in $E_{1/2}$ values between the mixed-valence couples. For the μ-pz complex **3**, $H_{ab}(1)$ is ≥17 % of $\Delta E_{1/2}$.

For symmetrical complexes, K_c varies from the statistical value of 4 for localized, completely noninteracting redox sites to as high as 2×10^{24}.[158] With a K_c value of this magnitude, there may be little question that the molecule is delocalized. However, interpretation of K_c values of lesser magnitude can be equivocal and it is not a sufficient criterion for distinguishing between Class III and Classes II or II−III. As examples, $K_c = 4 \times 10^{10}$ (DMSO) for **2** and 3.9×10^6 (H_2O) for **1** and yet both appear to be in Class II−III and not in Class III.

IT bandwidths have also been used as a criterion for distinguishing between localization and delocalization. In the classical limit the bandwidth ($\Delta\bar{\nu}_{1/2}$) is related to the free energy change ($\Delta G°$) and energy maximum (E_{abs}) as shown in eq 19.[19,20] In retrospect, this is a criterion for solvent averaging and not for distinguishing between electronic localization or delocalization. Narrow bandwidths point to Class II−III or Class III but do not distinguish between them.

$$(\Delta\bar{\nu}_{1/2})^2 = 16(E_{IT} - \Delta G°)k_B T \ln 2 = [2.31 \times 10^3(E_{IT} - \Delta G°)] \text{ (at 298 K in cm}^{-1}) \quad (19)$$

Care must also be taken in analyzing bandwidths since a typical IT "band" for first- and second-row transition-metal complexes is probably a superposition of three overlapping bands. Depending on the orbital coupling scheme, more than one may contribute significantly to the bandwidth and intensity. This results in bandwidths in excess of those predicted by eq 19, a situation that is commonly observed.[21,23] The converse is true for Class II−III. Because of the

greatly decreased bandwidths which result from the decoupling of the solvent from electron transfer, it is sometimes possible to observe separate IT bands even for complexes of Ru and Fe.[159,160]

There are a variety of possible origins for asymmetric mixed-valence bands. There may be contributions from a vibronic progression or progressions, overlapping mixed-valence bands, differences in the extent of electronic delocalization between the ground and mixed-valence excited states, or the band cutoff effect mentioned in section II. For the chemically linked triarylamine cations mentioned in section II, the half bandwidths on the low-energy side of the IT bands were attributed to a cutoff arising from thermal population at the top of the electron-transfer barrier.[47,48] These molecules still appear to be in Class II since the half bandwidths on the high-energy side are consistent with the classical prediction made by eq 19. For the Creutz−Taube ion and some of its analogues, there is also an asymmetry with band halfwidths narrower on the low-energy side but the bandwidths are far narrower than predicted by eq 19, consistent with solvent averaging, section III.D. These molecules appear to be in Class II−III with the band asymmetry arising from overlapping mixed-valence transitions.

Application of the classical band shape analysis to IT bands for Class II−III molecules is inappropriate. The classical analysis assumes that $\hbar\omega \ll k_BT$ for the coupled vibrations, which is invalid for all but the lowest frequency modes at room temperature since $k_BT \sim 200$ cm^{-1}. As long as the change in equilibrium displacement is large ($S \gg 0$) and the widths of the separate vibronic components larger than the vibrational spacing, the classical approximation can work reasonably well for calculational purposes, but in Class II−III there is minimal solvent broadening.

With specific knowledge of S and $\hbar\omega$, straightforward, semiclassical corrections can be made to expressions defining the electron-transfer barrier. Alternately, the coupled modes can be specifically included on a mode-by-mode basis or as part of an average by using the average mode approximation, section VI.A.[161−170] Values for S and $\hbar\omega$ can be extracted by a Franck−Condon analysis of spectral profiles or by use of the time-dependent generating function approach.[171−175] Measurement of IT(1) at low temperatures, ideally in single crystals, with the appearance of vibronic progressions and application of an appropriate band shape analysis, could provide S and $\hbar\omega$ on a mode-by-mode basis for all of the coupled modes. The same information can be obtained by analysis of the excitation dependence of resonance Raman band profiles even at room temperature in fluid solution.[152−155] Unfortunately, there are formidable technical difficulties associated with the measurement of Raman scattering from low-energy absorption bands.[86,150]

The standard methods for analyzing spectra make use of the Born−Oppenheimer approximation. For many, probably most, Class II−III molecules the extent of electronic coupling is sufficient that this approximation is no longer valid. For Class II−III molecules, the PKS model provides energy levels and wave functions for analyzing spectra by application of a band shape analysis. In this case, the energy levels and wave functions depend on both the electronic and nuclear coordinates, section II.[50,52,57−59]

2. Classification

(i) Molecules in Class II−III. On the basis of Criteria 1−3 in the previous section, a number of molecules in addition to **1**, **2**, and **3** can be placed in Class II−III. In $[(CN)_5Os(pz)Os(CN)_5]^{5-}$ in CH_3CN, ν_{8a}(pz) appears at 1581 cm^{-1} as well as ν(CN) stetching vibrations for both Os(II) and Os(III). Narrow IT bands appear in the near-IR and an IC band at 4000 cm^{-1}. For this complex, $K_c(CH_3CN) = 6 \times 10^8$.[176]

In $[(bpy)_2Ru(\mu\text{-adc-R})Ru(bpy)_2]^{3+}$ (adc-R^{2-} is the azodicarbonyl dianionic ligand shown below), K_c varies from 1×10^8 to 5×10^9 in 1,2-dichloroethane (DCE) as R is varied from OCH_2Ph to Ph. There are two different sets of Ru binding energies in the XPS spectrum and an intense IT feature at 1500 nm (6670 cm^{-1}). It is solvent independent and structured with evidence for the expected three IT bands separated by ~1000 cm^{-1}.[159,160]

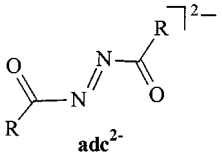

adc^{2-}

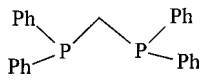

dppm

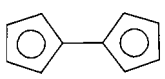

fulvalene

For [(fulvalenyl)$Mn_2(CO)_4(\mu$-dppm)]$^+$ (dppm is 1,2-diphenylphosphinomethane), a narrow, intense IT band appears at 6940 cm^{-1} in CH_2Cl_2 ($\epsilon = 5130$ M^{-1} cm^{-1}, $\Delta\bar{\nu}_{1/2} = 2450$ cm^{-1}) but the oxidation states are localized as shown by the appearance of two separate sets of two ν(CO) bands. This molecule may be in Class II−III or in a transition region between Classes II and II−III, section V.A.[178]

A second molecule close to the transition between Class II and Class II−III is the fulvalene-bridged carborane monocation $\{[(Et_2C_2B_4H_4)Co]_2$(fulvalenediyl)$\}^+$.[120] It was initially assumed to be delocalized based on the appearance of an averaged ν(B−H) stretch at 2515 cm^{-1} in CH_3CN. $K_c(THF) = 6 \times 10^7$ for this complex and, based on the properties of the IT band at 6240 cm^{-1} in CH_3CN, $H_{ab} = 1200$ cm^{-1}. There is evidence for localization in the solvent dependence of the IT band and in its width of 3600 cm^{-1} in CH_3CN. As for the linked triarylamine monocations mentioned in section II, the IT band is asymmetric with a decreased half bandwidth on the

low-energy side. The asymmetry could arise because of a band cutoff or because there are overlapping bands. If the latter is the case, IT(1) may appear at even lower energy in the spectrum.

(ii) Molecules in Class III. Other cases are clearly delocalized. Oxidation of bis(fulvalene)diiron to the mixed-valence cation results in a shortening of the Fe···Fe distance from 3.98 to 3.64 Å. Delocalization through a direct, through-space metal−metal interaction has been invoked.[177−179]

For $[(NH_3)_5Os(N_2)Os(NH_3)_5]^{5+}$, $K_c = 7 \times 10^{12}$(H_2O), $\nu(N_2)$ does not appear in the IR and the near-IR spectrum is not consistent with Os(III).[96,180] The spectrum can be interpreted by assuming electronic delocalization by including axial and rhombic distortions and spin−orbit coupling.[180] XPS measurements on $[(NH_3)_4(Cl)Os(N_2)Os(Cl)(NH_3)_4](Cl)_3$ reveal only one set of Os 4d binding energies consistent with delocalization.[181]

For $[(NH_3)_5Os(pz)Os(NH_3)_5]^{5+}$, $K_c = 1 \times 10^{13}$ (0.1 M HCl), ν_{8a}(pz) appears but is of very low intensity, and the usual pattern of Os(III) IC bands is missing.[114] The temperature dependence of the near-IR and MCD spectra of the $Cl_5 \cdot H_2O$ salt have been obtained in KCl disks or foils of poly(vinyl alcohol). The results were interpreted by using a parametrized model which assumed delocalization and included spin−orbit coupling and mixing with π^*(pz).[182] The delocalized effective pair model mentioned above was used to interpret the EPR g values and MCD spectra.[145]

In the X-ray crystal structure of *trans,trans*-$[(CH_3CN)(NH_3)_4Os(\mu\text{-}N_2)Os(NH_3)_4(CH_3CN)]^{5+}$, the coordination environments are equivalent at the two metal ions.[97] In the cyanogen-bridged complex, $[(NH_3)_5Ru(\mu\text{-}NCCN)Ru(NH_3)_5]^{5+}$, $K_c(H_2O) > 10^{13}$. There is evidence for delocalization in XPS spectra and in the pattern of cyanogen-based stretches from 2150 to 2350 cm^{-1}. A narrow, nearly solvent-independent band appears at 1430 nm in D_2O, and its low intensity can be explained if the electron hole is in d_{xy} rather than the d_{yz} or d_{xz} orbitals.[183]

In the μ-N_2 complex, $[(NH_3)_5Ru(\mu\text{-}N_2)Ru(NH_3)_5]^{5+}$, there is no $\nu(N_2)$ stretch in the IR. A narrow, solvent-independent absorption band appears at 9800 cm^{-1}, which is structured on the high-energy side.[96]

In the C−C linked *trans*-cyclam dimer, $[Ru_2C_{20}H_{36}N_8)Cl_4]^+$, $K_c = 3.5 \times 10^{15}$ (CH_3CN) and a single set of Ru(3p) binding energies are observed by XPS.[92] In $[(NH_3)_5Ru(\mu\text{-bqd})Ru(NH_3)_5]^{5+}$ (bqd is *p*-benzoquinone diimine), the two metal centers are structurally equivalent in the *p*-benzene-disulfonate and *m*-nitrobenzenesulfonate salts. Narrow, solvent-independent bands appear at 10 600, 7740, and 7590 cm^{-1}.[184]

For $[(NH_3)_5Ru(\mu\text{-bptz})Ru(NH_3)_5]^{5+}$ in CH_3CN, $K_c = 10^{15}$ and a narrow, solvent-independent, structured band appears at 1450 nm (7680 cm^{-1}). It is of low intensity with $\epsilon = 500$ M^{-1} cm^{-1}.[156]

The electronic spectra of the symmetrical *tri*-μ-halo-bridged complexes $[(NH_3)_3Ru(X)_3Ru(NH_3)_3]^{2+}$ (X = Cl, Br)[185,186] have been interpreted by assuming D_{3h} symmetry and delocalization.[187] Resonance enhancement of a series of low-frequency, symmetric Ru−X stretches occurred upon excitation into the visible $\sigma \rightarrow \sigma^*$ band, also consistent with delocalization.[188]

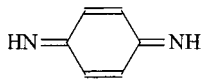

bqd

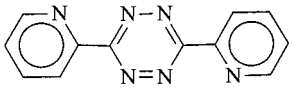

bptz

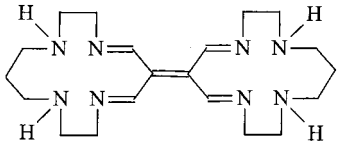

$C_{20}H_{36}N_8$

The intense absorption bands that appear in the visible−near-IR spectra of a series of N-based monocations such as *para*-phenylene-tetramethyldiamine monocation ($[p,p\text{-}Me_2N{-}C_6H_4NMe_2]^+$) have been analyzed by assuming delocalization.[189] The same conclusion has been reached for a series of helicene−bisquinone radical anions. For example, for the radical anion of the diquinone shown below, a band appears at 7500 cm^{-1} which is only slightly solvent dependent.[190]

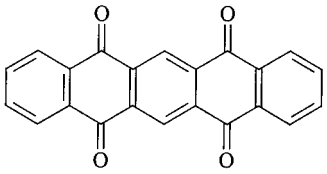

In other cases the odd electron is in a largely bridging-ligand-based molecular orbital[184,191] or there is a complicated interplay between the metal and bridging-ligand orbitals.[93,192] In $\{[(NH_3)_5Ru]_4(TCNE)\}^{8+}$ (TCNE is tetracyanoethylene) and related assemblies based on organic tetracyano bridging ligands, XPS measurements reveal that there is partial oxidation at the metals and partial reduction at the bridge and that the metals are equivalent.[93]

(iii) Ambiguous Cases. Other cases are equivocal because there are insufficient data to make a distinction. Conclusions that were reached earlier based on the widths of low-energy absorption bands, the magnitude of K_c, or the appearance of averaged spectator vibrations have to be reassessed in light of Criteria 1−3. This reassessment will include a significant number of molecules which have been placed in Class III (electronically delocalized) but which are probably in Class II−III (solvent delocalized) or in transition regions between Class II and Class II−III or between Class II−III and Class III, section V.[21−23]

In the bipyrimidine-bridged complex, $[(NH_3)_4Ru(\mu\text{-bpym})Ru(NH_3)_4]^{5+}$ (bpym is bipyrimidine), $K_c(CH_3CN) = 1 \times 10^5$ and a narrow absorption band appears at 3200 cm^{-1}.[193]

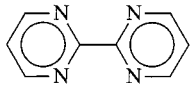

bpym

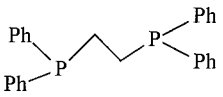

dppe

For the (*SS,RR*) isomer of the acetylide-bridged complex $\{[(\eta^5\text{-}C_5Me_5)(PPh_3)(NO)Re]_2(\mu\text{-}C_4)\}^+$, $K_c(CH_3CN) = 3 \times 10^7$, there is a single, averaged ν(NO) band at 1665 cm^{-1} and an averaged EPR spectrum. New absorption bands appear at 11 300 cm^{-1} (ϵ = 15 000 M^{-1} cm^{-1}), 10 000 cm^{-1} (ϵ = 9400 M^{-1} cm^{-1}), and 8330 cm^{-1} (ϵ = 3200 M^{-1} cm^{-1}) with bandwidths in the range 2000−2500 cm^{-1}. If the low-energy bands are IT(3), IT(2), and IT(1), calculated values for E(IC(1)) and E(IC(2)) are 1670 and 2970 cm^{-1} by using eq 12. This suggests that there may be additional bands at lower energy in the IR for this complex. The bandwidths are less than those calculated by eq 19 (4400−5100 cm^{-1}), and this complex may be on the borderline between Class II and Class II−III, section V.A.[194]

For the acetylide-bridged diiron complex $\{[(\eta^5\text{-}C_5Me_5)(dppe)Fe]_2(\mu\text{-}C_4)\}^+$, $K_c(CH_2Cl_2) = 1 \times 10^{12}$. The Fe Mössbauer spectrum is averaged, as are a series of ν(C═C) stretches, and an intense band appears at 7410 cm^{-1} with ϵ = 11 700 M^{-1} cm^{-1}. This complex is presumably delocalized, but there is no information about the width or solvent dependence of the mixed-valence band.[195]

There are two different isomers for the bridged butadienediyl complex $\{[(\eta^5\text{-}C_5H_5)(CO)(PPh_3)Fe]_2(\mu\text{-}CH{=}HCH{=}CH)\}^+$ for which $K_c(CH_2Cl_2) = 9 \times 10^5$ and 4×10^6. The EPR spectrum is averaged at −86 °C, and there is an averaged ν(CO) stretch at 1946 cm^{-1} (CH_2Cl_2 at −40 °C).[196] Unfortunately, there is no information about the low-energy electronic absorption spectrum.

The mixed-valence anion, $\{[\{HB(dmpz)_3\](NO)(Br)Mo]_2(\mu\text{-}pz)\}^-$, is almost surely delocalized with $K_c(CH_2Cl_2) = 2 \times 10^{24}$. There is an averaged EPR signal and a single ν(NO) stretch at 1585 cm^{-1}. There is no information about the low-energy absorption spectrum. The corresponding monocation has both a localized EPR spectrum and separate ν(NO) bands at 1720 and 1606 cm^{-1}.[158] For the diamidobenzene-bridged, mixed-valence complexes $\{[[HB(dmpz)_3(NO)(X)Mo]\}_2(\mu\text{-}1,2\text{- or }1,4\text{-}C_6H_4(NH)_2\}^-$ (X = Cl, Br, I) in CH_2Cl_2, $K_c = (1 \times 10^{13})-(1 \times 10^{16})$. The EPR signal is delocalized, but there are separate ν(NO) bands.[158,197] These molecules could be in Class II or Class II−III, but again, there is no information about the low-energy absorption spectra.

For the pyrazine-bridged complexes *trans,mer*-$\{[(P(^i Pr)_3)_2(CO)_3M]_2(\mu\text{-}pz)\}^+$ (^{i}Pr is isopropyl) in CH_2Cl_2, $K_c = 10^{11}$(M = W) and 2×10^6 (M = Mo). Upon oxidation from M(0)−M(0) to the once-oxidized mixed-valence forms in CH_2Cl_2, all three ν(CO) bands shift to higher energy (to 1962, 1898, and 1829 cm^{-1} for M = Mo) and narrow, intense absorption bands

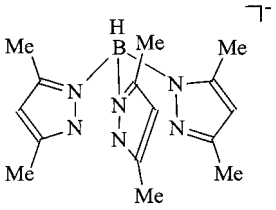

$HB(dmpz)_3$

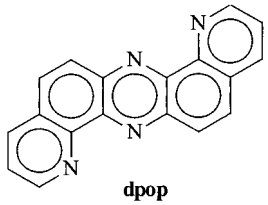

dpop

appear at 4990 cm^{-1} (M = W, $\Delta\bar{\nu}_{1/2}$ = 730 cm^{-1}, ϵ = 4600 M^{-1} cm^{-1}) and 4650 cm^{-1} (M = Mo, $\Delta\bar{\nu}_{1/2}$ = 700 cm^{-1}, ϵ = 7000 M^{-1} cm^{-1}), which are nearly solvent independent. These molecules are probably in Class III, but there is no mention of the ν(pz) stretch.[198,199]

Similarly, in the 2,2′-bipyrimidine complex $\{[(P(^n Bu)_3)_2(CO)_2Mo]_2(bpym)\}^+$ (^{n}Bu is *n*-butyl), $K_c(CH_2Cl_2) = 6 \times 10^8$ and there are only two ν(CO) bands at 1891 and 1808 cm^{-1}. A new absorption band appears at 2700 cm^{-1} ($\Delta\bar{\nu}_{1/2}$ = 1300 cm^{-1}) which is of low absorptivity.[200]

For doubly bridged $\{(biphenyl)[Cr(CO)_2]_2(\mu\text{-dppm})\}^+$ and related complexes with $(CH_3)_2PCH_2P(CH_3)_2$ and $Ph_2AsCH_2AsPh_2$ as the second bridge, $K_c(CH_2Cl_2) = (3 \times 10^8)-(2 \times 10^9)$ and only two ν(CO) bands are observed which are shifted 75−80 cm^{-1} to higher energy compared to the neutral molecules.[201] These molecules may also be electronically delocalized, but there is no mention of low-energy absorption bands.

For the complex $[(bpy)_2Os(dpop)Os(bpy)_2)]^{5+}$, $K_c(CH_3CN) = 1 \times 10^6$. New bands appear for the mixed-valence form at 13 330 and 8930 cm^{-1} ($\Delta\bar{\nu}_{1/2}$ = 1700 cm^{-1}, ϵ = 5500 M^{-1} cm^{-1}). Presumably, this molecule is related to mixed-valence complex **3** and is in Class II−III with the band at 8930 arising from IT(2) or IT(3) and additional IT and IC bands appearing at lower energy.[202]

V. Transitions Between Classes

Invoking Class II−III adds a complication to the localized-to-delocalized transition since there are two transitions to consider, the transition between Class II (solvent localized) and Class II−III (solvent delocalized) and between Class II−III and Class III (electronically delocalized). Invoking Class II−III has the advantage of providing an explanation for an otherwise puzzling series of experimental observations by invoking an intermediate class with well-defined properties of its own.

The transitions between classes are not abrupt. There are molecules with a continuous range of properties between the three limiting forms. This is to be expected given the coupling of the electron-transfer time scale to solvent and vibrational dynamics and the complexities arising from multiple coupled vibrations.

A. Class II to Class II–III

The transition between Classes II and II−III is tied to the onset of dynamical coupling of solvent dipole reorientations to intramolecular electron transfer. An expected experimental consequence is the appearance of IT bandwidths that are intermediate between those predicted for Class II by the classical analysis and the narrow bandwidths found with solvent averaging.

One of the first examples was found for the unsymmetrical complex [*cis*-$(bpy)_2(Cl)Os(pz)Ru(NH_3)_5]^{4+}$.[107,203,204] It exists as two oxidation-state isomers, $[(bpy)_2(Cl)Os^{II}(pz)Ru^{III}(NH_3)_5]^{4+}$($Os^{II}-Ru^{III}$) and $[(bpy)_2(Cl)Os^{III}(pz)Ru^{II}(NH_3)_5]^{4+}$($Os^{III}-Ru^{II}$). Isomer $Os^{II}-Ru^{III}$ is in Class II and is favored in high donor number solvents[205] such as DMSO and dimethylformamide which H-bond strongly to $-[Ru(NH_3)_5]^{3+}$. Overlapping, broad, solvent-dependent IT bands appear in the near-IR for this isomer (at 6600 cm^{-1} in DMSO).

Isomer $Os^{III}-Ru^{II}$ is favored in solvents of lower donor number (methanol, D_2O, acetonitrile,...) and is stabilized by enhanced $d\pi(Os^{III})-d\pi(Ru^{II})$ electronic coupling through the pz bridge. Both isomers are present in equilibrium amounts in trimethyl phosphate, which is a solvent of intermediate donor number, eq 20.

$$Os(III)-Ru(II) \rightleftharpoons Os(II)-Ru(III) \qquad (20)$$

There is evidence for electronic localization in isomer $Os^{III}-Ru^{II}$ by the appearance of the expected IC bands at Os(III) and characteristic ν(bpy) Os(III) marker bands that appear in the IR. A narrow, nearly solvent-independent band appears at 8300 cm^{-1} in CD_3CN ($\epsilon = 1850\ M^{-1}\ cm^{-1}$, $\Delta\bar{\nu}_{1/2} = 1850\ cm^{-1}$) much as for IT(2), IT(3) in **1**, section IV.A. This band is asymmetrical on the high-energy side and appears to be a convolution of two bands separated by ca. 1000 cm^{-1}. They were assigned to IT(2) and IT(3), but there was no definitive evidence for IT(1) at lower energy.

Changing the solvent from DMSO or DMF to CH_3CN or D_2O shifts the equilibrium in eq 20 and induces Os(II) → Ru(III) electron transfer. Electron transfer is accompanied by a transition from Class II to Class II−III. The transition is not abrupt. In nitromethane and nitrobenzene, solvents in which isomer Os(III)−Ru(II) is most highly favored over Os(II)−Ru(III), the IT band(s) shift to higher energy (to 9030 cm^{-1} in nitromethane-d_3) and increase in bandwidth (to $\Delta\bar{\nu}_{1/2} = 2210\ cm^{-1}$). For the 4,4′-bpy-bridged analogue, an analogous IT band appears at 10 200 cm^{-1} with $\Delta\bar{\nu}_{1/2} = 3540\ cm^{-1}$.

The increases in E_{IT} and $\Delta\bar{\nu}_{1/2}$ for nitrobenzene and nitromethane suggest that there is only partial solvent averaging in the mixed-valence ground state in these solvents. This could occur if the intramolecular electron-transfer time scale is comparable to the solvent relaxation time scale. As electron-transfer becomes more rapid than the ability of the solvent to respond, the effective λ_o decreases causing the absorption band energy and width to decrease and the intensity at the maximum to increase. Solvent motions are uncoupled dynamically and no longer in equilibrium with the exchanging electron. In the limit of fast electron transfer, the solvent is averaged and in orientations appropriate to the delocalized electronic distribution, $M^{II.5}-M^{II.5}$. The phenomenon of band narrowing is analogous to the broadening and coalescence of spectator vibrations described in section III.B.

Electron transfer is slower in nitromethane and nitrobenzene because these solvents stabilize isomer $Os^{III}-Ru^{II}$ over isomer $Os^{II}-Ru^{III}$. This increases the barrier for electron transfer by increasing $\Delta G°$, which decreases k_{ET}.

For $Os^{III}-Os^{II}$ in nitromethane or nitrobenzene compared to solvents such as CH_3CN where the solvent is averaged on the electron-transfer time scale, partial relaxation results in an increase in the IT band energy and width. The width increases by 360 cm^{-1} in nitromethane compared to CH_3CN but is still only 30% of the width expected if the solvent were fully coupled dynamically. From ultrafast solvent relaxation measurements, the average solvent relaxation time for nitromethane is 0.41 ps. This points to a time scale for Ru(II) → Os(III) intramolecular electron transfer of ∼1 ps in nitromethane.

From the data of Itoh and Kubiak et al. in CH_2Cl_2 at room temperature on the pyrazine-bridged clusters $\{[Ru_3(\mu_3\text{-}O)(\mu\text{-}O_2CCH_3)_6(CO)(L)]_2(\mu\text{-pz})\}^-$, k_{ET} and $\Delta\bar{\nu}_{1/2}$ values are L = 4-(dimethylamino)pyridine, $k_{ET} = 9 \times 10^{11}\ s^{-1}$, $\Delta\bar{\nu}_{1/2} = 3760\ cm^{-1}$; L = pyridine, $k_{ET} = 5 \times 10^{11}\ s^{-1}$, $\Delta\bar{\nu}_{1/2} = 3930\ cm^{-1}$; L = 4-cyanopyridine, $k_{ET} = 1 \times 10^{11}\ s^{-1}$, $\Delta\bar{\nu}_{1/2} = 5220\ cm^{-1}$.[117,118] There are probably multiple IT contributors to these band widths but the important point is that the bandwidths for the first two are considerably less than the bandwidth for the third. This provides evidence for band narrowing in the pz-bridged clusters as well. They undergo electron transfer on the 1−2 ps time scale, which approaches the average solvent relaxation time for CH_2Cl_2 of 0.56 ps.[27]

Related observations have been made for the 2,2′-bibenzimidazolate-bridged complexes $[(bpy)_2M(BiBzIm)M(bbp)_2]^{3+}$ (M = Ru, Os) for which $K_c(CH_3CN) = 1 \times 10^3$ for M = Os and 8×10^4 for M = Ru. For M = Os in CH_3CN, IC bands for Os(III) are observed at 4400 and 5400 cm^{-1} and IT bands at 4800 cm^{-1} ($\epsilon = 500\ M^{-1}\ cm^{-1}$) and 8180 cm^{-1}. For the Ru complex an IT band appears at 5130 cm^{-1}. The widths of both IT bands are narrower than predicted by eq 19, by 33% for Ru and by 23% for Os.[206]

In the superphane-bridged cyclopentadienylcobalt cyclobutadiene monocation bridged complex illustrated below, an IT band is observed in CH_2Cl_2 at 12 000 cm^{-1} ($\epsilon = 600\ M^{-1}\ cm^{-1}$) which is solvent dependent but to a lesser degree than predicted by dielectric continuum theory. The bandwidth is also considerably less (3510 cm^{-1}) than predicted by eq 19 (5170 cm^{-1}).[207]

The most interesting and comprehensive set of data illustrating IT band narrowing were reported by Curtis and co-workers.[43] They investigated the influence of L (L = NH_3, 3,5-Me_2py, py, 3-Fpy, 3-Clpy, 2,6-

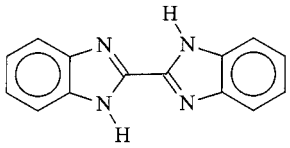

Bibzim

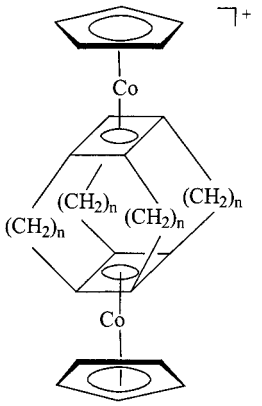

Dicobalt Superphane Complex

Me_2pz) on $\Delta E_{1/2}$ and E_{IT} in *cis*- and *trans*-$[(NH_3)_4(L)Ru(pz)(L)(NH_3)_4]^{5+}$ and in the unsymmetrical series *trans*-$[(NH_3)_4(L)Ru(pz)(NH_3)_5]^{5+}$.

For the symmetrical complexes, bandwidths increased as $\Delta E_{1/2}$ decreased. The variations were from $\Delta\bar{\nu}_{1/2} = 1480\ cm^{-1}$ at $\Delta E_{1/2} = 0.43$ ($K_c = 1.8 \times 10^7$) for L = NH_3 to $\Delta\bar{\nu}_{1/2} = 3300\ cm^{-1}$ at $\Delta E_{1/2} = 0.23$ ($K_c = 7.7 \times 10^3$) for L = 2,6-Me_2pz. $\Delta E_{1/2}$ decreases across the series because back-bonding with L competes with $d\pi(Ru^{II})-\pi^*(pz)$ mixing. This decreases electronic coupling across the bridge, increases the electron-transfer barrier, and decreases k_{ET}.

The increase in bandwidth as $\Delta E_{1/2}$ decreased was initially interpreted as direct experimental evidence for the delocalized to localized transition. It may also be indicative of the onset of solvent averaging and the transition between Classes II−III and II.

Through the series of complexes, $\Delta\bar{\nu}_{1/2}$ increased by 370−2500 cm^{-1} (compared to the bandwidth for **1** of 1480 cm^{-1}) as L was varied. The average solvent relaxation time for CH_3CN is 0.26 ps.[27] If the variations in bandwidth arise from solvent dynamics, these data point to electron transfer on time scales in the range <100 ps to >1 ps. The caveat must be added that the literature relaxation times were obtained by using the excited states of organic dyes. Part of the solvent relaxation may be slower for the ammine complexes because of specific H-bonding interactions with the NH_3 ligands, section III.D.

There is the additional caveat that these measurements were presumably made on IT(2),IT(3) rather than on IT(1), section IV.A. This further complicates the interpretation of the bandwidth data. Intermediate bandwidths could be a consequence of solvent localization in the ground state and delocalization in the excited state(s). This would decrease the solvent contribution to the bandwidth and energy. In fact, there could be a progression in behavior from solvent delocalization in both the ground and excited states as for **1** to solvent localization in both states. The data may also reflect differences in time scales for different solvent motions, section III.D.

A related band broadening effect has been observed in acetonitrile in the unsymmetrical series $[trans\text{-}(NH_3)_4(L)Ru_a(pz)Ru_b(NH_3)_5]^{5+}$.[43] Variations in L were used to stabilize isomer $Ru_a(II)-Ru_b(III)$ by Ru(II) back-bonding to L. This creates a redox asymmetry with $\Delta G°$ increasing for $Ru_a(II) \rightarrow Ru_b(III)$ electron transfer as the back-bonding ability of L increases. The increase in $\Delta G°$ decreases k_{ET} and $\Delta\bar{\nu}_{1/2}$ increases from 1480 to 3860 cm^{-1}. Band broadening is accompanied by an increase in E_{IT} from 6260 to 7440 cm^{-1}.

Even with electronic delocalization, the electronic distribution in the ground and mixed-valence excited states of these complexes is asymmetrical because of the asymmetrical ligand fields. There may be some charge-transfer character to low-energy mixed-valence transitions even if they occur between levels that are electronically delocalized.

A related effect was observed by Hupp et al. for **1** and *trans,trans*-$[(NH_3)_4(py)Ru(pz)Ru(py)(NH_3)_4]^{5+}$ in nitromethane in the presence of 1 equiv of the added crown ethers dibenzo-36-crown-12(DB-36-C-12) or dibenzo-30-crown-19 (DB-30-C-10).[208] Under these conditions, there is selective encapsulation of one end of the complexes. This creates a redox asymmetry, IT(2), IT(3) shifts from ~5700 to ~6700 cm^{-1} and $\Delta\bar{\nu}_{1/2}$ increases by ca. 1000 cm^{-1}. The original band shape is restored, with a slight shift in E_{abs} when a second equivalent of the crown is added.

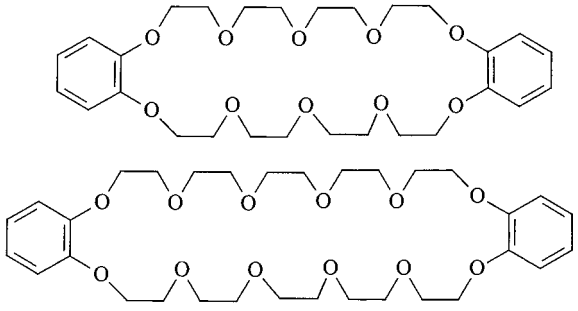

Crown Ethers

Deprotonation of the malonitrile bridge in the protonated precursor gives the mixed-valence ion $[(NH_3)_5Ru(NC-C(^tBu)-CN)Ru(NH_3)_5]^{4+}$ for which $K_c(H_2O) \geq 10^{10}$.[209] Electronic coupling is dominated by $d\pi-\pi(pz)-d\pi$ mixing. An intense band appears at 8550 cm^{-1} in D_2O ($\epsilon = 1.6 \times 10^4\ M^{-1}\ cm^{-1}$) which is somewhat solvent dependent and has an intermediate bandwidth of 2120 cm^{-1}. For the dialkylated analogue with the bridge $NC-C(^tBu)_2-CN$, a relatively weak IT band is observed at 10 800 cm^{-1} (ϵ = 180 $M^{-1}\ cm^{-1}$; $\Delta\bar{\nu}_{1/2} = 4990\ cm^{-1}$).

Crutchley et al. carried out a comprehensive study on a related series of 1,4-dicyanamidobenzene-complexes.[157] The structures of the bridging ligands are illustrated below. The complexes were $[(NH_3)_5Ru(\mu\text{-}L)Ru(NH_3)_5]^{3+}$, *trans,trans*-$[(NH_3)_4(py)Ru(\mu\text{-}L)Ru(py)(NH_3)_4]^{3+}$, and *mer,mer*-$[(bpy)(NH_3)_3Ru(\mu\text{-}L)(NH_3)_3(bpy)]^{3+}$.

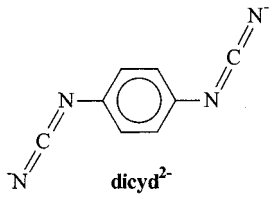

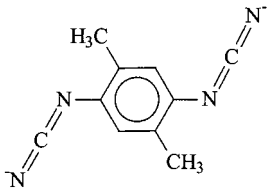

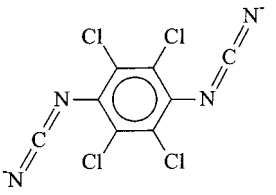

H_{ab}, estimated from $\Delta E_{1/2}$ values, increased for the most strongly reducing ligand Me_2dicyd^{2-} and for the most electron-deficient complexes, based on *mer*-$[Ru(NH_3)_3(bpy)]^{2+}$. In these complexes, electronic coupling is also dominated by $d\pi-\pi(\mu\text{-L})-d\pi$ mixing.

Intense IT bands appear in the visible with bandwidths varying from 1700 cm^{-1} for *mer,mer*-$[(bpy)(NH_3)_3Ru(\mu\text{-}Me_2dicyd^{2-})(NH_3)_3(bpy)]^{3+}$ in CH_3CN to 4530 cm^{-1} for $[(NH_3)_5Ru(\mu\text{-}Me_2dicyd^{2-})Ru(NH_3)_5]^{3+}$ in DMSO. $\Delta\bar{\nu}_{1/2}$ increased in solvents of higher donor number (DN) in the order nitromethane (DN = 2.7) < acetonitrile (DN = 14.1) < DMSO (DN = 29.8)). E_{IT} increased with bandwidth. These observations are also consistent with decreased solvent averaging as the time scale for electron transfer increases due to a decrease in electronic coupling.[157]

Effects related to the transition from Class II to Class II−III in solution have also been observed in the solid state. The clusters $[Fe_3(\mu_3\text{-}O)(\mu\text{-}O_2CCH_3)_6(L)_3]\cdot S$ (L = H_2O or a pyridine derivative; S is a molecule of solvation) are electronically localized with the oxidation-state configuration $Fe(III)_2Fe(II)$ based on temperature-dependent IR measurements.[210−213] They are also localized on the ^2H NMR and ^{57}Fe Mössbauer time scales at low temperatures. At higher temperatures the Mössbauer signals are averaged consistent with an increased rate of electron transfer. Mössbauer averaging is accompanied by the onset of motions of the solvate molecule and occurs in one or more phase transitions.[214−217]

Similar complex behavior was found in PF_6^- and SbF_6^- salts of the mixed-valence cations 1,1″-dichlorobiferrocenium, 1,1″-dibromobiferrocenium, and 1,1″-diiodobiferrocenium. All were shown to have localized oxidation states by the appearance of two infrared bands arising from C−H bending modes in the 815−850 cm^{-1} region. Temperature-dependent Mössbauer measurements revealed a complex array of behaviors depending on the salt and how it was prepared. Examples were found of localization at low temperatures and averaging as the temperature was increased, of localization over all temperature ranges, and of samples in which there were both localized and delocalized polymorphs. For the SbF_6^- salt of the diiodo cation, a transition from a localized to an averaged Mössbauer spectrum occurred in the same temperature range as the onset of motion of the SbF_6^- anion. These observations point to a contribution to the barrier from counterion motion that can be sufficiently slow to localize the exchanging electron on the Mössbauer time scale.[218−224] Similar effects as well as the role of ring tilting on Mössbauer line broadening were observed in I_3^- salts of a series of ethyl-substituted biferrocenium cations.[225]

B. Class II–III to Class III

There is only limited experimental information about the transition from Class II−III to Class III. The transition is described quantitatively by PKS theory, which is parametrized in terms of H_{ab} and λ, section II. In Class III there is no vibronic coupling to the intramolecular electronic distribution and the odd electron is delocalized. Mixed-valence bands arise from optical transitions between electronically delocalized ground and excited states.

There are gradations of behavior within Class II−III as the magnitude of H_{ab} increases. Varying the terminal ligand from 4-dimethylpyridine to 4-cyanopyridine in the μ-oxo Ru clusters of Itoh and Kubiak in CH_2Cl_2 increases H_{ab} and K_c from 1.7×10^4 to 2.7×10^7. This causes a change in the pattern of ν(CO) bands from two discrete bands to a single averaged band.[117,118]

For both *cis,cis*-$[(bpy)_2(Cl)Os(pz)Os(Cl)(bpy)_2]^{3+}$ (**3**) and $[(tpy)(bpy)Os(pz)Os(bpy)(tpy)]^{5+}$, ν(pz) appears at 1595−1600 cm^{-1} in CD_3CN. For **3** a series of ν(bpy) ring-stretching modes from 1400 to 1500 cm^{-1} are averaged.[111,112] There is less Os(II)−pz back-bonding in the tpy complex and evidence for the onset of dynamical effects in the pattern of ν(bpy) and ν(tpy) bands rather than averaging. A related observation has been made for the bpy bands in *cis,cis*-$[(bpy)_2(Cl)Os(N_2)Os(Cl)(bpy)_2]^{3+}$.[94,95] For **1**, a series of spectator vibrations are averaged but there is still localization as evidenced by the appearance of the three symmetrical ν(pz) vibrations, section III.A.

These observations show that there is a gradation of behavior in Class II−III in the extent to which vibrations are averaged. This is a time scale phenomenon much like solvent averaging in the transition between Class II and Class II−III. The response of the vibrations and the appearance of broadening or coalescence depend on the time scale for electron transfer, the difference in band maxima between oxidation states, and the band shapes. As electronic coupling is increased in a closely related series of molecules, there is a concomitant decrease in the electron-transfer barrier, which decreases the time scale for electron transfer and leads to vibrational averaging.

The appearance or nonappearance of symmetrical bridging-ligand stretches such as ν(pz) or $\nu(N_2)$ is the

most useful experimental criterion for distinguishing between electronic localization and delocalization. The intensities of these bands should be related at some level to the extent of delocalization and the magnitude of the local electric dipole created by the electronic asymmetry across the bridge. However, there are many factors that determine infrared band intensities.[226−228]

The available data are rudimentary, and there are no obvious trends. Molar extinction coefficients for ν_{8a}(pz) in CD_3CN are 2600 M^{-1} cm^{-1} for **3**, 600 M^{-1} cm^{-1} for *cis*-$[Os(bpy)_2(pz)(Cl)]^+$, ca. 450 M^{-1} cm^{-1} for **1**, and 50 M^{-1} cm^{-1} for *cis*,*cis*-$[(bpy)_2(Cl)Os(pz)Os(Cl)(bpy)_2]^{2+}$. The large value for **3** may arise from the mixing of charge-transfer character into the ring-stretching mode, section III.B.[111,112] ν_{8a}(pz) appears for the Os(II)−Os(II) dimer because the bridged complexes are asymmetrical and there are rotamers across the bridge which are noncentrosymmetric.[99]

As noted in section III.B, the appearance of the bridging-ligand stretches in the IR and the absence of solvent coupling provide a basis for estimating the time scales for electron transfer in **2** and **3**. These time scales overlap with the periods of barrier vibrations. For the 324 cm^{-1} Ru−N(pz) mode for **1**, the period is 100 fs (10^{-13} s). On these time scales, electronic and nuclear motions are dynamically coupled and it is no longer possible to apply the Born−Oppenheimer approximation.

In **1** there appears to be a residual barrier to electron transfer arising largely from the Ru−N stretching modes at 324 and 262 cm^{-1}.[86] This molecule is on the verge of being electronically delocalized. As shown by the Os analogue, which is delocalized, a further increase in through-bridge electronic coupling would presumably trigger delocalization.

It may be possible to probe the Class II−III to III transition in further experimental detail. One approach would be to apply the ligand modification strategy developed by Curtis and co-workers[43] but in an equivalent Os series $[(L)(NH_3)_4Os(pz)Os(NH_3)_4(L)]^{5+}$. Replacement of coordinated NH_3 by L would decrease Os(II) → pyrazine back-bonding and perhaps decrease electronic coupling to a degree sufficient to begin to map the Class III to II−III transition.

VI. Intervalence Transfer and Electron Transfer

A. Electron-Transfer Theory

If a single coupled harmonic mode or averaged mode is coupled to electron transfer in the classical limit and $H_{ab} \ll \lambda$, E(IT) is related to lambda and $\Delta G°$ as shown in eq 21, eq 21a if $\Delta G° = 0$. The bandwidth was defined in eq 19.[19,20]

$$E_{IT} = \Delta G^{o} + \lambda \tag{21a}$$

$$E_{IT} = \lambda \tag{21b}$$

The electron-transfer barrier is given by eq 22a, eq 22b if $\Delta G° = 0$.

$$\Delta G^{*} = \frac{(\Delta G° + \lambda)^2}{4\lambda} = \frac{E_{abs}{}^2}{4(E_{abs} - \Delta G°)} = \frac{578 E_{abs}{}^2}{(\Delta \nu_{1/2}^{-})^2}(\text{in cm}^{-1}) \tag{22a}$$

$$\Delta G^{*} = \frac{E_{abs}}{4} = \frac{\lambda}{4} \tag{22b}$$

In the classical limit, the rate constant for electron transfer is given by eq 23. In the nonadiabatic limit, the frequency factor, ν_{ET}, is the electron tunneling frequency. It is related to H_{ab} as shown in eq 24.

$$k_{ET} = \nu_{ET} \exp -(\Delta G^{*}/4RT) \tag{23}$$

$$\nu_{ET} = \nu_e = \frac{2\pi H_{ab}{}^2}{\hbar}\left(\frac{1}{4\pi\lambda RT}\right)^{1/2} \tag{24}$$

If there is a single coupled mode or averaged mode, the rate constant for electron transfer is given by eq 25. In eq 25, $\hbar\omega_j$ is the quantum spacing, v_j and v_j' the initial and final vibrational quantum numbers, S_j the electron-vibrational constant, and S_s is the electron-vibrational coupling constant for a single high or medium-frequency spectator vibration.[30,161,163,166−168,229−234] In this equation $L_{v_j}^{(v_j'-v_j)}(S_j)$ is a Laguerre polynomial which, assuming $\hbar\omega = \hbar\omega'$, is given by eq 26.

$$k_{ET} = \frac{2\pi}{\hbar}\frac{H_{DA}{}^2}{(4\pi\lambda_o RT)^{1/2}} \exp - (S_s)\sum_{v_j}\sum_{v_j'} p(v_j) \exp(-S_j) S_j^{(v_j'-v_j)} \frac{v_j!}{v_j'!}[L_{v_j}^{(v_j'-v_j)}(S_j)]^2 \times \exp[-(\Delta G° + \sum_j (v_j' - v_j)\hbar\omega_j + \lambda_o)^2/4\lambda_o RT] \tag{25}$$

$$L_{v_j}^{(v_j'-v_j)}(S_j) = \sum_{v=0}^{v_j} \frac{v_j'!(-S_j)^v}{(v_j - v)!(v_j' - v_j + v)!v!} \tag{26}$$

The Boltzmann population in level j, $p(v_j)$, is given by eq 27 with $\beta_j = \hbar\omega_j/k_B T$ and Z_j the vibrational partition function. For an harmonic oscillator, $Z_j = (1 - \exp - (\hbar\omega_j/k_B T)^{-1}$.

$$p(v_j) = \exp[-(v_j\hbar\omega_j/k_B T)]/Z_j = \exp[-(v_j\beta_j)]/Z_j \tag{27}$$

Equation 25 describes electron transfer as occurring through a series of vibrational channels from initial vibrational level j, with Boltzmann population $p_j(v_j)$, to final level j'. The contribution by the solvent to each channel is treated classically and included in λ_o. For a spectator vibration with $\hbar\omega \gg k_B T$, the transition between initial and final states occurs from $v = 0$ to $v' = 0$ through every channel. The macroscopic rate constant is the sum of the contributions through each microscopic channel. This result can be generalized to include multiple coupled vibrations on a mode-for-mode basis or by using mode averaging.[169,170]

These electron-transfer equations are parametrized in terms of spectroscopic quantities. In the classical limit, simple absorption band measurements and application of eqs 9 and 22 are sufficient to determine ΔG^* and ν_{ET}. For transition-metal complexes, where multiple IT bands are expected, eq 22 only applies to IT(1). In particular, the parameters in the electron-transfer rate constant equations are $H_{ab}(1)$ and $E_{IT}(1)$. If there is a single, broad overlapping IT band, deconvolution is required to acquire the band shape parameters for IT(1).

To use the quantum mechanical forms of the rate constant equation, it is necessary to have an independent evaluation of the kinetic parameters derived by spectral fitting or by analysis of excitation dependent resonance Raman profiles. The difficulties in applying the latter technique to low-energy absorption bands was noted above.

If H_{ab} is sufficiently large, electron tunneling is rapid and the transferring electron is always in equilibrium with the nuclear motions that are coupled to electron transfer. This is the adiabatic limit where a nuclear motion or motions dictate the dynamics of barrier crossing. In this limit ν_{ET} is given by eq 28. In eq 28 ν_{ET} is the product of the effective frequency for nuclear motion (or motions) along the reaction coordinate (ν_n) and κ the probability that electron transfer will occur at the coordinate(s) where the electron-transfer barrier is minimized.[30,161−165,229−236] κ is given by eq 29.[236]

$$\nu_{ET} = \nu_n \kappa \tag{28}$$

$$\kappa = \frac{2[1 - \exp(-\nu_e/2\nu_n)}{2 - \exp(-\nu_e/2\nu_n)} \tag{29}$$

The minimum in the energy barrier occurs when the slowest mode or modes dictate the barrier crossing dynamics. These are the collective dipole reorientational (frictional) motions in the solvent.[121,122,125−133,130,230,237−247] To put these limits into perspective, for a reorganizational energy of $\lambda = 8000$ cm^{-1} and $H_{ab} = 32$ cm^{-1}, $\nu_e = 10^{13}$ s^{-1} based on eq 24. Assuming a solvent relaxation time of 1 ps, $\nu_n = 10^{12}$ s^{-1} and from eq 29 $\kappa \sim 1$. Even weak electronic coupling is sufficient to ensure adiabatic electron transfer.

There is experimental evidence for solvent dynamical effects from ultrafast measurements on excited states,[164] in heterogeneous (electrochemical) electron transfer, and in self-exchange reactions such as $[Fe(Cp)_2]^{+/0}$ exchange measured by ^{1}H NMR line broadening.[238] The dynamics of solvent coupling to electron transfer have been studied theoretically both formally and by the use of molecular simulations.[125,241,248−252]

B. Electron Transfer in Class II–III

The analysis of electron-transfer barriers and rate constants in the previous section is based on time-dependent perturbation theory and the Golden Rule. It assumes localization and the Born−Oppenheimer approximation. The effects of electronic coupling appear in H_{ab} and in the barrier either treated classically, eq 8, or quantum mechanically, eq 25 with S_j and λ_o decreasing with H_{ab}.

These results and the assumption of localization are no longer valid as the magnitude of H_{ab} begins to approach lambda. With significant electronic coupling the energy levels and wave functions are dependent on both electron and nuclear coordinates, section II.

There is evidence for the breakdown of the localized approximation in the results of Nelsen and coworkers on intramolecular electron transfer in a series of chemically linked, bis-hydrazine monocations.[12−17] They were able to measure k_{ET} by EPR measurements and IT band energies and widths spectroscopically. The IT bands are broad and solvent dependent. In these molecules there are both large barriers to electron transfer and relatively strong electronic coupling. For the cation aBIT$^+$, illustrated below, $E_{IT} = 18\,100$ cm^{-1} ($\epsilon = 673$ M^{-1} cm^{-1}, $\Delta\bar{\nu}_{1/2} = 8310$ cm^{-1}) and $H_{ab} = 1330$ cm^{-1} in CH_3CN.[253,254]

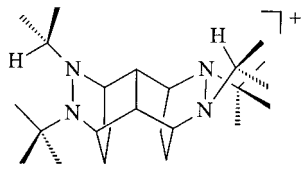

aBIT$^+$

Experimental rate constants in this series were consistently greater than values calculated by using electron-transfer theory by factors of 20−30 even with the inclusion of specific mode contributions based on UHF/AM1 dynamics calculations.[253−255] Excellent agreement was obtained between theory and experiment by using the semiclassical approach in section II but with an empirical modification to describe the upper and lower energy curves for calculating E_a from the IT band profile.[12] Instead of the harmonic approximation, variations in H_{aa} and H_{bb} with X were modified by adding a quartic term. This had the effect of greatly decreasing E_a and transferring the minima of the energy curves nearer to $X = a/2$. This empirical procedure provided a semiclassical barrier that adequately represented k_{ET} for these strongly adiabatic reactions where the wave functions and energy levels depend on both electron and nuclear coordinates, at least near the top of the barrier.

For transition-metal complexes, electron-transfer barriers tend to be smaller, 7000 and 2620 cm^{-1} for μ-N_2 and μ-pyrazine complexes **2** and **3**. A lesser degree of electronic coupling suffices to enter the same adiabatic regime. Attempted application of the semiclassical result in eq 8 with kinetic parameters derived from IT spectra consistently result in calculated values that are too low based on independent estimates for k_{ET}.[94,112] The disagreement between experiment and theory may have the same origin, a breakdown of the localized approximation.

There are other factors that ensure that electron-transfer theory will have to be significantly modified to deal with electron transfer in Class II−III and with the transitions between classes. A partial listing includes the following. (1) The effect on the frequency

factor and barrier to electron transfer of partial solvent averaging in the Class II to Class II−III transition must be included. (2) In Class II−III the solvent is averaged and no longer contributes to the dynamics of barrier crossing. There could be an intermediate case in which electron transfer remains dynamically coupled to the inertial (fast) solvent motions but not to the slower frictional motions. (3) Given the relatively modest degree of electronic coupling required to achieve rapid electron tunneling, barrier crossing dynamics in Class II−III must be largely dictated by vibrational motions with $\nu_{ET} = \nu_n$. For the low-frequency skeletal modes that are most strongly coupled to electron transfer, $\nu \sim 10^{13}$ s^{-1} (τ^{-1} = 100 fs). An appropriate theory must include the fact that vibrational dynamics are, in general, coupled directly to the motion of the exchanging electron. (4) The transition between Classes II−III and III with multiple coupled modes must be dealt with on a mode-for-mode basis with the extent of averaging depending on $H_{ab}(1)$ and S_j. (5) Depending on the orbital coupling scheme and the magnitude of H_{ab}-(1), the electronic distribution could still be oscillatory in Class III molecules on a measurable time scale. This could occur if strong dπ−dπ electronic coupling greatly decreases λ but the coupling between the dπ_3 donor and acceptor orbitals is small. Analysis of the distance dependence of the electronic distribution within H_2^+ as a function of the internuclear coordinate reveals a region where the electronic distribution is oscillatory with the frequency dependent on the extent of electronic coupling.[256,257]

VII. Postscript. Localized-to-Delocalized Behavior in Metal-to-Ligand Charge Transfer (MLCT) Excited States

Many of the conceptual issues that arise in describing the localized-to-delocalized mixed-valence transition also appear in the charge-transfer excited states of certain dπ^6 transition-metal complexes such as $[Ru(bpy)_3]^{2+}$ or *fac*-$[Re(bpy)(CO)_3(py)]^+$. The low-energy absorption spectra of these complexes are dominated by bands arising from metal-to-ligand charge transfer (MLCT) transitions. In the corresponding MLCT excited states, e.g., eq 30, there is considerable charge polarization in the wave functions describing the excited-state electronic distribution.[258−264]

$$\underset{(d\pi^6)}{fac\text{-}[Re^{I}(bpy)(CO)_3(py)]^+} \xrightarrow{h\nu} \underset{(d\pi^5\pi^{*1})}{fac\text{-}[Re^{II}(bpy^{-\bullet})(CO)_3(py)]^{+}*} \quad (30)$$

For the MLCT excited states of $[Ru(bpy)_3]^{2+}$ and other complexes with multiple acceptor ligands, there is an ambiguity in describing the excited state. The excited electron could be either localized, $[Ru^{III}(bpy^{-\bullet})(bpy)_2]^{2+}$*, or delocalized, $[Ru^{III}(bpy^{1/3-\bullet})_3]^{2+}$*, with the electron either occupying a π* orbital on one bpy or delocalized over all three. There has been considerable controversy in the literature over this point with different views strongly held much as for the Creutz−Taube ion.[265−274]

The microscopic factors that determine localization and delocalization are the same as in mixed-valence complexes. They are the magnitude of bpy$^{-\bullet}$−bpy electronic coupling (H_{ab}) and the reorganizational energy arising from the coupled vibrations and the solvent (λ).

When viewed as a mixed-valence molecule, the thermally equilibrated excited state $[Ru(bpy)_3]^{2+}$* is an organic analogue of the chemically linked quinones, hydrazines, and aromatic amines mentioned in previous sections. In this case, the metal ion acts as a bridge between the interacting ligands.

There is evidence for instantaneous localization in $[Ru(bpy)_3]^{2+}$* and $[Os(bpy)_3]^{2+}$* on the time scale for light absorption based on the solvent dependence of the MLCT absorption bands. From the magnitude of the spectral shifts, it has been estimated that the excited-state dipole moment in $[Ru(bpy)_3]^{2+}$* is 14.6 ± 6.1 D.[265] If the excited state were delocalized, the D_3 symmetry of the ground state would be retained giving an excited-state dipole moment of 0.

There is also direct evidence for localization in the equilibrated excited state by transient resonance Raman and IR measurements.[269,275−278]

Although the lowest MLCT excited state is localized, the excited electron undergoes rapid, subnanosecond ligand-to-ligand electron transfer as shown by time-resolved polarization measurements.[279−282] Ligand−ligand electron transfer is rapid compared to the excited-state lifetime of ~1 μs but slow relative to the time scales for the coupled vibrations and solvent motions.

When classified as a mixed-valence molecule, $[Os(bpy)_3]^{2+}$* and probably $[Ru(bpy)_3]^{2+}$* are in Class II. The evidence for this conclusion comes from the appearance of separate ν(bpy) and ν(bpy$^{-\bullet}$) vibrational modes in the excited-state IR spectrum[269] and the recent observation of broad, solvent-dependent bands in transient near-IR spectra. This band has been assigned to excited-state intervalence transfer, eq 31.[283]

$$[Os^{III}(bpy^{-\bullet})(bpy)(bpy)]^{2+}* \xrightarrow{h\nu} [Os^{III}(bpy)(bpy^{-\bullet})(bpy)]^{2+}* \quad (31)$$

The available experimental evidence suggests that $[Ru(bpy)_3]^{2+}$* is localized both immediately after light absorption and when thermally equilibrated, but the appropriate description on intermediate time scales is unknown. There may a period of delocalization if the time scale for electronic dephasing by ligand-ligand electron transfer is shorter than the vibrational and solvent relaxation times. On the basis of the Franck−Condon Principle, the excited state is formed instantaneously in the vibrational and solvent coordinates of the ground state. There is no microscopic basis for localizing the excited electron until the solvent and coupled vibrations relax to the new equilibrium coordinates of the excited state.

Localization vs delocalization is also an issue in ligand-bridged complexes in which MLCT excitation creates mixed-valence character.[284,285] An example is

shown in eq 32 in which the lowest-lying π^* acceptor level is on the 4,4′-bpy bridging ligand and oxidation states at Re could be either localized or delocalized.[286]

$$\begin{aligned} &\textit{fac,fac}\text{-}[(4,4'\text{-}Me_2bpy)(CO)_3Re^{I}(4,4'\text{-bpy})\\ &\qquad Re^{I}(CO)_3(4,4'\text{-}Me_2bpy)]^{2+} \xrightarrow{h\nu}\\ &\textit{fac,fac}\text{-}[(4,4'\text{-}Me_2bpy)(CO)_3Re^{II}(4,4'\text{-bpy}^-)\\ &\qquad Re^{I}(CO)_3(4,4'\text{-}Me_2bpy)^{2+}* \text{ or}\\ &\textit{fac,fac}\text{-}[(4,4'\text{-}Me_2bpy)(CO)_3Re^{I.5}(4,4'\text{-bpy}^-)\\ &\qquad Re^{I.5}(CO)_3(4,4'\text{-}Me_2bpy)^{2+}* \end{aligned} \quad (32)$$

There is an additional oxidation state ambiguity in these molecules. In the MLCT "excited state" of *fac,fac*-{[(bpy)(CO)$_3$Re]$_2$(4,4′-bpy)}$^{2+}$, there is a solvent-dependent equilibrium between ligand-based isomers. In one the excited electron is on bpy and in the other on the bridging ligand. The bpy-based isomer, [(bpy$^{-\bullet}$)(CO)$_3$Re^{II}(4,4′-bpy)Re^{I}(CO)$_3$(bpy)]$^+$ is presumably localized because of the asymmetric charge distribution which creates an uphill free energy gradient to Re(I) → Re(II) electron transfer.[286]

The mixed-valence MLCT excited states have one more electron than ground-state mixed-valence analogues—compare *cis,cis*-[(bpy)$_2$(Cl)Os(pz)Os(Cl)-(bpy)$_2$]$^{3+}$ (**3**) and *cis,cis*-[(bpy)$_2$(Cl)Os(pz^{-})Os(Cl)-(bpy)$_2$]$^{2+}$*. Ground-state complex **3** is known to be in Class II−III, section III.B but the state of localization in the excited-state analogue is unknown.

The question of localization vs delocalization in the MLCT excited state of [(tpy)Ru^{II}(tppz)Ru^{II}(tpy)]$^{4+}$ has been explored by transient absorption measurements in the near-IR. A relatively narrow ($\Delta\bar{\nu}_{1/2}$ = 1070 cm^{-1}), solvent-independent band is observed at 6300 cm^{-1} in CD_3CN, which has been assigned to a mixed-valence transition in the excited state [(tpy)Ru^{III}-(tppz$^{-\bullet}$)Ru^{II}(tpy)]$^{4+}$*.[283] A band appears at 6550 cm^{-1} ($\Delta\bar{\nu}_{1/2}$ = 970 cm^{-1}) for the mixed-valence ground-state [(tpy)Ru^{III}(tppz)Ru^{II}(tpy)]$^{5+}$. Either or both may be in Class II−III or Class III, but note the conclusion reached for {[(bpy)(Cl)Ru]$_2$(tppz)}$^{3+}$ in section III.B.

Application of transient IR spectroscopy has allowed the issue of localization versus delocalization to be resolved in ligand-bridged complexes containing CO and CN$^-$ ligands.[287] For the Re complex in eq 32, two sets of ν(CO) bands are observed consistent with localization.[288] Similar conclusions have been reached for the MLCT excited states of [(CO)$_5$W]$_2$(BL) (BL = pz, 4,4′-bpy)[289] and for the lowest MLCT excited states of cyano-bridged complexes such as [(bpy)$_2$-(CN)Ru(CN)Ru(CN)(bpy)]$^+$ with terminal cyanide ligands.[290−291]

Localization and delocalization appear as an issue in a third area of MLCT excited-state chemistry in which the extent of electronic coupling between the metal and acceptor ligand in the excited state can be varied. The MLCT excited states of [Ru(bpy)$_3$]$^{2+}$ and *fac*-[Re(bpy)(CO)$_3$(py)]$^+$ are true excited states with extensive dπ(M)−π^*(bpy) metal−ligand mixing, largely by dπ−2pN(π) overlap. Once formed, they decay by a combination of radiative and nonradiative processes.

In MLCT-based, chromophore−quencher complexes an electron-transfer donor or acceptor, or both, are chemically linked to a MLCT chromophore.[292,293] The extent of electronic coupling between the donor or acceptor and the MLCT chromophore in these molecules depends on the chemical link that connects them.

The structures of the acceptor ligands for three complexes of general formula, [Re(4,4′-X$_2$bpy)(CO)$_3$-(LA)]$^{n+}$ (X = Me or H; LA = acceptor ligand; n = 2 for LA = MQ$^+$, n = 1 for LA = BIQD and OQD) are illustrated below. In all three cases, dπ(Re) → 4,4′-X$_2$bpy excitation is followed by rapid 4,4′-bpy$^{-\bullet}$ → LA intramolecular electron transfer to give the photochemical transients [Re^{II}(4,4′-bpy)(CO)$_3$(LA$^{-\bullet}$)]$^+$.

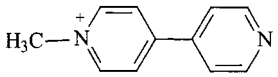

MQ$^+$

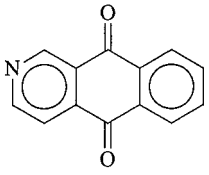

BIQD

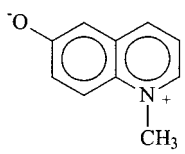

OQD

An appropriate description of the transients depends on the extent of Re(II)−LA$^{-\bullet}$ coupling. With MQ$^+$ as the acceptor, there is extensive dπ(Re(II))−π^*(MQ$^{\bullet}$) electronic coupling, $2H_{ab}/\lambda > 1$, and the photochemical transient is a lower MLCT excited state.[294,295] For BIQD as the acceptor, there are localized Re(II) and BIQD$^{-\bullet}$ sites with H_{ab} = 153 cm^{-1} and λ = 4980 cm^{-1} based on an analysis of the emission spectrum and the radiative lifetime. For LA = OQD, H_{ab} is only 4 cm^{-1} and Re(II)−(OQD$^{-\bullet}$) electronc coupling is weak.[296]

Weak electronic coupling and small excited-ground state mixing for the OQD complex is a consequence of poor overlap due to symmetry considerations and a change in spin from a largely triplet transient intermediate to the singlet ground state.[297,298]

This comparison reveals the existence of a localized-to-delocalized transition in MLCT excited states analogous to the transition from Class I to Class III in mixed-valence compounds. In this case, the deciding factor is the extent of electronic coupling between π^*(LA) and dπ_3(Re(II)). There are two types of photochemical transients, MLCT excited states for which $2H_{ab} > \lambda$ and "redox-separated" (RS) states for which $2H_{ab} < \lambda$. Both decay to the ground state with a large free energy change with $|\Delta G°| > \lambda$.

The effect of increasing electronic coupling on the energy-coordinate curves for the initial and final states in the region where $|\Delta G°| > \lambda$ is illustrated in

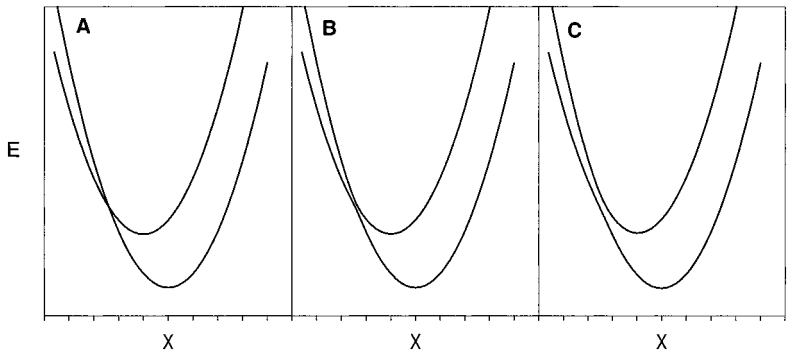

Figure 8. Energy-coordinate diagram following Figure 1 illustrating the effect of increasing electronic coupling and the transition between electron transfer in the inverted region (A) to nonradiative decay (C). The energy curves were calculated by using the following equations: $E_1 = [\lambda(2X^2 - 2X + 1 + \Delta E_o]/2 - \{[\lambda(2X - 1) - \Delta E_o]^2 + 4H_{ab}^2\}^{1/2}/2$; $E_2 = [\lambda(2X^2 - 2X + 1 + \Delta E_o]/2 + \{[\lambda(2X - 1) - \Delta E_o]^2 + 4\ H_{ab}^2\}^{1/2}/2$ (see ref 30a) and the parameters $\lambda = 5000\ cm^{-1}$, $\Delta E° = 19\ 000\ cm^{-1}$ and (A) $H_{ab} = 0\ cm^{-1}$, (B) $H_{ab} = 1000\ cm^{-1}$, and (C) $H_{ab} = 2500\ cm^{-1}$. Taken from ref 298.

Figure 8. For both the RS state in Figure 8A and the MLCT state in Figure 8C, the energy-coordinate curve for the initial state is imbedded in the curve of the final state. This allows emission to occur and emission is observed from all three of the Re complexes.

The RS state returns to the ground state by a combination of radiative decay (emission) and electron transfer in the inverted region, which is a nonadiabatic process. Electron transfer occurs between orbitals largely dπ(Re) and π*(LA) in character that are weakly mixed by an electrostatic perturbation. The decay of an MLCT excited state to the ground state occurs by a combination of radiative and nonradiative decay. Nonradiative decay of excited states is vibronically induced by a vibration or vibrations that have the appropriate symmetry to mix the electronic wave functions describing the two states, the "promoting" modes.[299−305] In this case, the wave functions are linear combinations of dπ_3(Re(II)) and π*($LA^{-\bullet}$). They describe eigenstates of the same Hamiltonian, and to zero order, the excited and ground states cannot mix.

If there are coupled medium- or high-frequency modes, the transition from the initial state to the final state for both inverted electron transfer and nonradiative decay is dominated by quantum vibrational transitions from $v^* = 0$ levels in the initial state to levels above $v = 0$ in the final state rather than by a classical barrier crossing.[299−309]

Just as for mixed-valence complexes, it is possible to predict the existence of a class of molecular excited states which fall between the limiting descriptions of RS states (localized) and MLCT states (delocalized). This will occur as metal−ligand electronic coupling is decreased and H_{ab} becomes comparable to lambda (=S$\hbar\omega$). In this region the same problems of description will exist as for mixed-valence complexes with wave functions and energies that are functions of both electronic and nuclear coordinates. There will probably also be an intermediate class of excited states analogous to Class II−III in which the solvent is delocalized but with oxidation states at the metal and acceptor ligand localized.

One place to look for such molecules is in polypyridyl complexes containing acceptor ligands in which the lowest π* acceptor level is part of the π system but not directly bonded to the metal. An example is the ligand dppz in which the lowest π* level is localized largely on the phenazine fragment.[310,311] Electronic coupling between this fragment and the metal in $[Ru(bpy)_2(dppz)]^{2+}$ is lower by a factor of ∼5 than with the bpy fragment.[312] It is conceivable that this or a related excited state or states could be the MLCT equivalent of the Creutz−Taube ion.

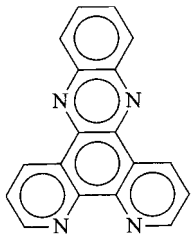

dppz

VIII. Acknowledgment

We thank the National Science Foundation for support in the writing of this review. Acknowledgments are also made to Henry Taube who invented this field and to Noel Hush who provided the tools to understand it. The authors also acknowledge Professor Juan-Pablo Claude of the University of Alabama at Birmingham for his help in constructing some of the figures.

IX. References

(1) *Mixed Valence Compounds*; Brown, D. M., Ed.; D. Reidel: Dordrecht, Holland, 1980.
(2) *Mixed Valence Systems: Applications in Chemistry, Physics and Biology*; Prassides, K., Ed.; NATO ASI Series 343; Kluwer Academic Publishers: Dordrecht, The Netherlands, 1990.
(3) Woodward, J. *Philos. Trans. R. Soc. London* **1724**, *33*, 15.
(4) Creutz, C.; Taube, H. *J. Am. Chem. Soc.* **1969**, *91*, 3988.
(5) Creutz, C.; Taube, H. *J. Am. Chem. Soc.* **1973**, *95*, 1086.
(6) Cowan, D. O.; Levanda, C.; Park, J.; Kaufman, F. *Acc. Chem. Res.* **1973**, *6*, 1.
(7) Le Vanda, C.; Bechgaard, K.; Cowan, D. O.; Rausch, M. D. *J. Am. Chem. Soc.* **1977**, *99*, 2964.
(8) Robin, M. B.; Day, P. *Adv. Inorg. Chem. Radiochem.* **1967**, *10*, 247.
(9) Allen, G. C.; Hush, N. S. *Prog. Inorg. Chem.* **1967**, *8*, 357.
(10) Powers, M. J.; Meyer, T. J. *J. Am. Chem. Soc.* **1980**, *102*, 1289.
(11) Meyer, T. J. *Acc. Chem. Res.* **1978**, *11*, 94.
(12) Nelsen, S. F.; Ismagilov, R. F.; Trieber, D. A., II *Science* **1997**, *278*, 846.

(13) Nelsen, S. F.; Ismagilov, R. F.; Powell, D. R. *J. Am. Chem. Soc.* **1997**, *119*, 10213.
(14) Nelsen, S. F.; Ismagilov, R. F.; Powell, D. R. *J. Am. Chem. Soc.* **1998**, *120*, 1924.
(15) Nelsen, S. F.; Adamus, J.; Wolff, J. J. *J. Am. Chem. Soc.* **1994**, *116*, 1589.
(16) Nelsen, S. F.; Trieber, D. A., II; Wolff, J. J.; Powell, D. R.; Rogers-Crowley, S. *J. Am. Chem. Soc.* **1997**, *119*, 6873.
(17) Nelsen, S. F.; Ismagilov, R. F.; Gentile, K. E.; Powell, D. R. *J. Am. Chem. Soc.* **1999**, *121*, 7108.
(18) Elliott, C. M.; Derr, D. L.; Matyushov, D. V.; Newton, M. D. *J. Am. Chem. Soc.* **1998**, *120*, 11714.
(19) Hush, N. S. *Prog. Inorg. Chem.* **1967**, *8*, 391.
(20) Hush, N. S. *Electrochim. Acta* **1968**, *13*, 1005.
(21) Crutchley, R. J. *Adv. Inorg. Chem.* **1994**, *41*, 273.
(22) Ward, M. D. *Chem. Soc. Rev.* **1995**, 187.
(23) Creutz, C. *Prog. Inorg. Chem.* **1983**, *30*, 1.
(24) Kaim, W.; Bruns, W.; Poppe, J.; Kasack, V. *J. Mol. Struct.* **1993**, *292*, 221.
(25) Richardson, D. E.; Taube, H. *Coord. Chem. Rev.* **1984**, *60*, 107.
(26) Chen, P.; Meyer, T. J. *Chem. Rev.* **1998**, *98*, 1439.
(27) Horng, M. L.; Gardecki, J. A.; Papazyan, A.; Maroncelli, M. *J. Phys. Chem.* **1995**, *99*, 17311.
(28) Kahlow, M. A.; Kang, T. J.; Barbara, P. F. *J. Phys. Chem.* **1987**, *91*, 6452.
(29) Fleming, G. R.; Cho, M. *Annu. Rev. Phys. Chem.* **1996**, *47*, 109.
(30) (a) Sutin, N. *Prog. Inorg. Chem.* **1983**, *30*, 441. (b) Brunschwig, B. S.; Sutin, N.; *Coord. Chem. Rev.* **1999**, *187*, 233. (c) Sutin, N. *Adv. Chem. Phys.* **1999**, *106*, 7.
(31) Newton, M. D. *Adv. Chem. Phys.* **1999**, *106*, 303.
(32) Hupp, J. T.; Dong, Y.; Blackburn, R. L.; Lu, H. *J. Phys. Chem.* **1993**, *97*, 3278.
(33) Mataga, N.; Kubota, T. *Molecular Interactions and Electronic Spectra*; Dekker: New York, 1970.
(34) Bublitz, G. U.; Laidlaw, W. M.; Denning, R. G.; Boxer, S. G. *J. Am. Chem. Soc.* **1998**, *120*, 6068.
(35) Creutz, C.; Newton, M. D.; Sutin, N. *J. Photochem. Photobiol. A: Chem.* **1994**, *82*, 47.
(36) Hush, N. S. *Trans. Faraday Soc.* **1961**, *57*, 557.
(37) The wave functions Ψ_a and Ψ_b are products of the associated one-electron wave functions. Thus, for a Ru(III)−Ru(II)′, $d\pi^5-d\pi^6$ mixed-valence ion with the $d\pi$ orbitals $d\pi_1$, $d\pi_2$, $d\pi_3$ and $d\pi_1'$, $d\pi_2'$, $d\pi_3'$, $\Psi_a = d\pi_1^2 d\pi_2^2 d\pi_3^1 d\pi_1'^2 d\pi_2'^2 d\pi_3'^2$, neglecting spin. With these wave functions and $H_{ab} = \langle\Psi_a|\hat{H}|\Psi_b\rangle$, $H_{ab} = \langle d\pi_3^1 d\pi_3'^2|\hat{H}|d\pi_3^2 d\pi_3'^1\rangle$. The one-electron wave functions are premixed with ligand orbitals including $d\pi-\pi$, π^* mixing with bridging-ligand orbitals. The $d\pi$ orbitals at Ru^{III} are linear combinations of the Cartesian orbitals d_{xy}, d_{xz}, d_{yz}, which are mixed by low symmetry and spin−orbit coupling in the $d\pi^5$ electronic core.
(38) This analysis assumes that the force constants (and quantum spacings, $\hbar\omega$) in the initial (ω) and final (ω') states are the same. More generally, they are different, which introduces a temperature dependence into E_{IT} and an additional temperature dependence into $\Delta\bar{\nu}_{1/2}$. In the limit that the frequency difference, $|\omega - \omega'|$, is small compared to the average, $\delta E_{IT}/\delta T = -\Delta S°$ where $\Delta S°$ is the entropy difference between the initial and final states. See: Hupp, J.; Neyhart, G.; Meyer, T. J.; Kober, E. K. *J. Phys. Chem.* **1992**, *96*, 10820.
(39) This is only true when the overlap of the electronic wave functions is neglected. More gererally, this difference is equal to $2(H_{ab} - S_{ab}H_{aa})/(1 - S_{ab}^2)$ where S_{ab} is the vibrational overlap integral, $\langle\Psi_a/\Psi_b\rangle$.
(40) Mulliken, R. S. *J. Am. Chem. Soc.* **1952**, *64*, 811.
(41) Mulliken, R. S.; Person, W. B. *Molecular Complexes*; Wiley: New York, 1969.
(42) Reimers, J. R.; Hush, N. S. *J. Am. Chem. Soc.* **1995**, *117*, 1302.
(43) Salaymeh, F.; Berhane, S.; Yusof, R.; de la Rosa, R.; Fung, E. Y.; Matamoros, R.; Lan, K. W.; Zheng, Q.; Kober, E. M.; Curtis, J. C. *Inorg. Chem.* **1993**, *32*, 3895.
(44) Nelsen, S. F.; Newton, M. D. *J. Phys. Chem. A* **2000**, *104*, 10023.
(45) (a) Oh, D. H.; Boxer, S. G. *J. Am. Chem. Soc.* **1990**, *112*, 8161. (b) Karki, L.; Lu, H. P.; Hupp, J. T. *J. Phys. Chem.* **1996**, *100*, 15637.
(46) Bublitz, G. U.; Boxer, S. G. *Annu. Rev. Phys. Chem.* **1997**, *48*, 213.
(47) Nelsen, S. F. *Chem. Eur. J.* **2000**, *6*, 581.
(48) Lambert, C.; Nöll, G. *J. Am. Chem. Soc.* **1999**, *121*, 8434.
(49) Huttner, G.; Evertz, K. *Acc. Chem. Res.* **1986**, *19*, 406.
(50) Hush, N. S. *NATO Adv. Study Inst., Ser. C* **1980**, *58*, 151.
(51) Reimers, J. R.; Hush, N. S. *Chem. Phys.* **1996**, *208*, 177.
(52) Piepho, S. B. *J. Am. Chem. Soc.* **1988**, *110*, 6319.
(53) Amos, A. T.; Burrows, B. L. *Adv. Quantum Chem.* **1973**, *7*, 289.
(54) Liptay, W. In *Excited States*; Lim, E. C., Ed.; Academic Press: New York, 1974; Vol. 1, p 129.
(55) Liptay, W. *Angew. Chem., Int. Ed. Engl.* **1969**, *8*, 177.
(56) Piepho, S. B.; Krausz, E. R.; Schatz, P. N. *J. Am. Chem. Soc.* **1978**, *100*, 2996.
(57) Wong, K. Y.; Schatz, P. N. *Prog. Inorg. Chem.* **1981**, *28*, 369.
(58) Schatz, P. N. *NATO Adv. Study Inst., Ser. C* **1980**, *58*, 115.
(59) Fulton, R. L.; Gouterman, M. *J. Phys. Chem.* **1961**, *35*, 1059.
(60) Rice, M. J.; Lipari, N. O.; Strässler, S. *Phys. Rev. Lett.* **1977**, *39*, 1359.
(61) Rice, M. J. *Phys. Rev. Lett.* **1976**, *37*, 36.
(62) Rice, M. J.; Yartsev, V. M.; Jacobsen, C. S. *Phys. Rev. B* **1980**, *21*, 3437.
(63) If there is no change in symmetry between donor and acceptor, only totally symmetric modes are coupled to electron transfer. For example, for $Fe(H_2O)_6^{3+}/Fe(H_2O)_6^{2+}$ self-exchange, the only coupled skeletal mode is the $\nu_{a_{1g}}$, totally symmetric Fe−O stretch. The coordinate in the original PKS treatment is an antisymmetric linear combination of such local modes. In the delocalized limit, the local modes are coupled to give a symmetric−antisymmetric pair. The degree to which they differ in energy depends on the extent of the Fermi resonance interaction between them. If there is a change in symmetry on electron transfer, local asymmetric modes are also coupled to electron transfer and must be included in the analysis.
(64) Hush, N. S. *ACS Symp. Ser.* **1982**, *198*, 201.
(65) Prassides, K.; Schatz P. N. *J. Phys. Chem.* **1989**, *93*, 8387.
(66) Ko, J.; Ondrechen, M. J. *Chem. Phys. Lett.* **1984**, *112*, 507.
(67) Ko, J.; Ondrechen, M. J. *J. Am. Chem. Soc.* **1985**, *107*, 6161.
(68) Ondrechen, M. J.; Ferretti, A.; Lami, A.; Villani, G. *J. Phys. Chem.* **1994**, *98*, 11230.
(69) Ferretti, A.; Lami, A.; Ondrechen, M. J.; Villani, G. *J. Phys. Chem.* **1995**, *99*, 10484.
(70) Murga, L. F.; Ondrechen, M. J. *Theor. Chim. Acta* **1995**, *90*, 331.
(71) Schatz, P. N. *NATO Adv. Study Inst., Ser. C* **1991**, *343*, 7.
(72) Creutz, C.; Chou, M. H. *Inorg. Chem.* **1987**, *26*, 2995.
(73) Oh, D. H.; Sano, M.; Boxer, S. G. *J. Am. Chem. Soc.* **1991**, *113*, 6880.
(74) Stebler, A.; Ammeter, J. H.; Fürholz, U.; Ludi, A. *Inorg. Chem.* **1984**, *23*, 2764.
(75) Beattie, J. K.; Hush, N. S.; Taylor, P. R. *Inorg. Chem.* **1976**, *15*, 992.
(76) Best, S. P.; Clark, R. J. H.; McQueen, R. C. S.; Joss, S. *J. Am. Chem. Soc.* **1989**, *111*, 548.
(77) Piepho, S. B. *J. Am. Chem. Soc.* **1990**, *112*, 4197.
(78) Broo, A.; Lincoln, P. *Inorg. Chem.* **1997**, *36*, 2544.
(79) Lauher, J. W. *Inorg. Chim. Acta* **1980**, *39*, 119.
(80) Broo, A.; Larsson, S. *Chem. Phys.* **1982**, *161*, 363.
(81) (a) Ondrechen, M. J.; Ko, J.; Root, L. J. *J. Phys. Chem.* **1984**, *88*, 5919. (b) Zhang, L. T.; Ko, J.; Ondrechen, M. J. *J. Phys. Chem.* **1989**, *93*, 3030.
(82) Ferretti, A.; Lami, A.; Villani, G. *Inorg. Chem.* **1998**, *37*, 2799.
(83) Bencini, A.; Ciofini, I.; Daul, C. A.; Ferretti, A. *J. Am. Chem. Soc.* **1999**, *121*, 11418.
(84) Fürholz, U.; Joss, S.; Bürgi, H. A.; Ludi, A. *Inorg. Chem.* **1985**, *24*, 9143.
(85) Fürholz, U.; Bürgi, H. A.; Wagner, F. E.; Stebler, A.; Ammeter, J. H.; Krausz, E.; Clark, R. J. H.; Stead, M. J.; Ludi, A. *J. Am. Chem. Soc.* **1984**, *106*, 121.
(86) Lu, H.; Petrov, V.; Hupp, J. T. *Chem. Phys. Lett.* **1995**, *235*, 521.
(87) Powers, M. J.; Salmon, D. J.; Callahan, R. W.; Meyer, T. J. *J. Am. Chem. Soc.* **1976**, *98*, 6731.
(88) Citrin, P. H. *J. Am. Chem. Soc.* **1973**, *95*, 6472.
(89) Hush, N. S. *Chem. Phys.* **1975**, *10*, 361.
(90) Citrin, P. H.; Ginsberg, A. P. *J. Am. Chem. Soc.* **1981**, *103*, 3673.
(91) Lazarus, M. S.; Sham, T. K. *J. Am. Chem. Soc.* **1979**, *101*, 7622.
(92) Spreer, L. O.; Allan, C. B.; MacQueen, D. B.; Otvos, J. W.; Calvin, M. *J. Am. Chem. Soc.* **1994**, *116*, 2187.
(93) Moscherosch, M.; Waldnör, E.; Binder, H.; Kaim, W.; Fiedler, J. *Inorg. Chem.* **1995**, *34*, 4326.
(94) Demadis, K. D.; El-Samanody, E.-S.; Coia, G. M.; Meyer, T. J. *J. Am. Chem. Soc.* **1999**, *121*, 535.
(95) Demadis, K. D.; Meyer, T. J.; White, P. S. *Inorg. Chem.* **1998**, *37*, 3610.
(96) Richardson, D. E.; Sen, J. P.; Buhr, J. D.; Taube, H. *Inorg. Chem.* **1982**, *21*, 3136.
(97) Che, C.-M.; Lam, H.-W.; Tong, W.-F.; Lai, T.-F.; Lau, T.-C. *J. Chem. Soc., Chem. Commun.* **1989**, 1883.
(98) Lam, H.-W.; Che, C.-M.; Wong, K.-Y. *J. Chem. Soc., Dalton Trans.* **1992**, 1411.
(99) The appearance or absence of a symmetrical bridging-ligand stretch must be used with care as a marker for localization. For example, low-intensity $\nu(N_2)$ or ν(pz) bands are observed for the "symmetrical" Os(II)−Os(II) complexes *cis*,*cis*-$[(bpy)_2(Cl)Os(BL)Os(Cl)(bpy)_2]^{2+}$ (BL = N_2,[94] pz[111,112]). This is because the complexes themselves are unsymmetrical. There are rotamers with respect to the bridge which are not centrosymmetric for which ν(pz) is weakly IR active.
(100) Goodman, B. A.; Raynor, J. B. *Adv. Inorg. Chem. Radiochem.* **1970**, *13*, 135.
(101) Sen, J.; Taube, H. *Acta Chem. Scand. Ser. A* **1979**, *33*, 125.
(102) Buhr, J. D.; Winkler, J. R.; Taube, H. *Inorg. Chem.* **1980**, *19*, 2416.
(103) Kober, E. M. Ph.D. Dissertation, University of North Carolina, 1982.

(104) Kober, E. M.; Goldsby, K. A.; Narayana, D. N. S.; Meyer, T. J. *J. Am. Chem. Soc.* **1983**, *105*, 4303.
(105) Hill, N. J. *J. Chem. Soc., Faraday Trans. 2* **1972**, *68*, 427.
(106) Kober, E. M.; Meyer, T. J. *Inorg. Chem.* **1983**, *22*, 1614.
(107) Neyhart, G. A.; Timpson, C. J.; Bates, W. D.; Meyer, T. J. *J. Am. Chem. Soc.* **1996**, *118*, 3730.
(108) Hudson, A.; Kennedy, M. J. *J. Chem. Soc. A* **1969**, 1116.
(109) Bhattacharya, S.; Ghosh, P.; Chakravarty, A. *Inorg. Chem.* **1985**, *24*, 3224.
(110) The relationships in eq 12 assume that the reorganizational energies for the IC bands are negligible so that $E_{IC}(1)$ and $E_{IC}(2)$ are the energy spacings between the Kramer's doublets.
(111) Demadis, K. D.; Neyhart, G. A.; Kober, E. M.; Meyer, T. J. *J. Am. Chem. Soc.* **1998**, *120*, 7121.
(112) Demadis, K. D.; Neyhart, G. A.; Kober, E. M.; Meyer, T. J. *Inorg. Chem.* **1999**, *38*, 5948.
(113) There are three totally symmetrical ring stretching modes for pyrazine, ν_{8a}, ν_{9a}, and ν_{6a}. See: Lord, R. C.; Marston, A. L.; Miller, F. A. *Spectrochim. Acta* **1957**, *9*, 113 and ref 86 in this work.
(114) (a) Lay, P. A.; Magnuson, R. H.; Taube, H. *Inorg. Chem.* **1988**, *27*, 2364. (b) Magnuson, R. H.; Lay, P. A.; Taube, H. *J. Am. Chem. Soc.* **1983**, *105*, 2507.
(115) Grevels, F.-W.; Kerpen, K.; Klotzbucher, W. E.; McClurg, R. E. D.; Russell, G.; Viotte, M.; Schaffner, K. *J. Am. Chem. Soc.* **1998**, *120*, 10423 and references therein.
(116) Wu, R.; Arap Koske, S. K.; White, R. P.; Anson, C. E.; Jayasooriya, U. A.; Cannon, R. D. *J. Chem. Soc., Chem. Commun.* **1994**, 1657.
(117) Ito, T.; Hamaguchi, T.; Nagino, H.; Yamaguchi, T.; Kido, H.; Zavarine, I. S.; Richmond, T.; Washington, J.; Kubiak, C. P. *J. Am. Chem. Soc.* **1999**, *121*, 4625.
(118) Ito, T.; Hamaguchi, T.; Nagino, H.; Yamaguchi, T.; Washington, J.; Kubiak, C. P. *Science* **1997**, *277*, 660.
(119) Hartshorn, C. M.; Daire, N.; Tondreau, V.; Loeb, B.; Meyer, T. J. Manuscript in preparation.
(120) Chin, T. T.; Grimes, R. N.; Geiger, W. E. *Inorg. Chem.* **1999**, *38*, 93.
(121) Maroncelli, M. *J. Mol. Liq.* **1993**, *57*, 1.
(122) Barbara, P. F.; Jarzeba, W. *Adv. Photochem.* **1990**, *15*, 1.
(123) Simon, J. D. *Acc. Chem. Res.* **1988**, *21*, 128.
(124) Bagchi, B.; Chandra, A. *Adv. Chem. Phys.* **1991**, *80*, 1.
(125) Bagchi, B. *Annu. Rev. Phys. Chem.* **1989**, *40*, 115.
(126) Raineri, F. O.; Zhou, Y.; Friedman, H. L. *Chem. Phys.* **1991**, *152*, 201.
(127) Ladanyi, B.; Shaf, M. S. *Annu. Rev. Phys. Chem.* **1993**, *44*, 335.
(128) Hynes, J. T. In *Ultrafast Dynamics of Chemical Systems*; Simon, J. D., Ed.; Klewer: Dordrecht, Holland, 1994; p 345.
(129) Smith, B. B.; Kim, H. J.; Borgis, D.; Hynes, J. T. In *Dynamics and Mechanism of Photoinduced Transfer and Related Phenomena*; Mataga, N., Okada, T., Masuhara, H., Eds.; Elsevier: Amsterdam, Holland, 1992; p 39.
(130) Kosower, E. M.; Huppert, D. *Annu. Rev. Phys. Chem.* **1986**, *37*, 127.
(131) Joo, T.; Jia, Y.; Yu, J.-Y.; Lang, M. J.; Fleming, G. R. *J. Chem. Phys.* **1996**, *104*, 6089.
(132) Stratt, R. M.; Cho, M. *J. Chem. Phys.* **1994**, *100*, 6700.
(133) Ladanyi, B. M.; Stratt, R. M. *J. Phys. Chem.* **1995**, *99*, 2502.
(134) Timpson, C. J.; Bignozzi, C. A.; Sullivan, B. P.; Kober, E. M.; Meyer, T. J. *J. Phys. Chem.* **1996**, *100*, 2915.
(135) Curtis, J. C.; Sullivan, B. P.; Meyer, T. J. *Inorg. Chem.* **1983**, *22*, 224.
(136) Stravrev, K. K.; Zerner, M. C.; Meyer, T. J. *J. Am. Chem. Soc.* **1995**, *117*, 8684.
(137) Zeng, J.; Hush, N. S.; Reimers, J. R. *J. Phys. Chem.* **1996**, *100*, 19292.
(138) Zeng, J.; Hush, N. S.; Reimers, J. R. *J. Am. Chem. Soc.* **1996**, *118*, 2059.
(139) Brunschwig, B. S.; Ehrenson, S.; Sutin, N. *J. Phys. Chem.* **1986**, *90*, 3657.
(140) Matyushov, D.; Schmid, R. *J. Phys. Chem.* **1994**, *98*, 5152.
(141) Matyushov, D. *Chem. Phys.* **1993**, *174*, 199.
(142) Hammack, W. S.; Lowery, M. D.; Hendrickson, D. N.; Drickamer, H. G. *J. Phys. Chem.* **1988**, *92*, 1771.
(143) Roberts, J. A.; Hupp, J. T. *Inorg. Chem.* **1992**, *31*, 157.
(144) (a) Krausz, E. R.; Mau, A. W. H. *Inorg. Chem.* **1986**, *25*, 1484. (b) Krausz, E. R. *Chem. Phys. Lett.* **1985**, *120*, 113.
(145) Dubicki, L.; Ferguson, J.; Krausz, E. R. *J. Am. Chem. Soc.* **1985**, *107*, 179.
(146) Zeng, J.; Hush, N. S.; Reimers, J. R. *J. Phys. Chem.* **1995**, *99*, 10459.
(147) Magnuson, R. H.; Taube, H. *J. Am. Chem. Soc.* **1975**, *97*, 5129.
(148) Winkler, J. R.; Netzel, T. L.; Creutz, C.; Sutin, N. *J. Am. Chem. Soc.* **1987**, *109*, 2381.
(149) Oh, D, H.; Boxer, S. G. *J. Am. Chem. Soc.* **1989**, *111*, 1130.
(150) Petrov, V.; Hupp, J. T.; Mottley, C.; Mann, L. C. *J. Am. Chem. Soc.* **1994**, *116*, 2171.
(151) In the average mode approximation the electron−vibrational coupling constant is the sum of S_j values for the individual modes that contribute with $S = \sum_j S_j$. The quantum spacing is the weighted average, $\hbar\omega_j = (\sum_j S_j \hbar\omega_j / \sum_j S_j)$.
(152) Myers, A. B. *Chem. Phys.* **1994**, *180*, 215.
(153) Heller, E. J. *Acc. Chem. Res.* **1981**, *14*, 368.
(154) Zink, J. I.; Shin, K.-C. K. *Adv. Photochem.* **1991**, *16*, 119.
(155) Myers, A. B. *J. Phys. Chem. A* **1999**, *103*, 6891.
(156) Poppe, J.; Moscherosch, M.; Kaim, W. *Inorg. Chem.* **1993**, *32*, 2640.
(157) Evans, C. E. B.; Naklicki, M. L.; Rezvani, A. R.; White, C. A.; Kondratiev, V. V.; Crutchley, R. J. *J. Am. Chem. Soc.* **1998**, *120*, 13096.
(158) Wlodarczyk, A.; Doyle, G. A.; Maher, J. P.; McCleverty, J. A.; Ward, M. D. *Chem. Commun.* **1997**, 769.
(159) Kasack, V.; Kaim, W.; Binder, H.; Jordanov, J.; Roth, E. *Inorg. Chem.* **1995**, *34*, 1924.
(160) Kaim, W.; Kasack, V.; Binder, H.; Roth, E.; Jordanov, J. *Angew. Chem., Int. Ed. Engl.* **1988**, *27*, 1174.
(161) Newton, M. D.; Sutin, N. *Annu. Rev. Phys. Chem.* **1984**, *35*, 437.
(162) Sutin, N. *Acc. Chem. Res.* **1982**, *15*, 275.
(163) Marcus, R. A.; Sutin, N. *Biochim. Biophys. Acta* **1985**, *811*, 265.
(164) Barbara, P. F.; Meyer, T. J.; Ratner, M. A. *J. Phys. Chem.* **1996**, *100*, 13148 and references therein.
(165) Hush, N. S. *Coord. Chem. Rev.* **1985**, *64*, 135.
(166) Kestner, N. R.; Logan, J.; Jortner, J. *J. Phys. Chem.* **1974**, *78*, 2148.
(167) Jortner, J. *J. Chem. Phys.* **1976**, *64*, 4860.
(168) Bixon, M.; Jortner, J. *Faraday Discuss. Chem. Soc.* **1982**, *74*, 17.
(169) Bixon, M.; Jortner, J.; Cortes, J.; Heitele, H.; Michel-Beyerle, M. E. *J. Phys. Chem.* **1994**, *98*, 7289.
(170) Kober, E. M.; Caspar, J. V.; Lumpkin, R. S.; Meyer, T. J. *J. Phys. Chem.* **1986**, *90*, 3722.
(171) Marcus, R. A. *J. Phys. Chem.* **1989**, *93*, 3078.
(172) Steinfeld, J. I. *Molecules and Radiation*; The MIT Press: Cambridge, 1985.
(173) Kubo, R.; Toyozawa, Y. *Prog. Theor. Phys.* **1955**, *13*, 160.
(174) Lax, M. J. *Chem. Phys.* **1952**, *20*, 1752.
(175) Myers, A. B. *Chem. Phys.* **1994**, *180*, 215.
(176) Hornung, F. M.; Baumann, F.; Kaim, W.; Olabe, J. A.; Slep, L. D.; Fiedler, J. *Inorg. Chem.* **1998**, *37*, 311.
(177) Atwood, C. G.; Geiger, W. E.; Rheingold, A. L. *J. Am. Chem. Soc.* **1993**, *115*, 5310.
(178) (a) Hillman, M.; Kvick, A. *Organometallics.* **1983**, *2*, 1780. (b) Levanda, C.; Bechgaard, K.; Cowan, D. O.; Mueller-Westerhoff, U. T.; Elbrecht, P.; Candela, G. A.; Collins, R. L. *J. Am. Chem. Soc.* **1976**, *98*, 3181.
(179) Kirchner, R. F.; Loew, G. H.; Mueller-Westerhoff, U. T. *Inorg. Chem.* **1976**, *15*, 2665.
(180) Dubicki, L.; Ferguson, J.; Krausz, E. R.; Lay, P. A.; Maeder, M.; Taube, H. *J. Phys. Chem.* **1984**, *88*, 3940.
(181) Lay, P. A.; Magnuson, R. H.; Sen, J.; Taube, H. *J. Am. Chem. Soc.* **1982**, *104*, 7658.
(182) Dubicki, L.; Ferguson, J.; Krausz, E. R.; Lay, P. A.; Maeder, M.; Magnuson, R. H.; Taube, H. *J. Am. Chem. Soc.* **1985**, *107*, 2167.
(183) Tom, G. M.; Taube, H. *J. Am. Chem. Soc.* **1975**, *97*, 5310.
(184) Joss, S.; Bürgi, H. B.; Ludi, A. *Inorg. Chem.* **1985**, *24*, 949.
(185) Beattie, J. K.; Del Favero, P.; Hambley, T. W.; Hush, N. S. *Inorg. Chem.* **1988**, *27*, 2000.
(186) Hughes, M. N.; O'Reardon, D.; Poole, R. K.; Hursthouse, M. B.; Thornton-Pett, M. *Polyhedron* **1987**, *6*, 1711.
(187) Hush, N. S.; Beattie, J. K.; Ellis, V. M. *Inorg. Chem.* **1984**, *23*, 3339.
(188) Armstrong, R. S.; Beattie, J. K.; Del Favero, P.; Ellis, V. M.; Hush, N. S. *Inorg. Chim. Acta* **1984**, *89*, L33.
(189) Nelsen, S. F.; Tran, H. Q.; Nagy, M. A. *J. Am. Chem. Soc.* **1998**, *120*, 298.
(190) Liberko, C. A.; Miller, L. L.; Katz, T. J.; Liu, L. *J. Am. Chem. Soc.* **1993**, *115*, 2478.
(191) Poppe, J.; Kaim, W.; Ben Albatef, A.; Katz, N. E. *J. Chem. Soc., Perkin Trans. 2* **1993**, 2105.
(192) Bell, S. E.; Field, S. S.; Haines, R. I.; Moscherosch, M.; Matheis, W.; Kaim, W. *Inorg. Chem.* **1992**, *31*, 3269.
(193) Baumann, F.; Kaim, W.; García Posse, M.; Katz, N. E. *Inorg. Chem.* **1998**, *37*, 658.
(194) Seyler, J. W.; Weng, W.; Zhou, Y.; Gladysz, J. A. *Organometallics* **1993**, *12*, 3802.
(195) Le Narvor, N.; Lapinte, C. *J. Chem. Soc., Chem. Commun.* **1993**, 357.
(196) Etzenhouser, B. A.; Dibiase Cavanaugh, M.; Spurgeon, H. N.; Sponsler, M. B. *J. Am. Chem. Soc.* **1994**, *116*, 2221.
(197) Wlodarczyk, A.; Maher, J. P.; McCleverty, J. A.; Ward, M. D. *J. Chem. Soc., Chem. Commun.* **1995**, 2397.
(198) Bruns, W.; Kaim, W.; Waldhör, E.; Krejik, M. *Inorg. Chem.* **1995**, *34*, 663.
(199) Bruns, W.; Kaim, W.; Waldhör, E.; Krejik, M. *J. Chem. Soc., Chem. Commun.* **1993**, 1868.
(200) Kaim, W.; Bruns, W.; Kohlmann, S.; Krejik, M. *Inorg. Chim. Acta* **1995**, *229*, 143.

(201) Geiger, W. E.; Atwood, C. G.; Chin, T. T. *Molecular Electrochemistry of Inorganic, Bioinorganic and Organometallic Compounds*; NATO ASI Ser. C; Kluwer Academic Publishers: Dordrecht, The Netherlands, 1993; Vol. 385, p 519.
(202) Ruminski, R. R.; Serveiss, D.; Jacquez, M. *Inorg. Chem.* **1995**, *34*, 3358.
(203) Hupp, J. T.; Neyhart, G. A.; Meyer, T. J. *J. Am. Chem. Soc.* **1986**, *108*, 5349.
(204) Neyhart, G. A.; Hupp, J. T.; Curtis, J. C.; Timpson, C. J.; Meyer, T. J. *J. Am. Chem. Soc.* **1996**, *118*, 3724.
(205) The donor number, as defined by Gutmann, is the molar reaction enthalpy in 1,2-dichloroethane for the formation of a 1:1 adduct between $SbCl_5$ and the added solvent as donor. See: Gutmann, V. *The Donor−Acceptor Approach to Molecular Interactions*; Plenum Press: New York, 1978.
(206) Haga, M.; Matsumura-Inoue, T.; Yamabe, S. *Inorg. Chem.* **1987**, *26*, 4148.
(207) (a) Stoll, M. E.; Lovelace, S. R.; Geiger, W. E.; Schimanke, H.; Hyla-Kryspin, I.; Gleiter, R. *J. Am. Chem. Soc.* **1999**, *121*, 9343. (b) Gleiter, R.; Röcker, H.; Pflästerer, G.; Treptow, B.; Kratz, D. *Tetrahedron Lett.* **1993**, *34*, 8075.
(208) Dong, Y.; Hupp, J. T.; Yoon, D. I. *J. Am. Chem. Soc.* **1993**, *115*, 4379.
(209) Krentzien, H.; Taube, H. *J. Am. Chem. Soc.* **1976**, *98*, 6379.
(210) Cannon, R. D.; White, R. P. *Prog. Inorg. Chem.* **1988**, *36*, 195.
(211) Meesuk, L.; Jayasooriya, U. A.; Cannon, R. D.; Powell, D. B. *J. Am. Chem. Soc.* **1987**, *109*, 2009.
(212) Johnson, M. K.; Cannon, R. D.; Powell, D. B. *Spectrochim. Acta* **1982**, *38A*, 307.
(213) Oh, S. M.; Hendrickson, D. N.; Hassett, K. L.; Davis, R. E. *J. Am. Chem. Soc.* **1985**, *107*, 8009.
(214) Oh, S. M.; Wilson, S. R.; Hendrickson, D. N.; Woehler, S. E.; Wittebort, R. J.; Inniss, D.; Strouse, C. E. *J. Am. Chem. Soc.* **1987**, *109*, 1073.
(215) Woehler, S. E.; Wittebort, R. J.; Oh, S. M.; Kambara, T.; Hendrickson, D. N.; Inniss, D.; Strouse, C. E. *J. Am. Chem. Soc.* **1987**, *109*, 1063.
(216) Kaneko, Y.; Nakano, M.; Sorai, M.; Jang, H. G.; Hendrickson, D. N. *Inorg. Chem.* **1989**, *28*, 1067.
(217) Sorai, M.; Hendrickson, D. N. *Pure Appl. Chem.* **1991**, *63*, 1503.
(218) Webb, R. J.; Hagen, P. M.; Wittebort, R. J.; Sorai, M.; Hendrickson, D. N. *Inorg. Chem.* **1992**, *31*, 1791.
(219) Sano, H. *Hyperfine Interact.* **1990**, *53*, 97 and references therein.
(220) Konno, M.; Sano, H. *Bull. Chem. Soc. Jpn.* **1988**, *61*, 4155.
(221) Dong, T.-Y.; Cohn, M. J.; Hendrickson, D. N.; Pierpont, C. G. *J. Am. Chem. Soc.* **1985**, *107*, 4777.
(222) Dong, T.-Y.; Schei, C.-C.; Hsu, T.-L.; Lee, S.-L.; Li, S.-J.. *Inorg. Chem.* **1991**, *30*, 2457.
(223) Cohn, M. J.; Dong, T.-Y.; Hendrickson, D. N.; Geib, S. J.; Rheingold, A. L. *J. Chem. Soc., Chem. Commun.* **1985**, 1095.
(224) Dong, T.-Y.; Kambara, T.; Hendrickson, D. N. *J. Am. Chem. Soc.* **1986**, *108*, 5857.
(225) Dong, T.-Y.; Huang, C.-H.; Chang, C.-K.; Wen, Y.-S.; Lee, S.-Y.; Chen, J.-A.; Yeh, W.-Y.; Yeh, A. *J. Am. Chem. Soc.* **1993**, *115*, 6357.
(226) Swanton, D. J.; Bacskay, G. D.; Hush, N. S. *Chem. Phys.* **1986**, *107*, 9.
(227) Swanton, D. J.; Bacskay, G. D.; Hush, N. S. *Chem. Phys.* **1986**, *107*, 25.
(228) Swanton, D. J.; Bacskay, G. D.; Hush, N. S. *J. Chem. Phys.* **1986**, *84*, 5715.
(229) Ulstrup, J.; Jortner, J. *J. Chem. Phys.* **1975**, *63*, 4358.
(230) Jortner, J.; Bixon, M. *J. Chem. Phys.* **1988**, *88*, 167.
(231) Siders, P.; Marcus, R. A. *J. Am. Chem. Soc.* **1981**, *103*, 741.
(232) Siders, P.; Marcus, R. A. *J. Am. Chem. Soc.* **1981**, *103*, 748.
(233) (a) Newton, M. D. *Chem. Rev.* **1991**, *91*, 767. (b) Newton, M. D.; Cave, R. J. In *Molecular Electronics*; Jortner, J., Ratner, M. A. ,Eds.; Blackwell Science Ltd.: Oxford, 1997; p 73.
(234) Marcus, R. A. *Annu. Rev. Phys. Chem.* **1966**, *15*, 155.
(235) Marcus, R. A. *Rev. Mod. Phys.* **1993**, *65*, 599.
(236) Sutin, N.; Brunschwig, B. S. *ACS Symp. Ser.* **1982**, *198*, 105.
(237) Simon, J. D. *Acc. Chem. Res.* **1988**, *21*, 128.
(238) Weaver, M. J. *Chem. Rev.* **1992**, *92*, 463.
(239) Calef, D. F.; Wolynes, P. G. *J. Phys. Chem.* **1983**, *87*, 3387.
(240) Heitele, H. *Angew. Chem., Int. Ed. Engl.* **1993**, *32*, 359.
(241) Sumi, H.; Marcus, R. A. *J. Chem. Phys.* **1986**, *84*, 4894.
(242) Zusman, L. D. *Chem. Phys.* **1988**, *119*, 51.
(243) Bixon, M.; Jortner, J. *Chem. Phys.* **1993**, *176*, 467.
(244) Simon, J. D.; Rossky, P. J. *Nature* **1994**, *370*, 263.
(245) Weaver, M. J.; Phelps, D. K.; Nielson, R. M.; Golovin, M. N.; McManis, G. E. *J. Phys. Chem.* **1990**, *94*, 2949.
(246) Jimenez, R.; Fleming, G. R.; Kumar, P. V.; Maroncelli, M *Nature* **1994**, *369*, 471.
(247) Yoshihara, K.; Tomonaga, K.; Nagasawa, Y. *Bull. Chem. Soc. Jpn.* **1995**, *68*, 696.
(248) Zusman, L. D. *Chem. Phys.* **1980**, *49*, 295.
(249) Hynes, J. T. In *The Theory of Chemical Reactions*; Baer, M., Ed.; CRC Press: Boca Raton, FL, 1985; Vol. 4, p 171.
(250) Onuchic, J. N.; Wolynes, P. G. *J. Phys. Chem.* **1988**, *92*, 6495.
(251) Zichi, D. A.; Cicotti, G.; Hynes, J. T.; Ferrario, M. *J. Phys. Chem.* **1989**, *93*, 6211.
(252) Bader, J. S.; Kuharski, R. A.; Chandler, D. *J. Chem. Phys.* **1990**, *93*, 230.
(253) Nelsen, S. F.; Ismagilov, R. F.; Powell, D. R. *J. Am. Chem. Soc.* **1996**, *118*, 6313.
(254) Nelsen, S. F. *J. Am. Chem. Soc.* **1996**, *118*, 2047.
(255) Nelsen, S. F.; Ramm, M. T.; Wolff, J. J.; Powell, D. R. *J. Am. Chem. Soc.* **1997**, *119*, 6863.
(256) Meyer, T. J. in *Mixed Valence Compounds*; Brown, D. M., Ed.; D. Reidel: Dordrecht, Holland, 1980; p 75 and references therein.
(257) Kauzman, W. *Quantum Chemistry: An Introduction*; Academic Press: New York, 1957.
(258) Crosby, G. A.; Highland, R. G.; Truesdell, K. A. *Coord. Chem. Rev.* **1985**, *64*, 41.
(259) DeArmond, M. K.; Hanck, K. W.; Wertz, D. W. *Coord. Chem. Rev.* **1985**, *64*, 65.
(260) Meyer, T. J. *Acc. Chem. Res.* **1989**, *22*, 163.
(261) Scandola, R.; Indelli, M. T.; Chiorboli, C.; Bignozzi, C. A. *Top. Curr. Chem.* **1990**, *158*, 73.
(262) Balzani, V.; Scandola, F. *Supramolecular Photochemistry*; Horwood: Chichester, U.K., 1991; Chapters 5 and 6.
(263) Kalyanasundaram, K. *Photochemistry of Polypyridine and Porphyrin Complexes*; Academic Press: London, 1992.
(264) (a) Crowley, C. E.; Clark, C. D.; Hoffman, M. Z. *Inorg. Chem.* **1998**, *37*, 5704. (b) Li, C.; Hoffman, M. Z. *Inorg. Chem.* **1998**, *37*, 830.
(265) Kober, E. M.; Sullivan, B. P. Meyer, T. J. *Inorg. Chem.* **1984**, *23*, 2098.
(266) Oh, D. H.; Boxer, S. G. *J. Am. Chem. Soc.* **1990**, *111*, 1130.
(267) Dallinger, R. F.; Woodruff, W. H. *J. Am. Chem. Soc.* **1979**, *101*, 4391.
(268) Bradley, P. G.; Kress, N.; Hornberger, B. A.; Dallinger, R. F.; Woodruff, W. H. *J. Am. Chem. Soc.* **1981**, *103*, 7441.
(269) Omberg, K. M.; Schoonover, J. R.; Treadway, J. A.; Leasure, R. M.; Dyer, R. B.; Meyer, T. J. *J. Am. Chem. Soc.* **1997**, *119*, 7013.
(270) For a review on $[Ru(bpy)_3]^{2+}$, see: Krausz, E.; Ferguson, J. *Prog. Inorg. Chem.* **1989**, *37*, 293.
(271) Miller, S. J. *Inorg. Chem.* **1989**, *28*, 868.
(272) Riesen, H.; Wallace, L.; Krausz, E. *Int. Rev. Phys. Chem.* **1997**, *16*, 291.
(273) Humbs, W.; Strasser, J.; Yersin, H. *J. Lumin.* **1997**, *72−4*, 658.
(274) Yersin, H.; Humbs, W.; Strasser, J. *Coord. Chem. Rev.* **1997**, *159*, 325.
(275) Caspar, J. V.; Westmoreland, T. D.; Allen, G. H.; Bradley, P. G.; Meyer, T. J.; Woodruff, W. H. *J. Am. Chem. Soc.* **1984**, *106*, 3492.
(276) Mabrouk, P. A.; Wrighton, M. S. *Inorg. Chem.* **1986**, *25*, 526.
(277) Maruszewski, K.; Bajdor, K.; Strommen, D. P.; Kincaid, J. R. *J. Phys. Chem.* **1995**, *99*, 6286.
(278) The lowest excited "state" is actually a series of three closely spaced, Boltzmann-populated states which share a common $d\pi-\pi^*$ MLCT origin and are in rapid equilibrium, see: Hager, G. D.; Crosby, G. A. *J. Am. Chem. Soc.* **1975**, *97*, 7031 and Striplin, D. R.; Crosby, G. A. *J. Phys. Chem.* **1995**, *99*, 7977.
(279) Cushing, J. P.; Butoi, C.; Kelley, D. F. *J. Phys. Chem. A* **1997**, *101*, 7222.
(280) Cooley, L. F.; Bergquist, P.; Kelley, D. F. *J. Am. Chem. Soc.* **1990**, *112*, 2612.
(281) Malone, R. A.; Kelley, D. F. *J. Chem. Phys.* **1991**, *95*, 8970.
(282) Pogge, J. L.; Kelley, D. F. *Chem. Phys. Lett.* **1995**, *238*, 16.
(283) Dattelbaum, D. M.; Meyer, T. J. Submitted for publication.
(284) Curtis, J. C.; Bernstein, R. H.; Schmehl, R. H.; Meyer, T. J. *Chem. Phys. Lett.* **1981**, *81*, 48.
(285) Schanze, K. S.; Neyhart, G. A.; Meyer, T. J. *J. Phys. Chem.* **1986**, *90*, 2182.
(286) Tapolsky, G.; Duesing, R.; Meyer, T. J. *J. Phys. Chem.* **1991**, *95*, 1105.
(287) Turner, J. J.; George, M. W.; Johnson, F. P. A.; Westwell, J. R. *Coord. Chem. Rev.* **1993**, *125*, 101.
(288) Omberg, K. M.; Schoonover, J. R.; Meyer, T. J. *J. Phys. Chem. A* **1997**, *101*, 9531.
(289) George, M. W.; Johnson, F. P. A.; Turner, J. J.; Westwell, J. R. *J. Chem. Soc., Dalton Trans.* **1995**, 2711.
(290) Bignozzi, C. A.; Argazzi, R.; Schoonover, J. R.; Gordon, K. C.; Dyer, R. B.; Scandola, F. *Inorg. Chem.* **1992**, *31*, 5260.
(291) Bignozzi, C. A.; Chiorboli, C.; Scandola, F.; Dyer, R. B.; Schoonover, J. R.; Meyer, T. J. *Inorg. Chem.* **1994**, *33*, 1652.
(292) Schanze, K. S.; Walters, K. A.; *Photoinduced Electron Transfer in Metal-Organic Dyads*; Ramamurthy, V., Schanze, K. S., Eds.; Marcel Dekker: New York, 1998; Vol 2.
(293) Sullivan, B. P.; Abruna, H. O.; Finklea, D. J.; Salmon, D. J.; Nagle, J. K.; Meyer, T. J.; Sprintschnik, H. *Chem. Phys. Lett.* **1978**, *58*, 389.
(294) Mecklenberg, S. L.; Opperman, K. A.; Chen, P. Y.; Meyer, T. J. *J. Phys. Chem.* **1996**, *100*, 15145.
(295) Chen, P. Y.; Palmer, R. A.; Meyer, T. J. *J. Phys. Chem. A* **1998**, *102*, 3042.

(296) The lowest excited state for the OQD complex is a $\sigma-\pi^*$ state of configuration $\sigma(\mathrm{ReO})^1\pi^{*1}$ rather than a $d\pi^5\pi^{*1}$ MLCT state.
(297) Claude, J. P.; Williams, D. S.; Meyer, T. J. *J. Am. Chem. Soc.* **1996**, *118*, 9782.
(298) Claude, J. P.; Omberg, K. M.; Williams, D. S.; Meyer, T. J. Manuscript in preparation.
(299) Kober, E. M.; Caspar, J. V.; Lumpkin, R. S.; Meyer, T. J. *J. Phys. Chem.* **1986**, *90*, 3722.
(300) Freed, K. M.; Jortner, J. *J. Chem. Phys.* **1970**, *52*, 6272.
(301) Bixon, M.; Jortner, J. *J. Chem. Phys.* **1968**, *48*, 715.
(302) Englman, R.; Jortner, J. *Mol. Phys.* **1970**, *18*, 145.
(303) Lin, S, H. *Radiationless Transitions*; Academic: New York, 1980.
(304) Freed, K. F. *Top. Curr. Chem.* **1972**, *31*, 65.
(305) Lin, S, H. *J. Chem. Phys.* **1966**, *44*, 3759.
(306) Bixon, M, Jortner, J., Verhoeven, J. W. *J. Am. Chem. Soc.* **1994**, *116*, 6, 7349.
(307) Closs, G. L.; Calcaterra, L. T.; Green, N. J.; Penfield, K. W. *J. Phys. Chem.* **1986**, *90*, 3673.
(308) Gould, I. R.; Noukakis, D.; Gomez-Jahn, L.; Young, R. H.; Goodman, J. L.; Farid, S. *Chem. Phys.* **1993**, *176*, 439.
(309) Gould, I. R.; Young, R. H.; Mueller, L. J.; Albrecht, A. C., Farid, S. *J. Am. Chem. Soc.* **1994**, *116*, 8188.
(310) Friedman, A. E.; Chambron, J.-C., Sauvage, J.-P.; Turro, N. J.; Barton, J. K. *J. Am. Chem. Soc.* **1990**, *112*, 4960.
(311) Chen, W.; Turro, C.; Friedman, L. A., Barton, J. K.; Turro, N. J. *J. Phys. Chem. B* **1997**, *101*, 6995.
(312) Schoonover, J. R.; Bates, W. D.; Meyer, T. J. *Inorg. Chem.* **1995**, *34*, 6421.

CR990413M